An Innovative Daylighting System Incorporating Active Light Collection

by

Sepideh Khosravi Simchi

B.Sc., The University of Tehran, 2007

M.Sc., The University of Tehran, 2010

A THESIS SUBMITTED IN PARTIAL FULFILLMENT OF

THE REQUIREMENTS FOR THE DEGREE OF

DOCTOR OF PHILOSOPHY

in

THE FACULTY OF GRADUATE AND POSTDOCTORAL STUDIES

(Physics)

THE UNIVERSITY OF BRITISH COLUMBIA

(Vancouver)

February 2015

Abstract

The building industry recognizes the importance of incorporating daylighting into the illumination of buildings to improve both the energy performance of the building and the overall lighting quality. There are several well-known methods to increase the daylighting level in buildings, including windows and skylights. However, they are usually not capable of illuminating the core of the building, and may increase the energy usage of the building due to poor insulation. There are other systems designed for illuminating the core of buildings with daylighting, but they all have some limitations that have impeded widespread adoption.

A daylighting system investigated in this PhD project offers a novel approach to illuminating the core of buildings. This system, so called the Two-Stage Core Sunlighting System, consists of active and passive optical elements that capture sunlight outside of the building and transfer it to the dark core. Active sunlight redirectors, mounted at the rooftop level edge of the building, track the sun throughout the day and redirect the sunlight towards building façades at a certain angle. Passive concentrator elements mounted on the façades of the building capture and concentrate the light and direct it into light guides. The sunlight is then distributed within the building via interior light guides that illuminate the building.

The performance of the Two-Stage Core Sunlighting System was evaluated for five different cities. The energy savings calculations and the cost estimation showed that the Two-Stage Core Sunlighting System can provide a practical approach to daylighting a building without negatively impacting its overall energy performance.

As a complement to the main research project, an analysis was carried out to determine whether performance improvements could be possible in the future. The analysis focused on modifications to the prismatic microstructured film, in particular the addition of reflective structures that may enhance the efficiency of the film by recapturing a portion of the energy that would otherwise be lost. Simulation results showed that such modifications do not substantially change the performance of the currently available microstructured films, but that they can improve the performance of a nanostructured film in future applications.

Preface

All the work presented in this PhD research project was conducted in the Sustainable Solutions Applied Physics Laboratory at the University of British Columbia, Vancouver campus. The knowledge about both published [1] [2] and unpublished optical design concepts was provided by the Sustainable Solutions Applied Physics Laboratory. The research described is a detailed scientific evaluation of some of those optical design concepts.

A summarized version of Chapters 3 to 6 was presented at the 2013 Solar World Congress of the International Solar Energy Society at Cancun, Mexico and the paper presented there was published in Energy Procedia by Elsevier Online Journal. I was the lead investigator for this scientific evaluation work and was responsible for all aspects of research, including computer modeling, data collection and analysis and manuscript composition. Dr. Lorne Whitehead and Dr. Michele Mossman were the co-authors of the Energy Procedia paper, and provided supervision for the research project and editorial guidance for the manuscript composition.

I was the lead investigator for the research presented in Chapters 7 and 8 (unpublished) for which I was responsible for all of the scientific research, including calculation analysis, simulation modeling, data collection and analysis. Dr. Lorne Whitehead and Dr. Michele Mossman provided supervision for the research and also editorial guidance for this thesis.

Table of contents

List of tables

List of figures

List of abbreviations

ADS - Anidolic Daylighting System: A system installed above the window that uses nonimaging (anidolic) optics to increase the penetration depth of sunlight inside the room

CPC - Compound Parabolic Concentrator: A concentrator with the shape of a parabola which is designed to effectively collet light within certain acceptance angle.

CR - Concentration Ratio: The ratio of the output beam diameter over input beam diameter in a concentrator.

CRI - Colour Rendering Index: A quantitative index that compares the ability of light source to reproduce different colours compare to sunlight on a scale of 0-100, with sunlight as source of reference.

CSL –Core Sunlighting System: An active daylighting system that captures sun outside the building and transfer it into the building core.

ESR - Enhanced Specular Reflector: Highly specular reflective film based on multilayers of dielectric, produced by 3M Company.

FDTD - Finite Difference Time Domain: is a common and simple numerical method that approximates the value of the electromagnetic wave across the desired boundary condition over the course of the time.

GHG - Greenhouse Gas: An atmospheric gas that absorbs and emits radiation within the infrared range and cause the temperature of atmosphere to rise. The excessive aggregation of greenhouse gasses in the atmosphere is known as the main reason of the global warming problem

IES – Illuminating Engineering Society: A non-profit society with the mission of improving the lighting quality by translating knowledge into actions that benefit the public.

LED – Liquid Emitting Diode: A semiconductor light source that activates p-n junction diode to emit light.

LEED - Leadership in Energy and Environment Design: A set of rating system for design, construction and operation of the building developed by U.S. Green Building Council to help building designers to measure the performance of the buildings in terms of sustainability.

OLF - Prismatic microstructured film: A thin film with microstructured prism developed at 3M with large optical applications.

PV- Photovoltaic Cells: A cell that converts sunlight into electricity using semiconductor material through photovoltaic effect.

SCIS - Solar Canopy Illumination System: An active solar lighting system for illuminating the interior spaces of building with natural sunlight.

Acknowledgements

I would like to give special thanks to all those people who made this dissertation possible.

First, I would like to express my gratitude to my supervisor Prof. Lorne Whitehead, who patiently guided me with his immense knowledge and idea, and supported me at the rough situations I went through couple of times. He gave me this opportunity to be part of a great research lab and gaining precious experience in the world of applied science.

I would like to thank Dr. Michele Mossman, the SSAP laboratory manager, for her scientific input and guidance during my research project and writing my thesis, and for making so much effort to provide a productive work environment.

I would like to thank my PhD committee members, Dr. Andrzej Kotlicki, Prof. Chris Waltham and Prof. Murray Hodgson, for their guidance and support during my research project.

Special thanks to the Sustainable Building Science Program at the University of British Columbia for funding this research through the NSERC grant and providing valuable knowledge through courses and seminars.

I would also like to thank all my lab mates, especially my dear friends, Jakob Emmel, Jason Radel, Angel Valerio, and Megan Ogilvie for giving me scientific feedback on my research and providing a lovely and friendly work environment in the past four years.

Finally, I would like to express my gratitude toward my beloved family for their unconditional everlasting love and for their encouragement and support through all these years, and my lovely friends whom without them, life wouldn't be just as beautiful as it is now!

Dedication

I would like to dedicate this dissertation to Soraya and Ahmad, the most caring lovely parents I could ever imagine, for their unconditional love and emotional support throughout all these years; and to my beloved brothers Khosro and Farshad, who taught me never to stop believing in myself and to always pursue my dreams.

Chapter 1: Introduction

Buildings have a significant impact on the modern lifestyle because most people spend most of their time within the indoor environment. It is important to design a building at a high quality level, such that it satisfies the needs of occupants while also achieving a reasonable energy performance. However, meeting these two requirements at the same time can be quite challenging for building designers. Many aspects of building design, including lighting, ventilation, heating, acoustics and visual aesthetics are highly connected and improving one aspect often diminishes other factors and leads to a net increase in the energy usage of the building. The Green Building Society addressed this problem in recent years by challenging the industry to achieve sustainable building design; that is minimizing the negative impact of a building on the environment while maintaining high performance.

One of the most important challenges in building design, which was the subject of interest in this research project, is illumination. People usually tend to be very aware of lighting quality and in general do not accept poor lighting quality. Thus, it is important to keep the quality of lighting at a high level while optimizing the energy performance of the building. One of the best methods to reach this goal is supplementing electric lighting with sunlight, which is a renewable source of energy. This can improve the energy performance of the building as well as minimizing the negative impact of the building on the environment.

In the past few years electrical light sources have substantially improved. However, most people still prefer sunlight over electrical lighting and they say that they simply feel better under natural light. Moreover, recent research suggests that sunlight may have a positive effect on the health, productivity and happiness of the occupants. Thus illuminating a building with sunlight not only decreases the required energy use but also improves the quality of the lighting.

One of the most conventional methods of daylighting is via windows, but a large glazing area can have negative impacts on the other characteristics of building, as explained in more detail in Section 2.4.1. Buildings with large glazing area usually require higher energy load for heating in winter and cooling in summer due to poor thermal insulation of windows. Glare and visual discomfort as well as poor acoustics and inadequate privacy are other common problems in those types of buildings. To overcome the limitations of a largely glazed façade, other lighting systems, such as skylights and more advanced fenestration systems can be implemented in a building. However, they cannot efficiently deliver light into the core of the building. Thus there is a need for more practical method for bringing sunlight into the building core, and this is the main focus of this research project.

An active solar lighting system is an advanced method of daylighting that can be implemented in buildings to improve the level of daylighting. In general these systems capture sunlight outside the building in an efficient way and deliver it to the core of the building for illumination. Typically such system has an active light collector element, which is installed outside the building either on the rooftop level or on the building façade and it tracks the sun position throughout the day to capture sunlight. The active solar system typically has little effect on the thermal energy usage of the building because it does not require large expanses of glazing. In the next chapter, a few examples of active solar lighting systems are described.

The work presented in this thesis represents a new configuration of an active redirecting system that was designed at the University of British Columbia. This lighting system, which in this thesis is referred to as the “Two-Stage Core Sunlighting System”, has three major components: an active light collector component that is installed at the rooftop at the perimeter edge of the building and tracks the sun position to redirect sunlight toward the building façade from all directions; a light collector that is installed at the façade of the building and that captures and concentrates the redirected light; and a light guide system that distributes the captured sunlight throughout the building.

All these optical elements were designed and optimized to determine the best possible performance and efficiency of the system. The optical performance was analyzed using commercially available raytracing software [3]. Based on this analysis, the system was proven capable of illuminating a multi-storey building with up to six floors. It can be applied to buildings of most common shapes, sizes and orientation. The main target of this solar lighting system is commercial buildings for which the illumination energy loads are highest during the daytime, when sunlight is available.

The next chapter presents a general review of the relevant background information required to best understand the work presented in this thesis. It begins with a brief description of the impact of daylighting on the occupant’s health and happiness and the importance of daylighting from the perspective of global energy usage and the greenhouse gas emission problem. Different types of existing daylighting systems are described and the advantages and limitations of each are discussed.

The general concept of a “Two-Stage Core Sunlighting System” is discussed in the Chapter 3. The key features intended to overcome the limitations of previous daylighting systems are explained in this chapter. This is followed by a discussion of the methodology which was used to optimize the performance and determine the efficiency of the system.

The optical design and optimization process of all three components of the Two-Stage Core Sunlighting System are discussed in detail in Chapters 4 to 6. The overall performance and efficiency of each of the components was evaluated. The system was then modeled as a whole by combining all components together and evaluating the performance for different sun positions.

Chapter 7 discusses the potential for the new daylighting system to be practical and cost-effective. The expected daylighting level in the office area illuminated by the Two-Stage Core Sunlighting System is presented for several typical latitudes to show the potential practicality of the system at different locations. Five cities at different latitudes, with different climate conditions were chosen and the average energy saving at each city was calculated throughout the year for a typical six floor building.

As an extension to the main project, further studies were carried out to investigate a potential improvement in the primary element that is used in the light guide, namely the prismatic microstructured film. Chapter 8 includes a comprehensive study of this film, including the efficiency and sources of loss in the film, and the impact of the loss in the film on the overall performance of the Two-Stage Core Sunlighting System. A few design modifications were proposed to reduce the loss and thus improve the performance of the prismatic microstructural film. The modified film was studied using electromagnetic field modeling software and the performance was compared with that of the original film. One of the suggested modifications showed the potential to reduce the loss in the prismatic film and the result is presented in Chapter 8. The practicality of applying the suggested modifications to the actual prismatic film is discussed, as well as the impact of this improvement on the overall efficiency of the Two-Stage Core Sunlighting System.

Chapter 2: Daylighting in buildings

The importance of daylighting is well known to architects and building designers. In this chapter a literature review is presented to give a better understanding of the impacts of daylighting on the occupants and on the functionality of the building. That is followed by a discussion of the global impact of electrical lighting on the greenhouse gas emission problem and the possible benefits available by substituting electric lighting with daylighting in commercial buildings. It also includes a discussion of previous daylighting techniques that provide daylighting in buildings, as well as their advantages and limitations.

2.1 Impact of daylighting on the occupants

It is important for building designers to consider all the requirements of occupants in order to provide a pleasant environment for them, especially since most people spend much of their time in a workplace environment where they have minimum control on their environmental factors. Thus, it is the job of building designers to consider the preference of occupants and design buildings based on that.

2.1.1 Occupant preference

Most people would like to work in offices with large windows and a nice view and would prefer to sit beside a window in spite of visual glare and thermal discomfort they may experience [4]. Windows have two main functionalities in buildings. First, they provide a visual opening for the occupants which enables them to keep track of the weather and outdoor environment and thus feel connected to the outdoors. Second, they can provide natural sunlight in the building and make the atmosphere of the building more pleasant for the occupants. In one research study, the preference of occupants for daylighting was assessed in terms of psychological factors, pleasantness, general health and etc., was investigated [5]. The results indicate that there is a higher preference for daylighting over electrical lighting. Other research results suggest that the view provided by the window can be as important as the daylighting for the occupant [6]. However, sunlight has benefits beyond the preferences of occupants, as discussed in the next section.

2.1.2 Lighting and health

One problem associated with new energy-efficient electrical light sources is that they do not adequately reproduce the solar spectrum. Life has evolved under sunlight and our body has variety of physiological response to the spectral characteristic of solar radiation. A recent discovery of new circadian photoreceptor in human eye that controls at least one important hormone level suggests that light, apart from the visual effect, has undeniable biological effect on our body as well [7] [8]. This suggests that it is important that the light we are exposed to has a similar spectral characteristic to that of the solar spectrum. Fluorescent lamps, which are widely used in commercial buildings, are designed to be efficient and inexpensive and thus do not have a spectrum like that of sunlight.

Another consequence of an unnatural spectrum is distorted colour appearances. The Colour Rendering Index (CRI) is a quantitative index that assesses the ability of a light source to cause objects to have the same colour appearance as they would under sunlight or incandescent light [9]. Higher CRI means that the colour of objects and people look more realistic and closer to what they look under natural sunlight and a score of 100 is perfect. The CRI of T8 fluorescent lamps, which are widely used for illumination, ranges from 78 to 85 [10]. According to Illumination Engineer Society (IES), the minimum acceptable CRI for a light source for office lighting is 80 [9]. This allows some colour distortion of objects inside the building, which some people may find unpleasant. In general, the light sources with higher colour rendering are more likely to render objects naturally.

2.2 Global impact of electrical lighting

One of the main concerns in building design is the energy performance of the building, not only because it affects the building maintenance cost, but more importantly because of its global impact on the environment. Every year 6.5×10^{12} kg of CO_2 are emitted globally. According to U.S. Environmental Protection Agency, 33% of Greenhouse Gas, GHG, emissions are produced by electric power generation. Residential and commercial buildings use 22% of the generated electricity, thus a noticeable portion of GHG emission is produced in building industry sector [11].

Most buildings have dimensions and interior features that make it challenging to illuminate the whole interior with sunlight. Until recently, there was no serious attempt to address this issue. As a consequence, the electrical load for illumination is quite high in commercial buildings. Making matters worse, they usually require a higher lighting level than residential buildings, and most of that used during the day. According to U.S. Department of Energy, more than 25% of electrical energy usage in commercial building is used for the purpose of illumination, as shown in Figure 1 [12]. Increasing daylighting can also positively affect the cooling and heating load of a building and hence improves the overall energy performance of the building.

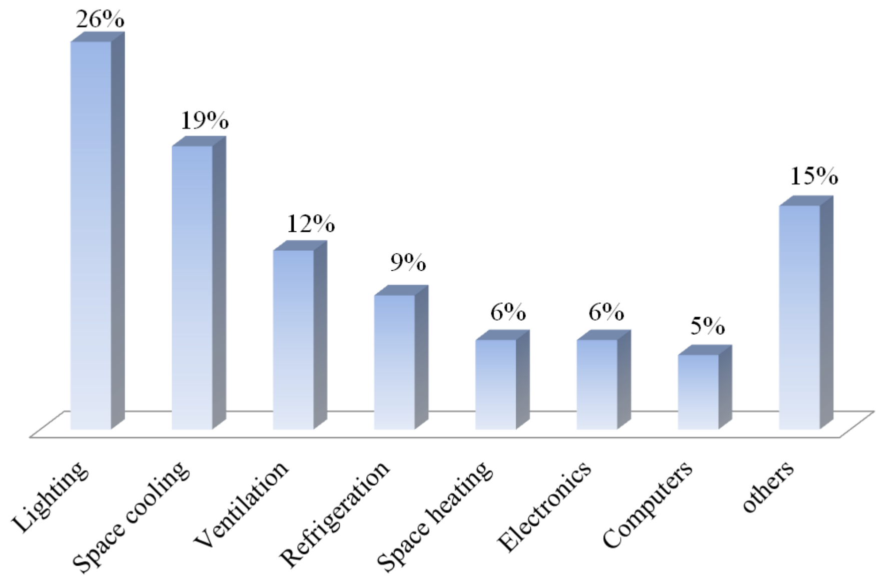

Figure 1. Commercial sector, electrical energy use

2.3 Importance of daylighting for meeting Green Building standard

One of the main challenges for architects today is to successfully meet the needs and requirements of building occupants, while causing minimum environmental degradation. In the recent years, this issue has been addressed by the Green Building Council, which is promoting Green Building design and sustainability in building industry.

A green or sustainable building refers to a construction that is environmentally responsible and resource-efficient throughout its life cycle, from design and construction, to operation and maintenance and eventually renovation and demolition. A major concern with green buildings is their construction cost. Usually upfront cost of design and construction for green buildings is higher than other buildings since more advanced technology and high quality material is used in their construction. However, green buildings have a better energy performance in comparison to the other buildings and their maintenance and other operation costs are often lower throughout the entire life cycle, which ideally will compensate for the upfront cost. Moreover, the energy saving due to efficient design and use of renewable energy on the site, as well as improving the health and happiness of the occupants and productivity of employee, can lead to significant economic saving [13].

The U.S. Green Building Society developed a rating system, Leadership in Energy and Environment Design (LEED), to help building designers assess the performance of the buildings in terms of sustainability. This evaluation tool is now largely used in Canada and the U.S. and similar tool kits have been developed in other countries. This evaluation tools assesses a building under seven major categories and for each a certain number of credits may be assigned [14]. Using the Canadian LEED standard toolkit, buildings that achieve at least 40 credits out of 110 may be considered green buildings. Depending on the number of credits they receive, these buildings are rated as “certified” (40-49), “silver” (50-59), “gold” (60-79) or “platinum” (80 and above).

One of the most important factors in the sustainability of the building is daylighting. It is so important that there are certain legislations to ensure that adequate level of daylighting is provided for the building occupants. In addition to the minimum required level, it is desired to increase the daylighting to improve the energy performance of building, which makes it more sustainable. Daylighting can also improve the performance of the building indirectly in some other aspects as well. Table 1 provides a summary of factors that are important in the sustainability of a building, indicating which of them can be improved by increasing daylighting. In the following sections, both conventional and modern techniques that were used to improve the lighting in the building are discussed in more detail.

Category	Criteria	Earned points	Improved by daylighting
Energy and atmosphere	Fundamental Commissioning of Building Energy Systems	Required	✓
	Minimum Energy Performance	Required	✓
	Fundamental Refrigerant Management	Required	✓
	Optimize Energy Performance	1-19	✓
	On-Site Renewable Energy	1-7	✓
	Enhanced Commissioning	2	✓
	Enhanced Refrigerant Management	2	✓
	Measurement and Verification	3	✓
	Green Power	2	✓
Indoor environmental quality	Minimum Indoor Air Quality Performance	Required	—
	Environmental Tobacco Smoke (ETS) Control	Required	—
	Outdoor Air Delivery Monitoring	1	—
	Increased Ventilation	1	✓
	Construction Indoor Air Quality Management Plan	2	—
	Low-Emitting Materials:	4	✓
	Indoor Chemical and Pollutant Source Control	1	—
	Controllability of System: Lighting	1	✓
	Controllability of System: Thermal Comfort	1	—
	Thermal comfort	2	✓
	Daylight and view	2	✓
Innovation in design	Innovation in design	1-5	✓
	LEED accredited Professional	1	✓
Regional priority	Durable building	1	✓
	Regional Priority credit	1-3	—

Table 1. How daylighting can impact different criteria in the sustainability of a building [14]

2.4 Passive solar illumination

To improve the daylighting in buildings, architects and building designers apply numerous techniques. Some of them are more conventional and have been using for centuries, while some are more advanced. They can be divided into two broad categories, passive and active solar illuminating systems. A passive solar system is a fixed system installed either outside or inside the building to capture sunlight. In this section, different types of passive solar illumination systems, and their advantages and limitations, are discussed.

2.4.1 Windows

Windows have been known as the primary method of daylighting, however, most of the time they cannot provide enough light to illuminate the whole building. The effective penetration depth of daylight is typically 2 to 3 meters inside the building, depending on the orientation of the window and the sun position. Thus, windows can only illuminate the perimeter portions in the building. This may be sufficient for most residential buildings, but when it comes to commercial buildings with larger floor plates, it is not sufficient. Increasing the ceiling height can increase the penetration depth of daylight somewhat, but this enlarges the whole building unnecessarily which increases the energy usage and the upfront construction cost.

To capture more daylight, some buildings are designed with fully or largely glazed facade. Although buildings of this style seem to be very bright and aesthetically pleasant, they actually are not very energy efficient, as described in the following section.

2.4.1.1 Effect of windows on the energy performance of building

One of the important factors in the energy performance of the building is the heat loss and heat gain through the façade. The amount of this heat flow depends on the temperature difference between inside and outside of the building and also the heat transfer coefficient of the façade. The heat transfer coefficient indicates how well heat flows through an element and depends on the thermal conductivity of the material. For example, single paned windows have a relatively large heat transfer coefficient, $\sim 7.4\ \mathrm{W/K\,m^2}$, thus the heat loss through them is high. To reduce the heat loss through the window, double or triple paned windows and/or specialized coatings and gas fillings are sometimes used. Although the heat transfer coefficient of these layered windows is smaller than the single paned windows, $\sim 4\,\mathrm{W/K\,m^2}$, they are not nearly as good as thermally insulated walls with the heat transfer coefficient smaller than $0.5\ \mathrm{W/K\,m^2}$, while they add a lot to the upfront cost of the building.

In addition to the heat loss and gain due to the temperature gradient, the solar radiation gain throughout the windows on the sun-facing façade can affect the energy performance of the building as well. The solar radiation throughout the windows heats the interior, which may reduce heating costs during winter, but which generally causes a greater increase in cooling costs during the summer.

A case study done for a multi-story building in Chicago shows that increasing the glazing area can decrease the required electricity for lighting by as much as 80%, however the energy consumption for heating and cooling was increased by 10% [15]. It was shown that the overall energy performance of the building (lighting, cooling and heating) was only decreased by 12%, while the upfront capital cost of the building increased about 20%. This makes the economic payback period of this building modification unacceptably long (about 90 years in this particular case study). [15].

2.4.1.2 Effect of windows on the thermal comfort of occupants

Thermal discomfort due to the radiation loss caused by the temperature gradient between windows and internal walls on cold days is another limitation of windows. To avoid thermal discomfort, the ambient temperature needs to be higher to reduce the radiation heat loss of the occupants. This increases the energy load of the building and negatively impacts its energy performance.

2.4.1.3 Effect of windows on the visual comfort of occupants

Visual discomfort and glare caused by bright sunlight at the workplace close by the window is another limitation of windows. To avoid sunlight glare at offices, an expensive shading system, either internal or external, is required. Shading systems reduce glare but also block sunlight, which leads to a decrease in the penetration depth of daylight. Moreover, in buildings with a largely glazed façade, the perimeter spaces are usually too bright on sunny days. Thus, to keep the light distribution uniform across the building floor plate, the lighting level at the core of the building must be greater than would otherwise be the case. This may even increase the overall electrical load of the building in some cases.

2.4.1.4 Effect of windows on the acoustic characteristics

Open plan designs are commonly used in commercial buildings with large glazing area to increase the penetration depth of daylight. Such office areas are often designed to be large open spaces with short partition walls to divide the workstations, and the result is that high background-noise levels, excessive reverberation, and inadequate speech privacy often occur. This is due to inadequate sound insulation of internal, external and partition walls.

In fully or largely glazed buildings, external walls of offices are covered with glass, which is a hard material with a low sound absorption coefficient. The sound absorption coefficient is a coefficient that describes the fraction of sound energy that is absorbed at the surface of a material. The sound absorption coefficient value for glass is fairly low, which means that almost all of the sound that strikes the glass surface will rebound toward the office and that causes significant reverberation.

2.4.2 Advanced fenestration system

Windows are not very efficient in providing daylight for the building and excessive glazing negatively impacts the performance of the building. Hence, it is desired to modify conventional windows, such that they capture light more efficiently. Advanced fenestration systems are a combination of conventional windows with some optical structure installed adjacent to the windows to capture sunlight more effectively. In this section, a few examples of advanced fenestration system are discussed.

2.4.2.1 Anidolic daylighting system

The Anidolic Daylighting System refers to a daylighting system that is installed above the window to increase the penetration depth of sunlight inside the room. It has three elements, a collector that is mounted on the external side of the façade, a reflective canal, and distributor at the end of the canal. The collector is designed based on the anidolic or non-imaging optics where the light concentration factor is more important than a clear image [16].The concentrator captures and concentrates solar radiation and sends it to the reflective canal and the distributor distributes the light efficiently in the room, Figure 2.

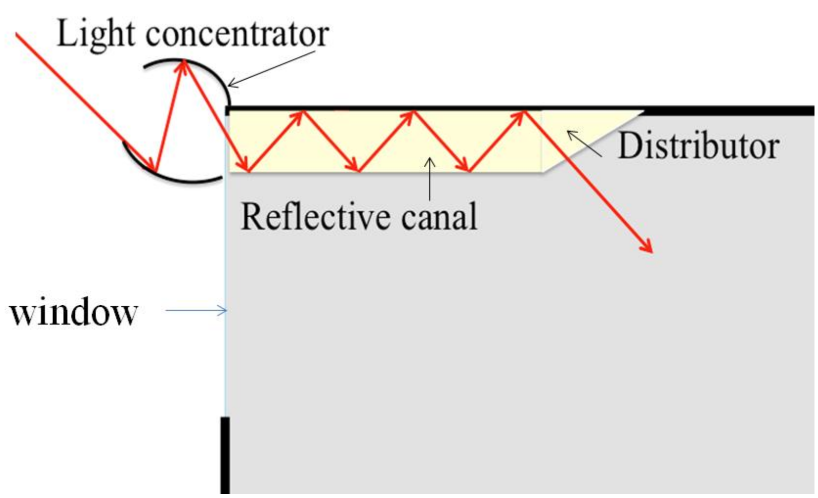

Figure 2. Window equipped with an anidolic daylighting system

The efficiency of the whole system varies according to the opening angle of the concentrator, from 32% for a 90° opening angle to 15% for a 50° opening angle. On a bright sunny day when the illuminance of sunlight may reach up to 120,000 lux, a 1 m wide system can deliver 3,000 lm to 6,000 lm to the room [16] (where the lumen, abbreviated as lm, is the unit of luminous flux of light beam and lux is the unit of illuminance in photometry [17]). According to the Illuminating Engineering Society, a minimum illumination level of 500 lux is required in a typical office area where occupants use a computer station and carry out paper work tasks [18]. Thus, with this daylighting system, it is possible to increase the penetration depth of daylight to 6 m for a room at the sun facing façade [19].

2.4.2.2 Light shelves for daylighting and shading

A light shelf is a horizontal surface mounted on the top part of window, intended to increase the penetration depth of the light into the building as well as reducing the glare effect beside the window. Part of the light shelf is mounted at the exterior part of the facade and the rest is installed inside the room. The light shelf acts like a shade and eliminates the glare effect while also reflecting sunlight into the building off the top surface. The light then strikes the ceiling and is reflected downward, Figure 3. Thus, the reflectance of the ceiling affects the overall efficiency of the system. The diffused light is spread out inside the room and penetration depth of light increases compared to a conventional window. This approach also avoids bright spots in the room [20].

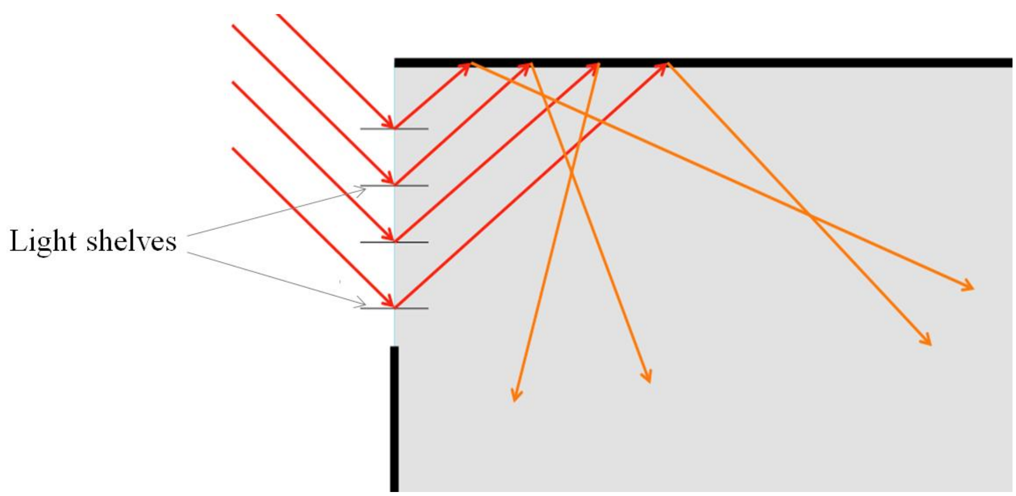

Figure 3. A window equipped with light shelves

In some models, the light shelf contains parallel mirrors that can move simultaneously just like a Venetian blind and the occupants can adjust the inclination angle of the mirrors to optimize the illuminance in the room. However, the result of some post-occupancy surveys showed that the occupants usually fail to adjust the light shelf optimally during the day. Thus the effective efficiency of the system is low [20]. Although light shelves can increase the penetration depth of the sunlight by few meters and avoid glare, they all share the same limitations. For example, they can capture less light compared to the conventional windows [21] and they can only improve the performance of window on the most sun-facing side of the building.

2.4.3 Atria

An atrium is a hollow empty space within the building. This is a conventional method to increase daylighting, especially in buildings with larger floor plates. Atria are often included in building design in order to make the building more aesthetically pleasing. However they increase the property cost and the energy usage of the building, since there is a large empty space in the building which is not effectively used but consumes some resources in construction and use. In addition, the hollow space with inadequate noise insulation acts like a sound guide that may deliver the sound of each floor to another one, and this in some cases could be problematic.

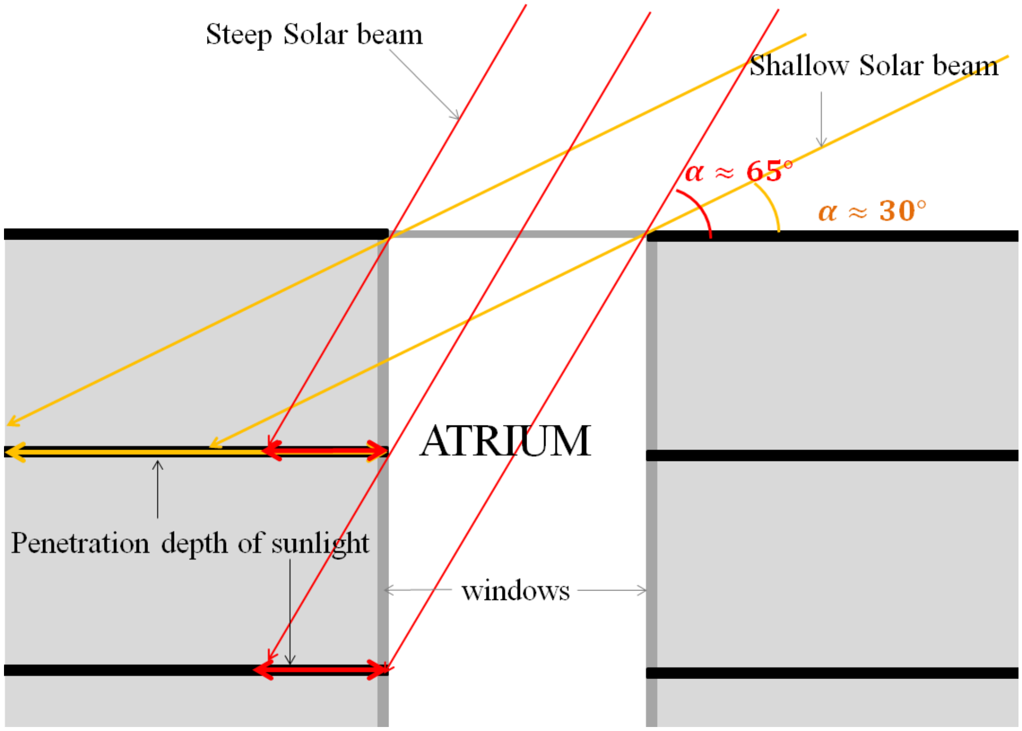

Figure 4. Penetration of sunlight from an atrium into building for different solar altitude

Moreover, atria are not very efficient in delivering daylighting to the core of the building. As illustrated in Figure 4, in an average size atrium (5 m by 5 m or more) only the top two floors can receive sunlight. When incoming light is at shallow angle, the front side of the atrium blocks most of the sunlight. Steep sunlight rays can reach the lower floors, but in that case the penetration depth of the light inside the room is much smaller and therefore atrium cannot effectively illuminate the building core, as illustrated in Figure 4.

2.4.4 Skylights

A skylight is a system which allows sunlight to get into the building from the roof. An example of a skylight in ancient architecture is large dome with an opening on top that lets the sunlight enter the building. Modern architecture uses the same concept to improve daylighting in buildings. The most conventional skylight systems are roof windows, which are either sloped or flat glazing, as shown in Figure 5. The roof windows can only provide daylight for the top floor in the building, and the glare problem they may cause limits their application in the buildings.

A “tubular skylight” or “sunscoop” is a more sophisticated type of skylight that has a wider range of applications in buildings. Tubular skylights often have a dome shaped collector installed at the roof and sometimes they include optical elements to enhance light capture. The collector is often connected to a light pipe that delivers light to a desired location. The light pipe is a hollow clear tube, the interior face of which is lined with highly reflective material. Tubular skylights provide sunlight best on the top floor and are sometimes used to deliver light with less efficiency on lower floors, as illustrated in Figure 5.

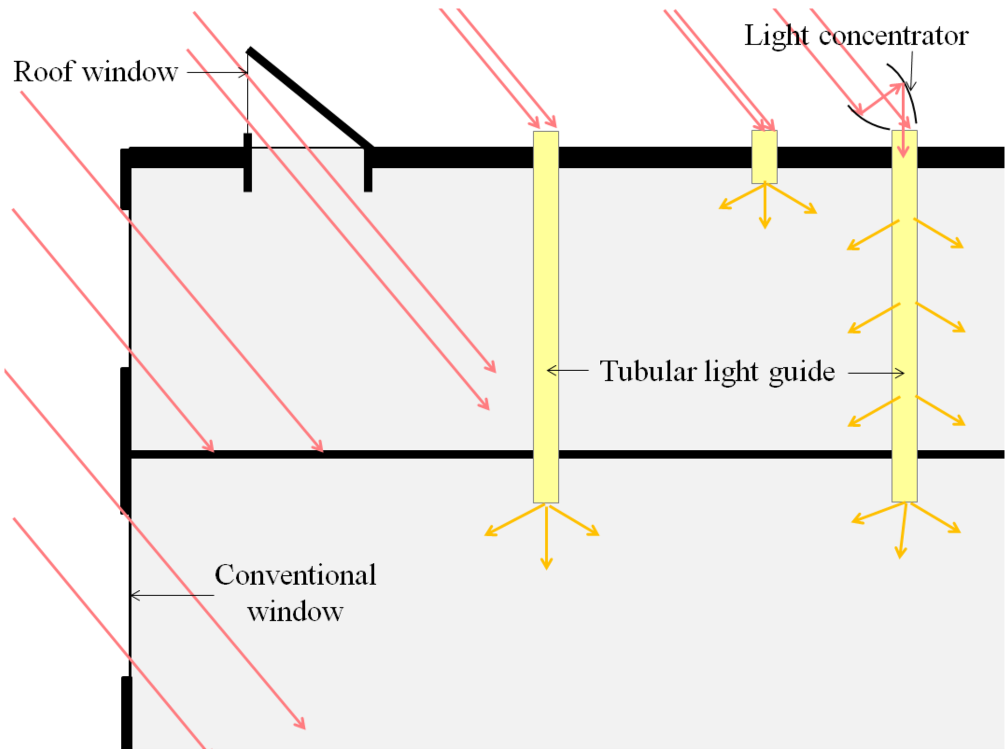

Figure 5. Different types of skylight

Several types of tubular skylights are commercially available, each with a different light collector design. The size of the commercially available products varies between 20 cm and 150 cm in diameter and 6m and 25 m in length, and their efficiency is 50% on average [22]. Thus, a 50 cm wide tubular skylight can capture 14,000 lumens on a bright sunny day, which is theoretically enough for 28 m^2 of floor area [22]. However, since the output light is concentrated in a small tube, it can be challenging to distribute this light uniformly over this area [23]. The bright spot produced by the skylight may cause glare problems as well.

In such systems, the light guides need to pass through every floor to reach the proper location. This greatly affects the design of the building, since they interfere with the design and function of the spaces through which they pass. Some of the available products have more flexible (although also less efficient) light guides that make this process a bit easier, but still it is a challenge to fit the light guide in the building. Furthermore, these adjustments need to be done in the construction process of the building and they cannot easily be applied to existing buildings.

Each of the mentioned passive daylighting systems can improve daylighting level to some extent; however it is impractical to illuminate the core of the building with them. Moreover, the performance of the passive daylighting systems highly depends on the solar position in the sky. Thus, the delivered flux varies significantly with changes of season and throughout day. To reduce this problem, the active daylighting system was designed. In the next section, this is described in more detail.

2.5 Active solar illumination

Active solar illumination systems consist of multiple optical elements that capture direct sunlight outside the building and deliver it to the core of the building. They have three main components: a light collector, a concentrator and a distributor. The light collector is an active system and differs from those in passive daylighting systems – this is the primary difference between them. The active collector, which is installed either at the rooftop or on sun-facing façades, physically adapts to the motion of the sun throughout the day by orienting its optical components such that the maximum amount of light can be captured and delivered at a given time. The active solar illumination system can only capture direct sunlight and therefore on cloudy or overcast days windows are the only source of daylight for the building. In this section few example of active solar illumination system is described in more detail.

2.5.1 ARTHELIO system

ARTHELIO was a European research project having the primary goal of delivering daylight to the dark core of lower floors of a multi-storey building and combining that light with electrically generated light which supplemented the sunlight to the extent necessary. This project was demonstrated in two buildings, the 3M Distribution Center in Italy and Semperlux building in Berlin, Germany. Light was captured at the roof by light collectors and then fed into a vertical light guide. Two different light collectors were used in each of these prototypes.

In the 3M building, the light collector was a combination of a linear Fresnel lens and an anidolic mirror, which is a compound parabolic concentrator, CPC [24]. The collector assembly can only rotate around the vertical axis, which enables the system to track the azimuthal movement of the sun, but not the elevation variation. When light is captured and concentrated by the light collectors, it is redirected downward into a 28 m long light pipe to be delivered to the very lower floor in the building. A dimmable electrical light source, which is installed on top of the light guide, provides electrical light based on the daylight level [25]. This system provided solar illuminance of 100 to 400 lux at the workplace depending on the time of the year [26].

A different light collector was used in the Berlin prototype. The light collector was a large 6.25 m^2 mirror that followed the movement of the sun and reflected light toward a Fresnel lens assembly that concentrated it. The concentrated light was fed into a 13 m long vertical light pipe equipped with a sulphur lamp which provided back-up illumination as required [25].

2.5.2 Hybrid solar lighting system

The Hybrid Solar Lighting system is another daylighting system, developed by Oak Ridge National Laboratory in the USA. The sun-tracker is a 1.22 m diameter parabolic acrylic mirror mounted at the rooftop, which has biaxial movement. A micro controller uses a sun position calculation to reorient the sun-tracker throughout the day to maximize the captured sunlight [27]. The parabolic mirror concentrates the sunlight and with the use of a secondary mirror, redirects it toward a bundle of 3 mm diameter optical fibres that transfer light.

The optical fibre cable acts as a flexible light guide and delivers light to a luminaire. Two types of luminaires are used in this daylighting system. In one design, light leads to an acrylic rod from the optical fibre. The acrylic rods emit light from the side and are located inside a conventional luminaire alongside dimmable fluorescent lamps. When the sunlight level is insufficient, electrical lighting supplements it. In another design, light exits from the fibre bundle at its end and shines on a diffuser panel, which in turn illuminates the room [26] [28]. On a bright sunny day one collector can capture 50,000 lumens of sunlight, which is adequate to illuminate eight luminaires, which can then illuminate a total area of 100 m^2 [27] at a level of 700-1000 lux [26].

2.5.3 Universal fibre optics project

The Universal Fibre Optics (UFO) project, coordinated by University of North London and funded by European commission "Energie Programme", created yet another active solar illumination system [29]. The light collectors were mounted on the roof and light was delivered with liquid-core optical fibres to the desired location in the building. A 1 m diameter Fresnel lens, mounted on a bi-axial movable dish, follows the sun movement throughout the day and concentrates light towards a 10 m long, 20 mm diameter liquid-filled light guide. The light guide transmits light using total internal reflection. By using a liquid interior, it can be less expensive and more flexible than a solid core optical fibre of the same diameter. One disadvantage of the liquid-filled guide is the high absorption of infrared light. This may cause blurring or vesication of the liquid core due to temperature rise in the liquid. To avoid heating the liquid light guide an infrared filter was placed before its input end [29].

Two 150 W metal halide lamps and two backup T5 fluorescent lamps (39 W each) were located beside the light collectors to provide additional electrical light when necessary. The light from sunlight and electrical light was guided to the edge sides of a 20 mm thick sheet of "PRISMEX", an acrylic sheet with a white dot pattern printed on it [26]. Light was trapped inside the acrylic sheet by total internal reflection and escaped from the panel via interaction with the dots. The pattern and size of dot were chosen such that Prismex can create a uniformly emitting surface.

A control system measured the intensity of solar radiation constantly and set the output of the electrical light accordingly to compensate for variations in sunlight. Due to the large number of optical stages, the overall efficiency of the system was low, about 3.4%. Thus, on a sunny day with the illuminance of 90,000 lux, this system could only deliver 3060 lm to the interior space, which is only enough to illuminate 6 m^2 [30].

2.5.4 Commercial fibre optics based solar systems

A few other commercial solar lighting systems were developed that make use of Fresnel lenses and fibre optics. The Himawari system developed in Japan had an active 2-axis sun-tracking system that consisted of 36 to 198 Fresnel lenses, each 95 mm diameter [31]. Every six Fresnel lenses formed a hexagon that concentrated light onto a cable made of 6 quartz glass fibre optics, each with 1 mm diameter. The efficiency of the system depends on the length of the fibre optics. For a 15 m long fibre the efficiency was about 15%. Each light collector fed 6 to 33 terminals and each terminal was enough to provide on average 420 lux of illuminance for 3.8 m^2 at the work plane [32]. A main advantage of the Himawari systems is that it can be applied to existing buildings. The system is self-powered but the capital cost of the system is so high that it is not economically justifiable [26] [33].

The Parans Solar system, developed in Sweden, resembles the Himiwari lighting system in many ways. The light collector can be mounted either on the roof or at the façade and each collector contains 64 Fresnel lenses. The collector uses a bi-axial tracking system that follows the sun to maintain the Fresnel lenses perpendicular to sun. Each lens concentrates light onto a 0.7 mm diameter optical fibre and every 16 fibre forms a bundle that transfers light into the building core up to 20 m depth. The Parans system has various luminaire options. Some of them are coupled with dimmable energy efficient LEDs or fluorescent lamps that supplement electrical lighting automatically when solar lighting is not enough [26] [34]. Assuming solar radiation of 75,000 lux, the output of one unit of light collector, 1 m^2, is 10,000 lm after 4 m long fibre optics and 7,500 lm after 10 m optics fibre. The efficiency of the system is 13.3% and 10% respectively [26].

2.5.5 Solar canopy illumination system (SCIS)

The Solar Canopy Illumination System, previously developed at University of British Columbia in Canada, is another active solar lighting system with a different approach. The light collector includes 70 flat, 16 cm wide, motorized mirrors, called an Adaptive Butterfly Array (ABA). The ABA is controlled by a microprocessor that moves all the mirrors simultaneously to follow the sun's movement throughout the day. Flat mirrors redirect sunlight at a constant angle toward two large parabolic mirrors. The large parabolic mirror concentrates light and redirects it toward a second, recollimating, parabolic mirror, which redirects light toward the light guide, Figure 6. The light collector is housed inside a 3 m by 1.2 m canopy and is mounted above the window at each floor on the most sun facing façade [35] [36].

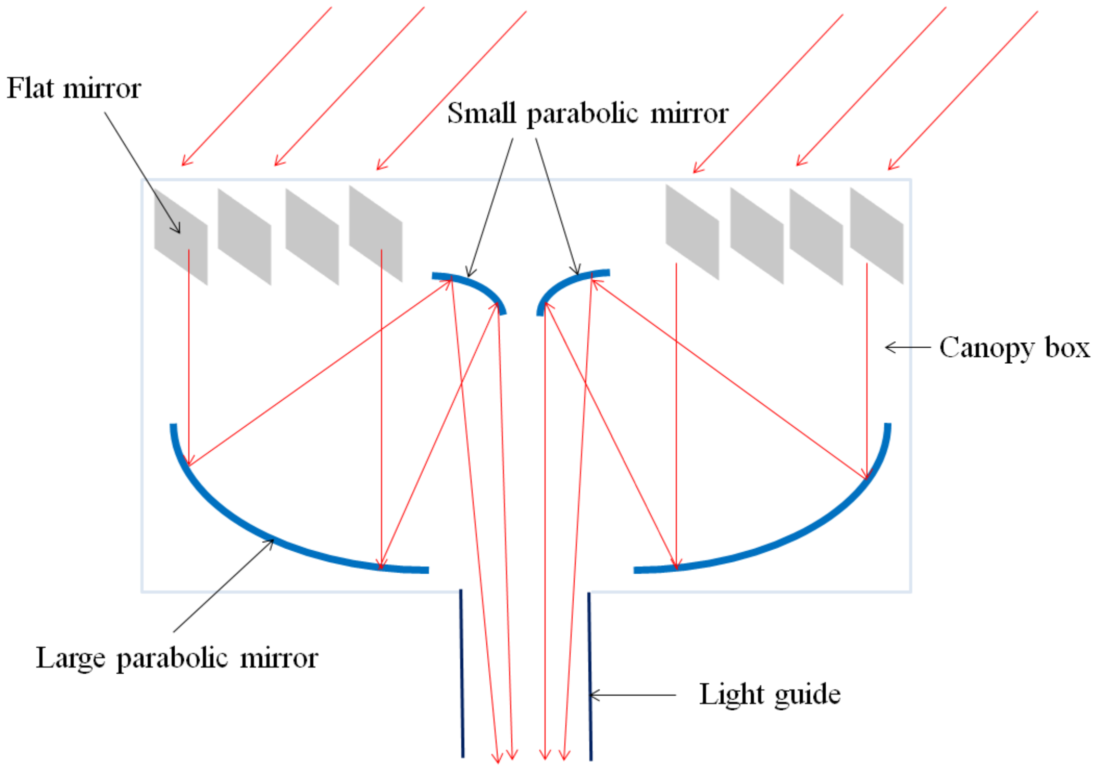

Figure 6. Plan view of the canopy system

Once light is collected by the ABA, it is delivered to the building core and distributed across the building with the light guide. There are different types of light guides that can be used in conjunction with this system. A common type is a hollow rectangular structure, ~ 30 cm by 20 cm, with three of the interior surfaces covered with highly specular reflective material and the bottom surface made out of a microstructured prismatic film. The prismatic film has the dual functionality of either transmitting light or reflecting it back to the light guide depending on the characteristics of the light. Thus it can transfer light across the building while transmitting part of it to illuminate the building area. The light guide is designed such that a uniform amount of light is extracted at all points along the guide. The detailed description of the light guide and the dual functionality of the prismatic film are provided in Section 6.1.

The light guide is installed at the ceiling of the room and light is emitted uniformly from it. It is integrated with dimmable electric lamps that are programmed to supplement the daylight as necessary. Each light guide is fed by one light collector canopy and it can deliver light up to 10 m deep into the core of the building.

Two prototypes of the SCIS were installed, one at the British Columbia Institute of Technology (BCIT) and a second at the Biological Sciences building at University of British Columbia. On a bright sunny day with the solar illuminance of 100,000 lux, the SCIS is reported to deliver an average illuminance of 500 lux over a floor area of 15 m^2.

2.5.6 Limitations of the previous active lighting systems

All of the mentioned designs have some advantages and disadvantages, and they all have several limitations in common. In the system with a light collector mounted at the façade, the operational period of the system is limited to the time when sun is facing that façade. This also means that the system cannot be applicable in a high density area where neighbouring buildings shadow one another's façades. Moreover, since light is collected only from one side of a building, it is only applicable to buildings with a narrow floor plate, in the North-South direction. The collectors also impact the appearance of the building in a manner that many architects would dislike. Another concern is that each floor requires separate motorized equipment, which could represent a maintenance challenge.

In the other approach, wherein the light collector is installed at the rooftop, delivering light to the lower floors is the main challenge. Optical fibres as the delivery tool can be excessively expensive or inefficient and tubular light guides can impact the design of the building and can be quite challenging to implement, especially when applied to existing building structures. Due to the mentioned problem, these systems are at most applicable to 2-3 floor buildings.

The main focus of this research study is to overcome the limitations and disadvantages of the previous daylighting technique and design a new system that would be more practical and efficient during larger portion of day and also has less of a negative impact on the aesthetics of the building. In a new approach to daylighting problem, a new active sunlighting system was designed to overcome some of the major limitations of the former active daylighting systems. The following chapter describes the central idea of the new design.

Chapter 3: The Two-Stage Core Sunlighting System

The Solar Canopy Illumination System (SCIS) mentioned in Section 2.5.5 showed considerable potential to improve the building illumination by providing sunlight to the core of the building. However, it has some significant limitations that can be overcome. The output of the Solar Canopy Illumination system varies highly with the sun movement, which is the main limitation of the system. When the solar altitude increases, the mirrors in the ABA redirector begin to shadow each other, which decreases the efficiency and the amount of light output by the system. Shadowing also negatively impacts the efficiency of the ABA light collectors for solar azimuthal angles close to 90° or 270°. Preliminary raytracing results showed that the light collector works most effectively for solar altitudes ranging from 20° to 60° and azimuthal angles from 120° to 240°. For latitudes less than 40°, the solar altitude angles exceeds 60° for 2 to 4 hours per day at summer solstice, and the azimuthal angle is out of the acceptable range the other portion of the day. This impacts the performance of the system in lower latitude locations, especially during the summer days which tend to have the highest sunshine probability.

The main focus of this research project was to overcome the limitations of the existing SCIS and improve the performance in order to make it more efficient and practical. Some of the main components of the Solar Canopy Illumination System were redesigned and the optical performance of each element was studied using raytracing software. This chapter explains the unique features of the new system.

3.1 Key features of Two-Stage Core Sunlighting System

3.1.1 Rooftop light collectors

The concept of the Two-Stage Core Sunlighting System is similar to the Solar Canopy Illumination System. It captures sunlight with an active light collector installed outside the building and delivers it into the core of the building for illumination. However, in the Two-Stage Core Sunlighting System, light collectors are mounted at the rooftop level instead of on the building façade. Thus light can be collected from all sides of the building instead of only the most sun-facing façade. Capturing light at the rooftop level is not a new approach in itself, but the concentration and delivery process described here is new. Other techniques that capture light at the rooftop level use a vertical pipe or optical fibre bundle to deliver the light to lower floors. As mentioned in Section 2.4.4, this requires some modifications in the building construction and is usually only applicable to 2-3 floor buildings.

In contrast, in the Two-Stage Core Sunlighting System, light is delivered to the lower floors using the unused space immediately adjacent to the building façade. In this design, the light collector was decoupled into two separate components: the active redirector element mounted at rooftop level and the passive concentrator element mounted on the building façade. The active redirector element follows the sun movement throughout the day and redirects sunlight toward the exterior façade of the building (or the walls of an interior atrium) at a predetermined angle. As a result, all four façades can be bathed with approximately equal amounts of sunlight, and the light can be distributed uniformly between multiple floors, as shown in Figure 7.

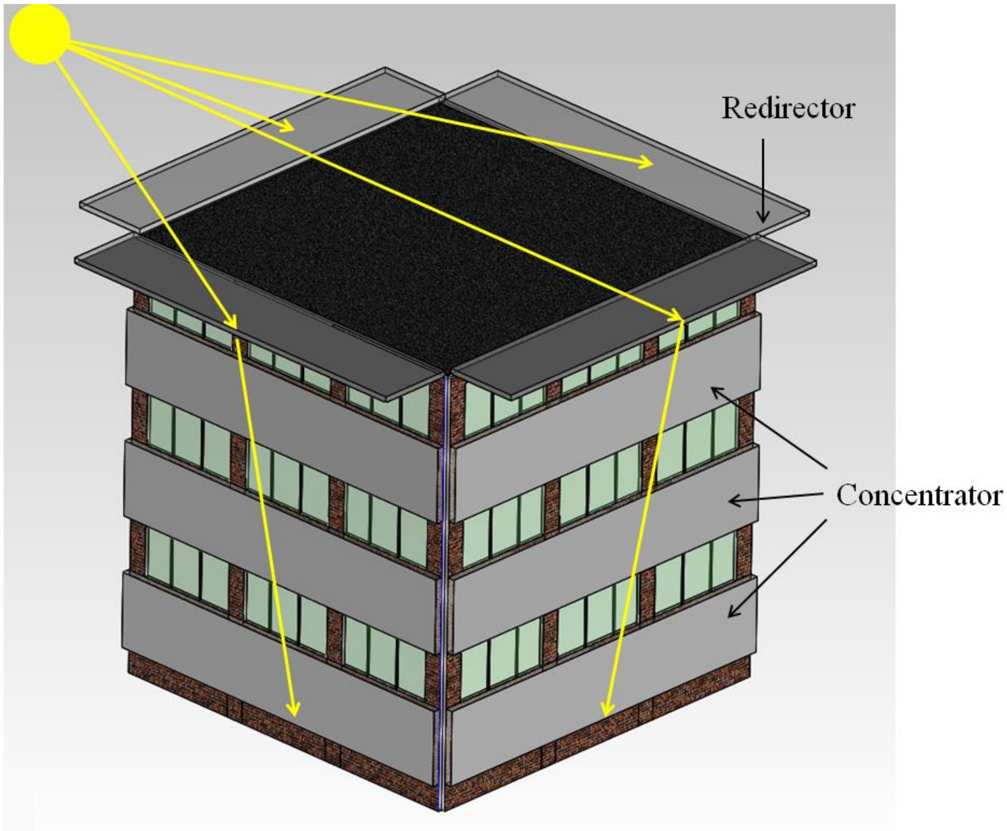

Figure 7. The rooftop light collectors redirect sunlight toward the building façade

(The internal details of the redirector and the concentrator are shown in Figure 12 and Figure 33)

The concentrator component, which is a fixed optical structure, is mounted on the façade of the building at each floor between the windows. The redirected light from the rooftop collectors strikes the concentrator and is captured at each floor. The façade light concentrator focuses sunlight into a much smaller light guide to be distributed across the building floor plate, as depicted in Figure 8. To protect the optical elements against dirt and corrosion, they are housed inside a glass enclosure. The enclosure can possibly be made out of acrylic; however it may require replacement every few years due to UV degradation which increases the maintenance cost, and so this may be a better approach only in applications where a long life cycle is not required.

Since the sunlight is captured from all sides of the building, and all facades are equally bathed with sunshine, it is easier to transport light to all regions of the building because the average guided distance is reduced. This enables a more uniform light distribution across the floor plate, even for larger buildings. Moreover, the building geometry and orientation have less influence on the distribution and uniformity of light, so the Two-Stage Core Sunlighting System can be applied to a wider variety of buildings.

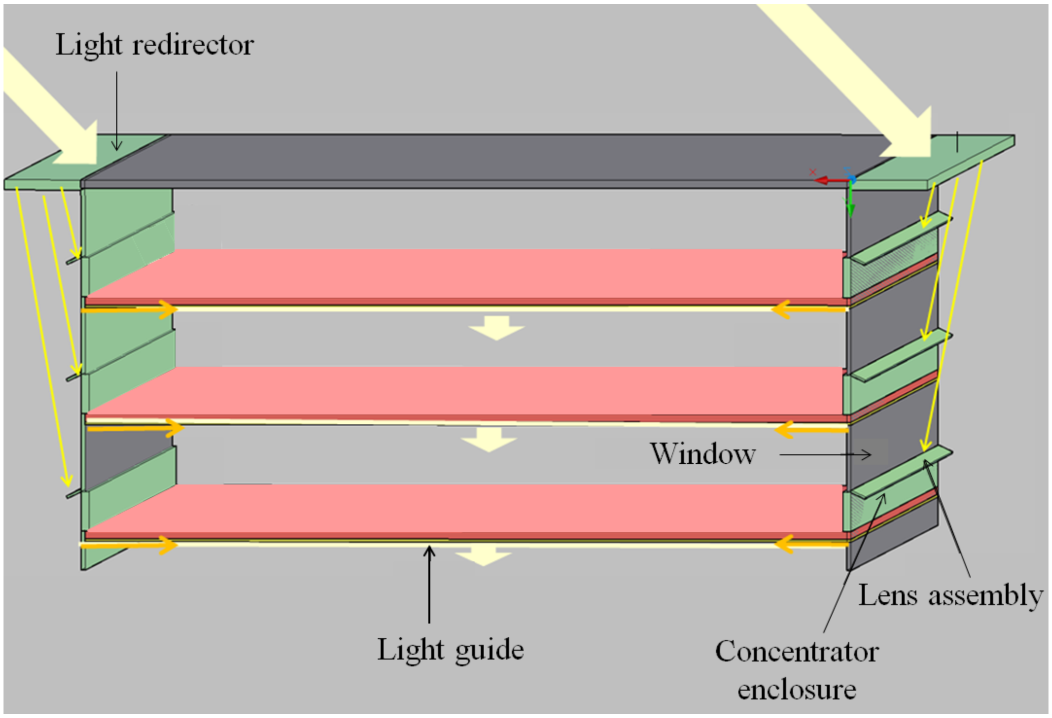

Figure 8. The Two-Stage Core Sunlighting System captures sunlight from both directions and delivers it to the building core

Another advantage of this approach is that all movable components are contained in the rooftop assembly. Thus, the system is expected to be easier to maintain compared to the Solar Canopy approach where each floor required individual tracking systems. Also, capturing light at the roof level allows higher solar exposure compared to the façade, specifically in high density areas.

It is expected that the Two-Stage Core Sunlighting System can provide enough daylighting for a typical six floor commercial building (detailed analysis is shown in Section 7.3). According to the U.S. Energy Information Administration, 75% of commercial buildings are between one and four floors and 15% are between four and nine floors [37]. Thus the new Two-Stage Core Sunlighting System can serve a large fraction of the existing building stock.

3.1.2 Bi-layer rotary light redirector

One of the main improvements of the Two-Stage Core Sunlighting System over the SCIS is the light redirector component. In the Two-Stage Core Sunlighting System, the light collector is installed horizontally at the roof edge of the building, instead of the vertical canopy box. The rectangular mirror array is replaced by parallel rotating slats of mirror (explained further in Section 4.1). The redirector operates in two different modes based on the solar elevation. This enables the system to maintain higher and more consistent efficiency throughout the day. This is specifically important for locations at low latitude where solar elevation is high during a large portion of day. The redirector is designed such that the azimuthal movement of sun will not significantly affect the efficiency of the system. Thus the amount of light that is redirected toward the building is the same for all facades and a relatively uniform light distribution can be achieved across the building floor plate.

3.1.3 The concentrator element

The concentrator element of the light collector is decoupled from the redirector element. It is installed on the façade of the building and has two main components: a lens assembly installed outside the building beneath the window of the floor above and protruding only 40 cm from the façade, and the 1 m tall concentrator enclosure installed either inside or outside of the building, between the windows of adjacent floors, that protrudes only 15 cm from the façade. The impact of this concentrator on the building appearance is minimal, Figure 9.

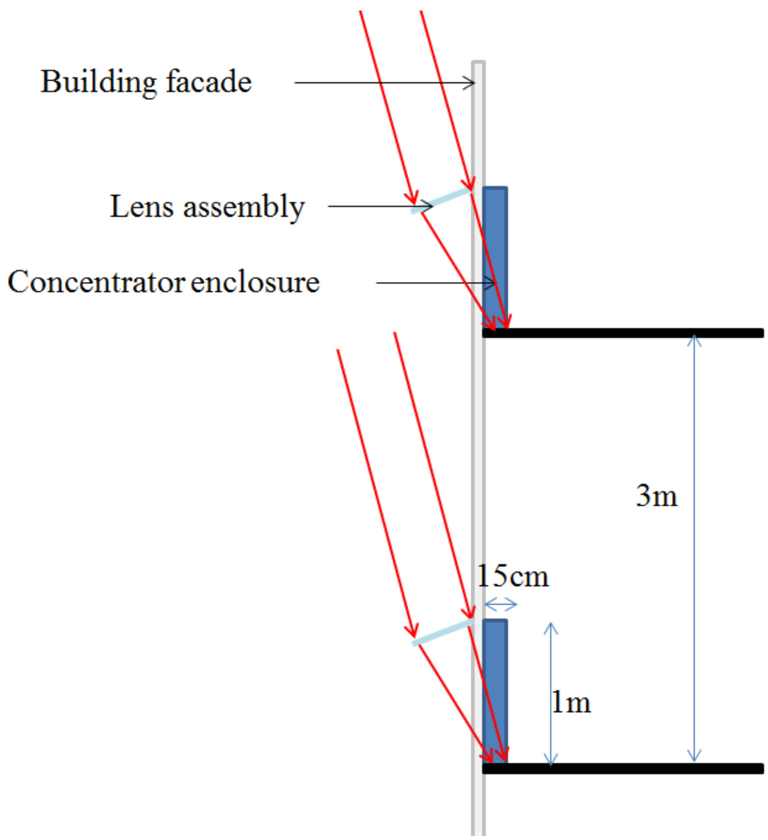

Figure 9. Concentrator installed at the building facade (side view)

The concentrator captures redirected light and concentrates it in order to fit into the smaller light guide, while also maintaining a high level of collimation of the resulting sun beam. This is the key feature of the concentrator, since the collimation of light is essential for subsequently transporting the light with minimal loss. In Section 5.3, the operation of the concentrator is fully described.

3.1.4 Thin light pipe for transferring sunlight 15 m deep into the building core

The excellent collimation of the light output from the concentrator enabled improvement of the light guide as well. In the SCIS, the light guide could provide daylighting at the adequate level along a distance of only 10 m from the windows [35], and to do so it had to be quite large, with a cross-section of approximately 0.2 m by 0.4 m. In the new Two-Stage Core Sunlighting System, it is possible to deliver sunlight more than 15 m into the building core.

Also, since the light fed into the light guide is highly concentrated and collimated, a much smaller light guide can be used in the new Two-Stage Core Sunlighting System, 30 cm by 7 cm (further explanation is provided in Section 6.1). The light guide resembles an ordinary luminaire commonly used in commercial buildings. This minimizes the impact of the light guide on the interior design, and makes the application of the light guide easier in existing buildings more straightforward. The details of each of these components are explained in the subsequent chapters. In the next section the methodology for the design and analysis procedure is described.

3.2 Methodology

The main goal of this research project was to design and analyze the elements of the Two-Stage Core Sunlighting System. To analyse the optical performance of the elements and optimize the efficiency, all elements were studied using computational simulation. To study the interaction of light with an optical system, two different approaches may be used, geometrical optics, where light is formulated in the language of geometry, and physical optics, where the propagation of light is described by the Maxwell equations. Since different simulation approaches use different methodology and have different advantages and disadvantages, it is important to choose the best approach for each case.

The Two-Stage Core Sunlighting System described in this dissertation uses primarily imaging optical elements to deliver light rays to the desired locations. The dimension of the optical elements, such as mirrors and lenses, are considerably larger than the wavelength of visible light and so they can be studied using the laws of geometrical optics. However, in the light guide, where prismatic microstructured film is used, diffraction effects can be important. As described in Chapter 8, diffraction effects in the prismatic film were studied using electromagnetic field modeling based on the Maxwell equations.

The geometric modeling was carried out using raytracing software “TracePro”, developed by Lambda Research Corporation [38]. TracePro uses laws of geometrical optics to study the interaction of a light with different optical structure within a 3-D geometry. Properties of the light sources, such as orientation, wavelength and the divergence can be specified, as well as the properties of surfaces in the 3 dimensional model [38].

TracePro uses numerical techniques to simulate the system, thus the number of rays affects the accuracy of the simulation. To obtain an accurate result, a large number of rays must be used, which requires a large memory capacity and long processing time. Thus, to ensure simulation is done in a reasonable time with an appropriate level of accuracy, the appropriate number of rays must be selected. To ensure that a sufficient and not excessive number of rays was used, simulations were repeated by increasing the number of rays, up to a point where increasing the number of rays did not change the simulation result more than 2% which is negligible, since most people typically cannot perceive variation of light intensity which is less than 10%. In some simulations where the distribution of light was measured, a larger number of rays was required to obtain a smooth variation over the detector. In Section 6.1.5, this is described in more detail.

TracePro uses two different numerical methods to analyze the system: ray splitting, and Monte Carlo method. In the ray splitting technique, as a light ray travels from one medium into another one, it is split into two new rays, a reflected ray and a transmitted ray, and the energy of each of these two rays depends on the reflection and transmission coefficients at the interface. To measure the intensity of light at a given surface, the software calculates the total energy of the combined rays that strike that particular surface.

The major disadvantage of this method is that, in a complicated system, light rays have many interactions, yielding an exponentially large number of rays. As a result the computational time is often excessively long and sometimes even impossible for the software to model. To avoid this problem, a lower energy limit can be set for the rays. If the energy of a ray is less than this threshold value, the software deletes it. The problem is that if the threshold value is set high enough to make the computational time manageable, a significant and unacceptable fraction of the rays may be deleted, which is a common problem with the prismatic structures studied in this project.

An alternative is to use the Monte Carlo technique, in which the interaction of light rays at an interface is treated with certain probability density functions [38]. When a light ray strikes a new boundary condition, it will either transmit through or reflect back and, as a result, the number of rays does not increase. However, the probability of reflection or transmission is calculated based on the geometry and optical properties of the materials. The energy of the light ray is reduced after the interaction depending on the absorption of the surface. This numerical method enables us to track the path that each ray follows all the way from the source to the detector. With this technique, a greater number of rays can be used with lower computational time and capacity; as a result the accuracy of the simulation will be higher. All simulations in this research project were done using this Monte Carlo technique.

The performance of the system was studied using TracePro to optimize different parameters associated with each element. To measure the efficiency of the system for different sun position, a series of automated simulations were carried out using a "macro" tool in TracePro. In each simulation, the light source was moved by few degrees to represent the movement of sun. The following chapters include the detailed description of each component as well as optimization procedures for different variables and the performance result of each component.

The system described here was not constructed in its entirety. However, to assess the accuracy of the modeling, several experimental measurements were made in the laboratory, using well-established principles of photometry, as occasionally described in subsequent chapters.

Chapter 4: The active light collector component: the rotary redirector

The light collector component in the Solar Canopy Illumination System has significant limitations that impact the performance of the system for some solar positions. In order to overcome these limitations, the Adaptive Butterfly Array was replaced with a new light collector component, a so-called rotary redirector. This chapter provides a comprehensive description of the optical design, the optimization procedure and the expected efficiency of the light redirector component.

4.1 The rotary redirector: the general concept

In order to obtain relatively uniform light distribution across the building, the same amount of light need to be captured at all sides of building with less than 10% variation, which is not noticeable by most people. Thus, a rotating assembly was used in the redirector canopy to adapt to the changing azimuthal sun position. This assembly consists of parallel sets of reflective slats contained inside a support ring. These slats can move in a similar fashion to the slats in a Venetian window blind, as depicted in Figure 10. The whole assembly is mounted at the rooftop, oriented horizontally, such that it protrudes from the edge, as illustrated in Figure 9.

The design of the redirector allows for two independent rotations: one rotation about the normal axis of the whole assembly set and the other about the individual slat axes, Figure 10. To follow the solar azimuthal angle movement, the whole assembly rotates about its axis, and thus the light redirector is oriented towards the sun at all times. The efficiency of the system is almost independent of the solar azimuthal angle. Each slat rotates about its individual axis and the rotation angle of the slats is calculated based upon the known solar altitude angle. Two inexpensive actuators control the movement of the redirector. For each sun position, the slats can be rotated in unison about these axes such that incident sunlight will be redirected at a predetermined angle.

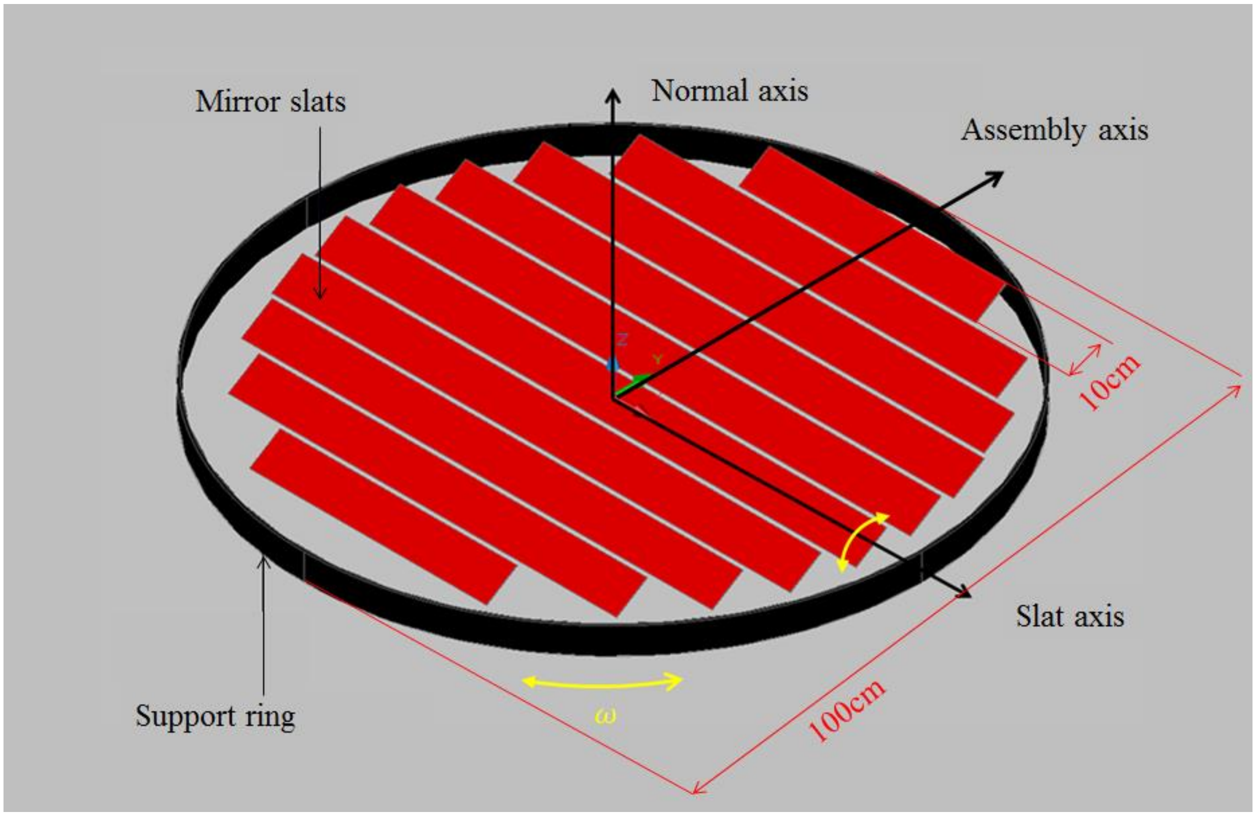

Figure 10. Schematic diagram of rotary redirector

This redirector can effectively capture light for lower solar altitudes, whereby most of the incoming rays strike the reflective slats and are redirected downward, Figure 11 (a). However, at higher solar altitudes, a large portion of the light rays pass through the reflective slats without interacting with them, Figure 11 (b). As a result, the intensity of captured light and the efficiency of the redirector are reduced. This can significantly impair the performance, especially for systems located near to the equator.

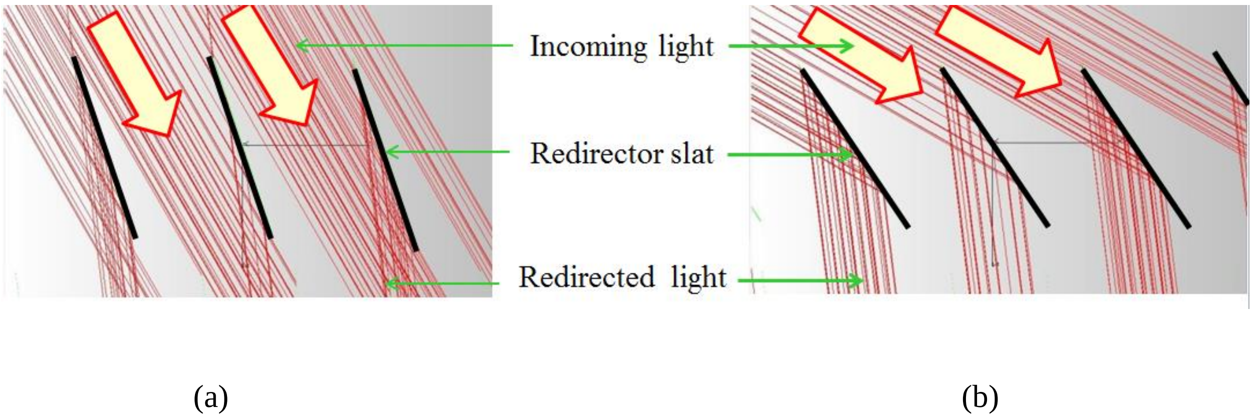

Figure 11. The reflective slats redirect sunlight at a predetermined angle, (a)at high solar altitude , (b) at low solar altitude

To overcome this limitation, the redirector was modified such that it can function in two different modes according to the solar altitude. In the bi-layer redirector, each slat pair consists of two individual mirrors connected together at the slat axis, possibly with a hinge like mechanism. Each mirror can rotate around the slat axis independently and the slat pair can be set in two different modes, single reflection and double reflection mode, as shown in the oblique view in Figure 12 and the cross-section in Figure 14.

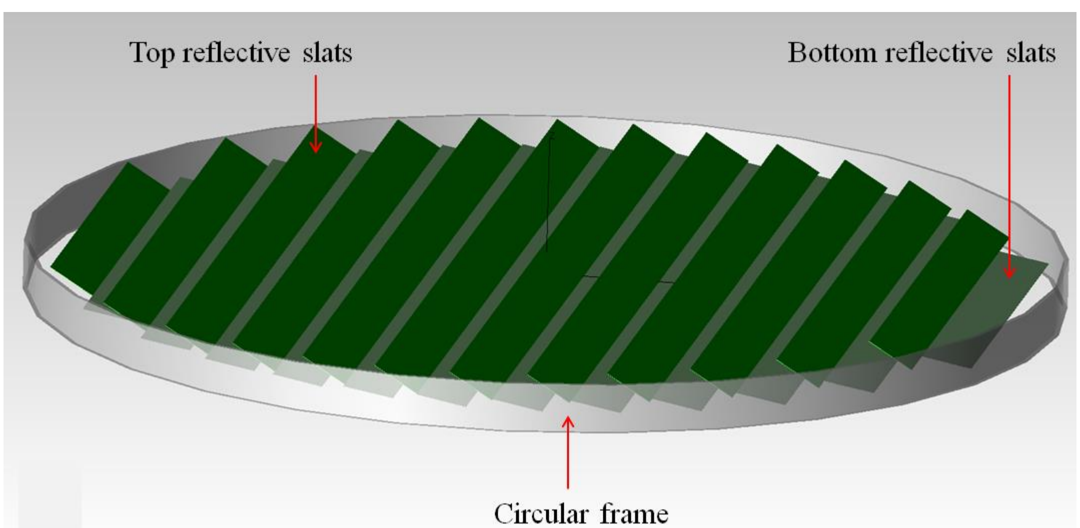

Figure 12. The schematic diagram of the bi-layer rotary redirector

In single reflection mode, used for lower solar altitudes, the two slat mirrors are co-planar, and thus light rays would interact with each slat pair only once, as depicted in Figure 13 (a). At higher solar altitudes, the double reflection mode is used wherein the slats are repositioned to predetermined angles such that most rays interact both with the top reflective slat and the bottom reflective slat, as depicted in Figure 13 (b). The bottom mirror slats must be mirrored on both sides so that it can be used both in single reflection mode and double reflection mode.

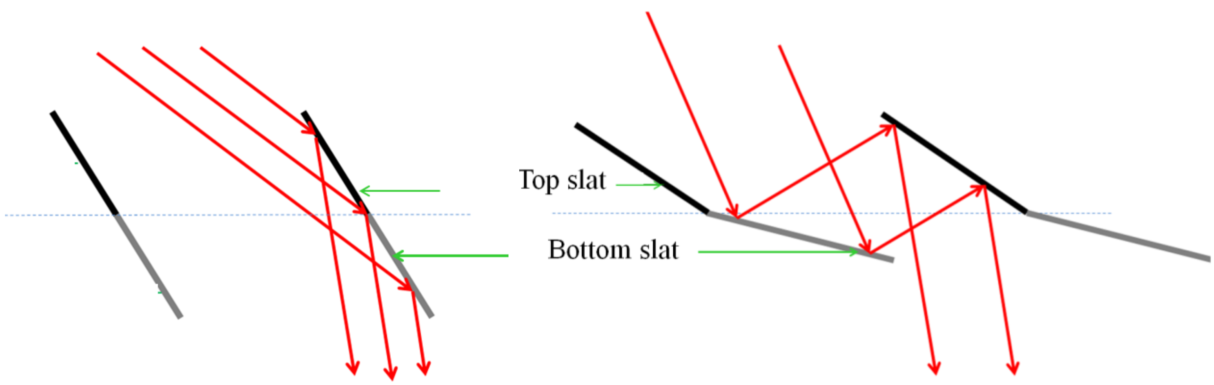

(a) (b)

Figure 13. Bi-layer redirector from side view, (a) Single reflection mode, (b) Double reflection mode

The ability to switch between the two modes as needed enables capturing a more constant level of light throughout the day. However, the bi-layer redirector requires a somewhat more complex control system compared to simple rotary redirector and the additional energy savings provided by the bi-layer redirector depends on the locations. Therefore, a careful cost analysis should be carried out to determine if it is economically advantageous to use bi-layer redirector in a given location.

4.2 Adjusting the redirector slats properly

As illustrated in Figure 14, the light should be redirected toward the building at an angle slightly deviating from the vertical direction. To redirect the sunlight toward the building façade at a predetermined angle, the mirror slats in the rotary redirector must be set properly, based on the sun angle.

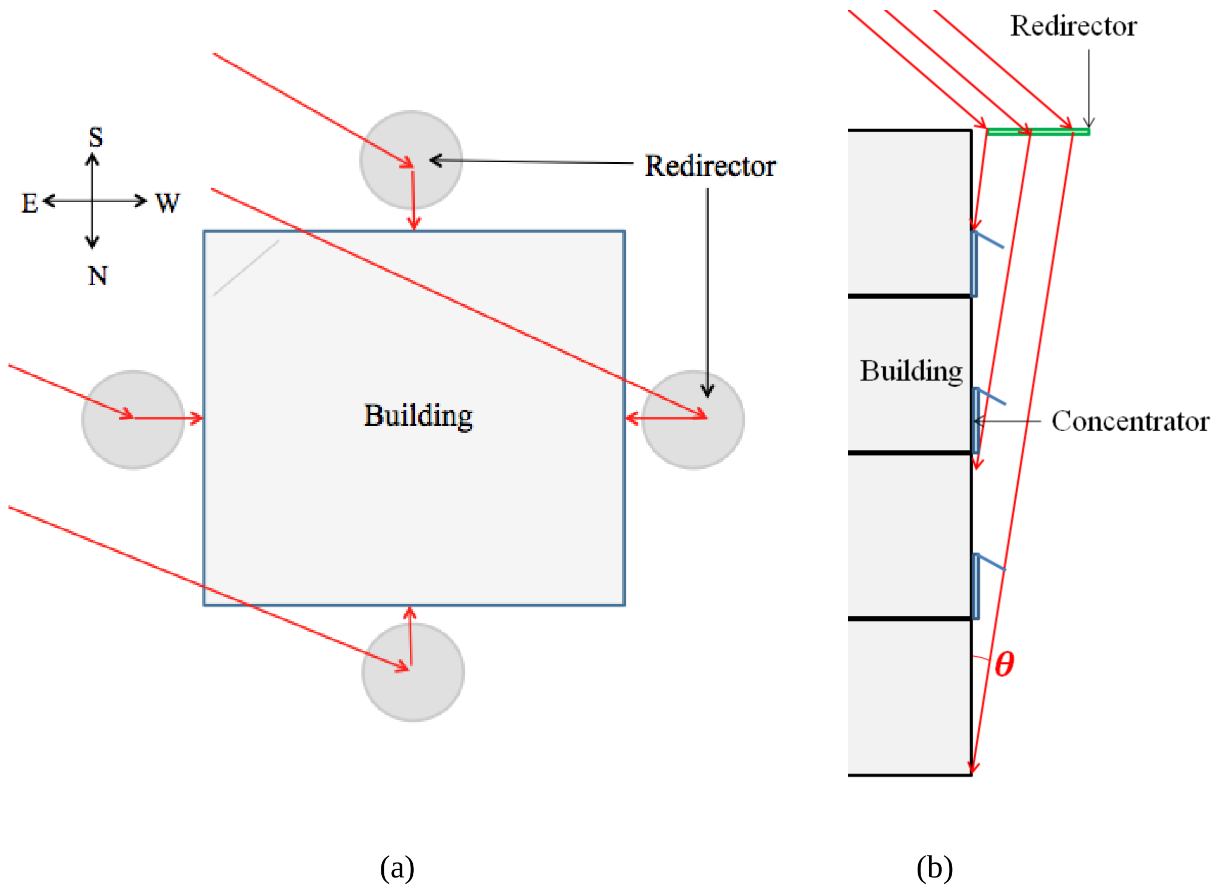

Figure 14. Light redirector reflecting sunlight toward the building at a predetermined angle, (a) Building from top view, (b) Building from side view (Redirectors are out of scale)

From simple geometrical considerations, in order to bathe the whole façade of a 6 floor building with sunlight via a redirector that protrudes 2.5 m away from the building edge, the redirector must reflect sunlight at an angle deviating about 7° from the vertical direction. This angle may vary slightly according to the building height and the width of the redirector unit, but the overall performance of the system would not be substantially affected. The next section describes the basic calculation algorithm for determining the orientation angles of the slats.

4.2.1 Reflection of the light ray off a flat surface

When a light ray strikes an interface, the incoming ray and the reflected ray form a plane that includes the normal vector of the interface surface as well, $\hat{n}$. This plane is called the plane of incidence. The angle between incoming light and the normal vector of the surface is described as incidence angle, θ_i, and the angle of reflected ray with respect to the normal vector of the surface is described as the reflected angle, θ_r, Figure 15. According the law of reflection the angle of incidence equals the angle of reflection [39]. Thus, when the direction of the incident and the reflected rays are both known, as is the case with the light redirector, the normal vector of the reflective surface is fully determined. The normal vector direction can be calculated from the incident light direction, $\hat{\imath}$ and the reflected light direction, $\hat{r}$, as follows:

$$\hat{n} = \frac{\hat{r} - \hat{\imath}}{|\hat{r} - \hat{\imath}|} \qquad (4\text{-}1)$$

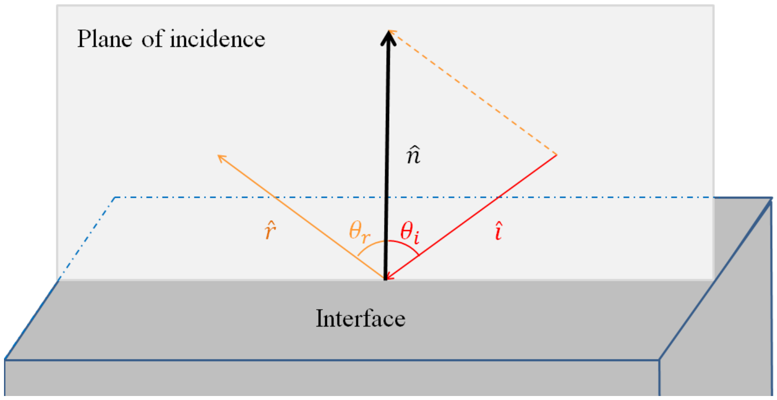

Figure 15. Light ray reflecting off a flat plane

4.2.2 Translating the sun position into the vector coordinate

The directions to the sun and other celestial objects, in the reference frame of the earth, change in the sky throughout the day and year due to rotation of the Earth and its revolution around the sun. The angular coordinates of the direction of celestial objects are often denoted on the "meridian sphere", which is an imaginary hemisphere whose base encompasses the local horizon, with the observer at the origin, as shown in Figure 16. The angle between the object direction and the plane of horizon is the altitude angle, α, and the azimuthal angle, φ, is defined in the standard manner, relative to the direction North.

The solar altitude and azimuth angles can be calculated at any given location and any time of the year using a standard solar direction calculation, explained further in Appendix A. To calculate the orientation of the mirror properly in order to redirect light from any incoming direction, it is appropriate to translate the direction of the sun's rays into Cartesian coordinates as follows:

$$\hat{\imath} = (-\cos\alpha\cos\varphi\,, -\cos\alpha\cos\varphi\,, \sin\alpha) \qquad (4\text{-}2)$$

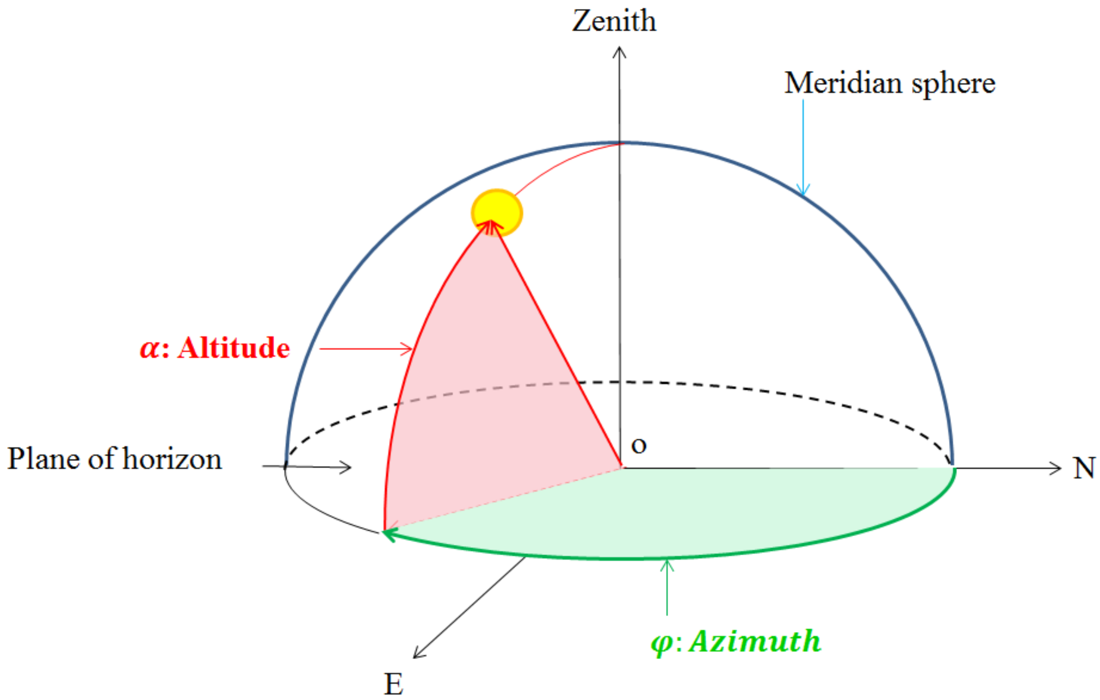

Figure 16. The movement of a celestial object in the meridian sphere

In this case, the Cartesian coordinates are defined such that the x-y plane is the plane of the horizon and the z direction is parallel to the zenith vector in the negative direction, as depicted in Figure 17. The redirected vector is calculated according to the angle θ, where θ is the angle at which light is redirected towards the building façade and is different for each façade, Figure 17:

$$\widehat{r_S} = (\sin\theta, 0, \cos\theta)$$

$$\widehat{r_N} = (-\sin\theta, 0, \cos\theta) \qquad (4\text{-}3)$$

$$\widehat{r_W} = (0, \sin\theta, \cos\theta)$$

$$\widehat{r_E} = (0, -\sin\theta, \cos\theta)$$

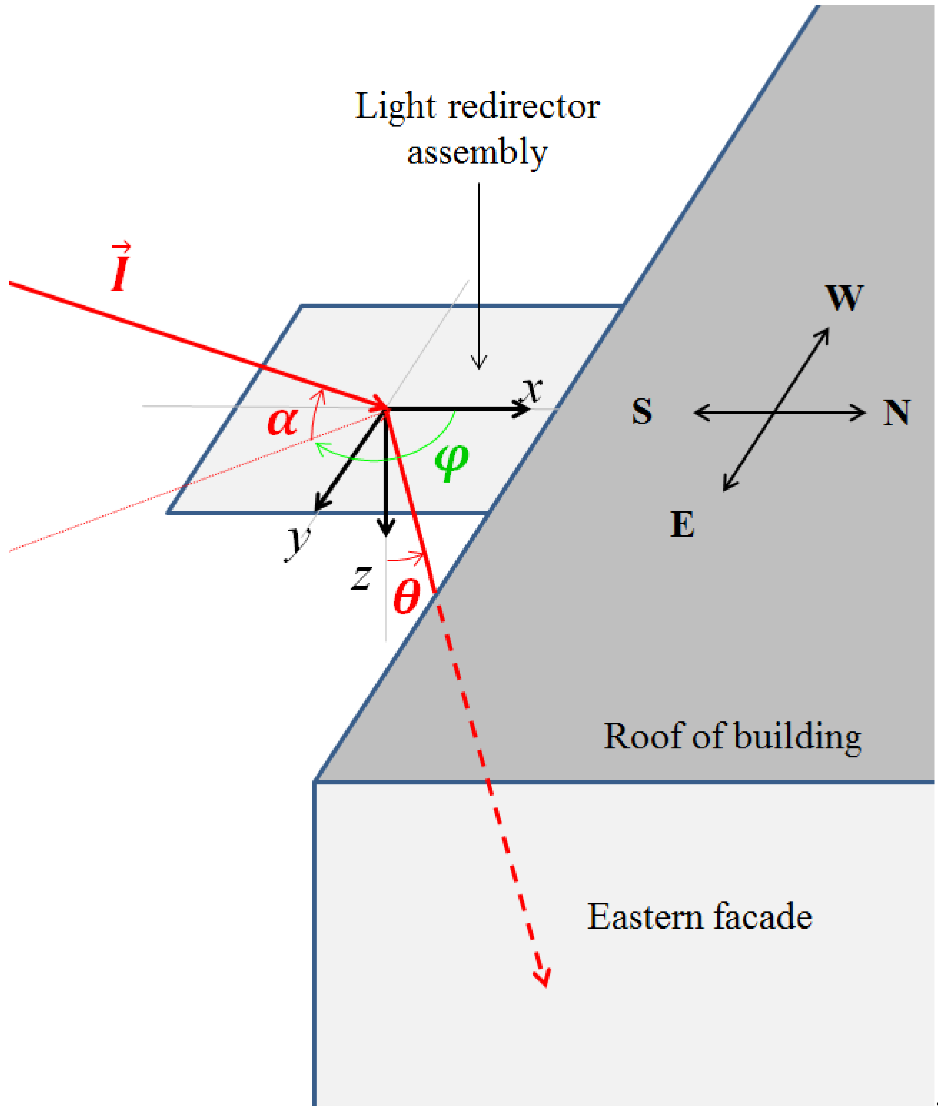

Figure 17. Light redirector assembly reflects the sunlight toward the building façade

4.2.3 Orientation of reflective slats in the single reflection mode

As described in Section 4.1, when the slats are orientated in the single reflection mode, the light strikes the reflective surface once and is reflected toward the building. Thus the interaction of light is simply described using Equation 4-1. Once the direction of the incident ray and the reflected ray are described in 3D Cartesian coordinates, the normal vector of the mirrors in the redirector can be calculated via Equation 4-1.

To redirect light at the desired angle, a control system orients the reflective slat along the calculated normal vector via a computer-controlled actuation system. With this design, the axis of the slat in the redirector assembly must remain in the x-y plane in Figure 17. Figure 18 illustrates how the reflective slats in the redirector unit are moved in two steps to change the normal vector of the surface from the initial $\widehat{n_0}$ to $\hat{n}$, in a way that the slat axis remains in the x-y plane. The slat is first rotated $\delta°$ around the y axis that moves it from stage 1 to stage 2. It is then rotated $\gamma°$ around the z axis, which moves the slat from stage 2 to stage 3, Figure 18. This rotation can be described using the Euler angle and rotation matrix [40]. If angle $\gamma, \delta,$ and μ represent the rotation angle around z, y, and x respectively, the rotation matrix is:

$$R = R_z(\gamma) R_y(\delta) R_x(\mu) \tag{4-4}$$

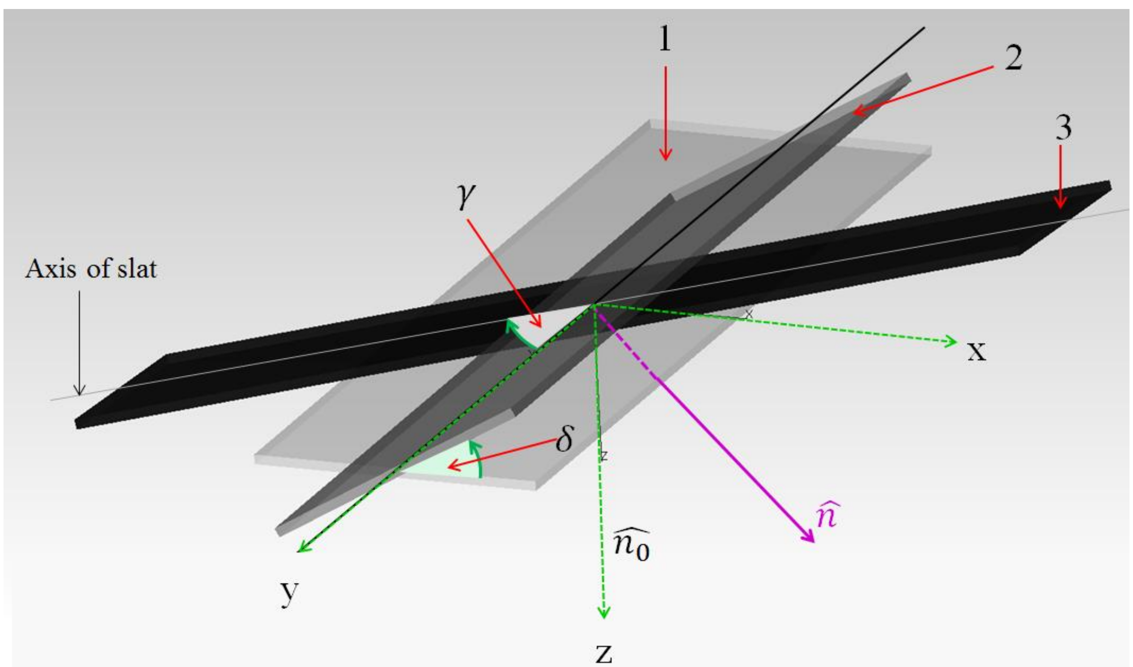

Figure 18. Orienting the reflective slats to the proper direction in two steps

where R_i represent the rotation matrix around the i-axis [40]. Assuming the normal vector of the slat is initially along the z axis, the new normal vector of the slat is calculated as:

$$\hat{n} = R \times \widehat{n_0} = R_z(\gamma)R_y(\delta)R_x(\mu) \times \begin{pmatrix} 0 \\ 0 \\ 1 \end{pmatrix} = \begin{pmatrix} \sin\mu \sin\gamma + \cos\mu \sin\delta \cos\gamma \\ -\sin\mu \sin\gamma + \cos\mu \sin\delta \sin\gamma \\ \cos\delta \cos\mu \end{pmatrix} \tag{4-5}$$

To keep the redirector assembly confined within the x-y plane, the rotation around x axis, μ, is zero, thus the rotation matrix can be rewritten in the following form:

$$\hat{n} = \begin{pmatrix} \sin\delta \cos\gamma \\ \sin\delta \sin\gamma \\ \cos\delta \end{pmatrix} = \begin{pmatrix} n_x \\ n_y \\ n_z \end{pmatrix} \tag{4-6}$$

The $\hat{n}$ vector can be calculated using Equation (4-1). Thus the angles δ and ω are calculated as:

$$\gamma = \tan^{-1}(\frac{n_y}{n_x}) \tag{4-7}$$

$$\delta = \tan^{-1}(\frac{n_x}{n_z \cos\gamma}) \tag{4-8}$$

4.2.4 Orientation of reflective slats in the double reflection mode

The reflection calculation is a bit more complicated for the double reflection mode, where both the top slats and bottom slats revolve around the slat axis independently. Three different variables, including the rotation angles of the top mirror and the bottom mirror around the slat axis and the rotation angle of the slat pair around the normal axis must be changed to redirect the incident sunlight to the proper angle. Using the following equations, each of these angles were calculated. Like the calculation in the single reflection mode, it is assumed that the axis of slat was initially along the y direction and the normal axis is along the z axis.

In the double reflection mode the incident ray, $\vec{I}$, strikes the bottom slat first. If the normal vector of the bottom slat was initially $\widehat{n_0} = (0, 0, -1)$, revolving $\beta°$ around the y axis and $\gamma°$ around the z axis moves the normal vector to new position $\hat{n}$, Figure 19:

$$\hat{n} = R_z(\gamma) R_y(\beta)\, \widehat{n_0} = \begin{pmatrix} -\sin\beta\cos\gamma \\ -\sin\beta\sin\gamma \\ -\cos\beta \end{pmatrix} \tag{4-9}$$

Using Equation (4-1), the reflected vector $\vec{R}$ can be calculated. The reflected ray then strikes the bottom slat, thus the normalized incident ray would be:

$$\widehat{I'} = \frac{\vec{R}}{|\vec{R}|} \tag{4-10}$$

Revolving the reflective slats $\delta°$ around the y axis and $\gamma°$ around the z axis moves the normal vector initially $\widehat{n'}_0 = (0, 0, 1)$ to new position $\widehat{n'}$:

$$\widehat{n'} = \begin{pmatrix} \sin\delta\cos\gamma \\ \sin\delta\sin\gamma \\ \cos\delta \end{pmatrix} \tag{4-11}$$

The final reflected beam is calculated using Equation (4-1) as follow:

$$\overrightarrow{R'} = \widehat{I'} + \widehat{n'} \tag{4-12}$$

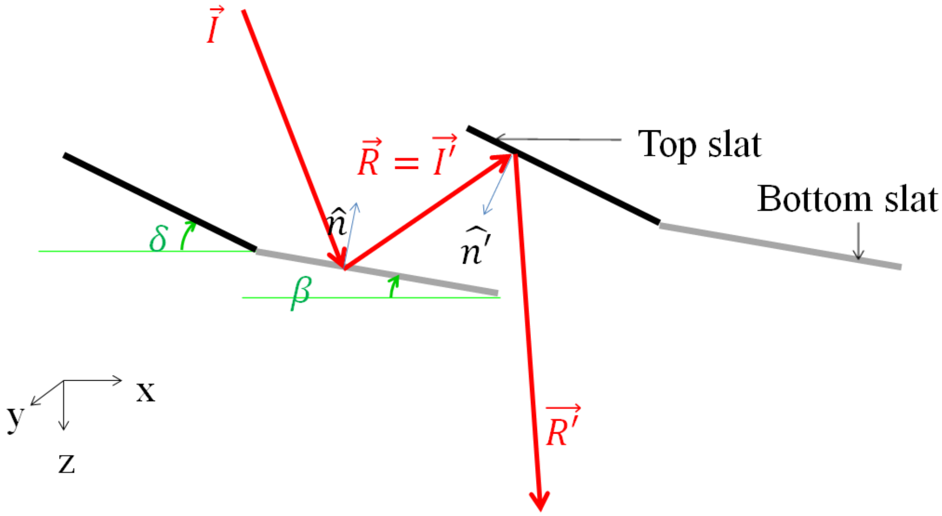

(a)

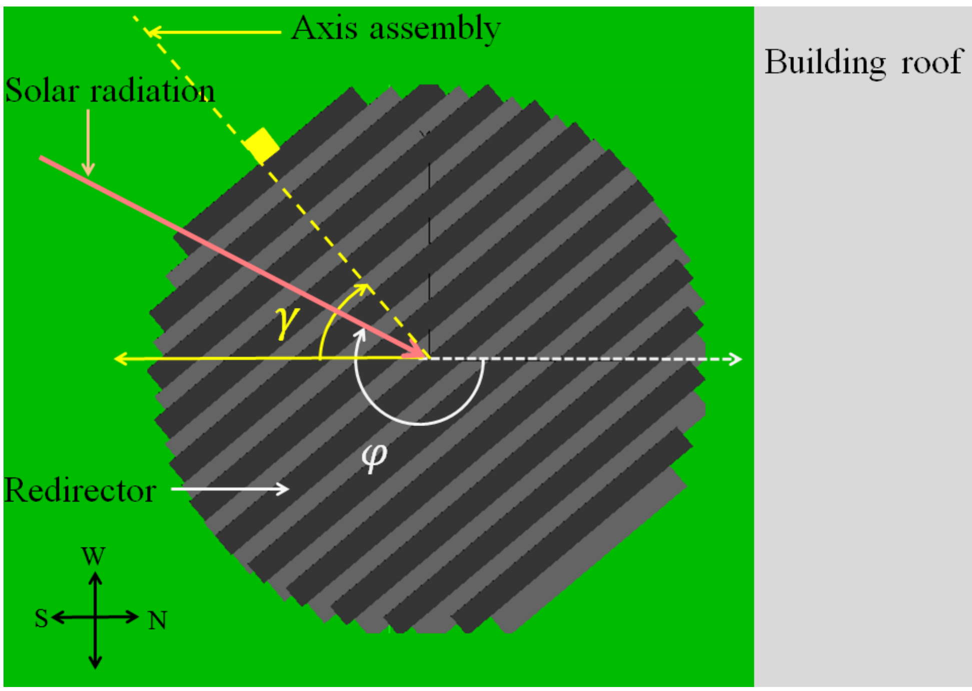

(b)

Figure 19. Light redirector at double reflection mode,

(a) two slats of the redirector from side view, (b) the whole redirector from top view

To redirect light toward the building at the desired angle, the reflected vector, $\overrightarrow{R'}$ is calculated via Equations (4-3) for each façade. For the south façade:

$$\varepsilon = \tan^{-1}\left(\frac{R'_x}{R'_z}\right) \equiv \theta \tag{4-13}$$

$$\sigma = \tan^{-1}\left(\frac{R'_y}{R'_z}\right) \equiv 0 \tag{4-14}$$

These equations do not have an analytical solution, so they were solved numerically using the optimizer tool in the Matlab, which minimizes the delta function, where delta function is defined as the variation of the reflected ray from the desired direction:

$$\Delta = (\varepsilon - \theta)^2 - (\sigma - 0)^2 \tag{4-15}$$

The optimization is done by changing the three variables, γ, β and δ , until find the optimum value for the delta function is achieved. Interestingly, Equations (4-13) and (4-14) do not have a single unique solution. For any given β angle, there is always a γ and δ that minimizes the delta function and so reflects light in the desired direction. However the efficiency of the system is different for different values of β angle. Thus, to maximize the overall efficiency of the system, the best value of β needed to be determined. In Section 4.3.1, the procedure for determining the best value of the β angle for different solar altitude is described. Once the optimized value of β was calculated for each solar altitude, $\beta_{opt}(\alpha)$, the other two variables were optimized using the optimizer tool in Matlab. The Matlab code which was used to find the optimized value of γ, δ is provided in Appendix B.

4.3 Rotary redirector optimization

All parameters in the light redirector component needed to be optimized to maximize the output of the redirectors both for the single reflection mode and the double reflection mode. Most of the parameters have some interdependence and so the optimum value of each parameter depends on the value of other parameters. All parameters were optimized one at a time while keeping the other parameters constant at some approximated value. In this section, the procedure for optimizing each parameter is explained in detail.

4.3.1 Optimizing the orientation of slats in the double reflection mode

As mentioned earlier the variable angles in the double reflection mode cannot be solved analytically in general, but for the special case that solar azimuth angle at 180°, the problem is simplified and can be solved using simple reflection theory. The derived value of the optimum β was used to optimize the delta function described in Equation (4-14) for other azimuthal angles. When the solar azimuth angle is 180°, the reflected rays $\hat{r}$ and $\widehat{r'}$ are co-planar with the incident ray $\hat{\imath}$. Thus, the reflected angles, φ and θ, can be calculated as function of slat angles δ and β[1]:

$$\varphi = \alpha - 2\beta \tag{4-16}$$

$$\theta = 90 - \varphi - 2\delta \tag{4-17}$$

[1] For simplicity in calculation, the sign of the angles was not considered here.

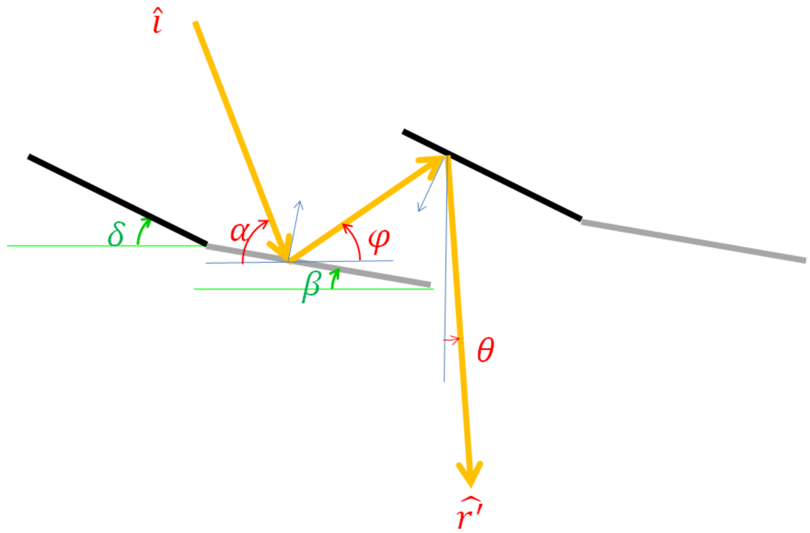

Figure 20. Light redirector at double reflective mode

The two equations can be combined and reformulated as:

$$\delta = \frac{90 - \theta - (\alpha - 2\beta)}{2} \tag{4-18}$$

This equation does not have a unique solution for a known θ *and* α value, thus one of these angles needs to be fixed and the other angle can be calculated based on that. The optimum value of the angle β needs to be found in order to maximize the performance of the system.

Reducing the beta angle increases the effective area of the collector at high solar altitudes; however, this may require the slat sets to be closer together. If the spacing between slats is too small, the bottom slats blocks some of the reflected rays, and these rays would be lost, as illustrated in Figure 21 (a). On the other hand, larger beta angles require larger spacing, which would cause some rays to be lost because they pass between the slats without interacting with them, as illustrated in Figure 21 (b). Thus, the optimum value of beta depends on the width ratio of the slats, W, which is the ratio of the distance between slats divided the by slat width, $^{d}/_{w}$. In order to maximize the efficiency of the redirector, both of these two variables needed to be optimized.

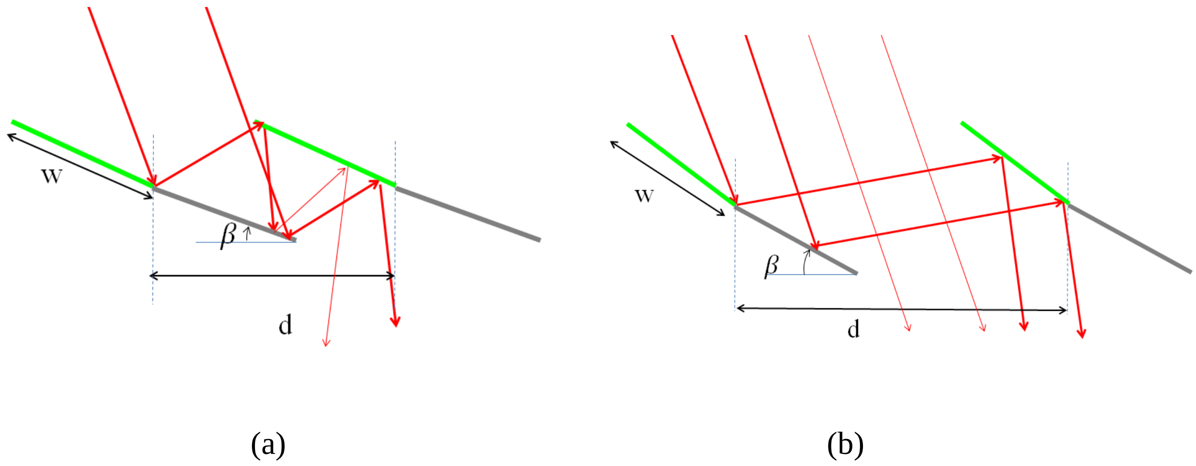

Figure 21. Light redirector at double reflection mode,

(a) Small spacing between slats, (b) Large spacing between slats

To address this problem, we find the optimum value of β and W for an average solar altitude for which the double reflection mode is expected to perform, 70°. The performance of the system was analysed by modeling two slat pairs in TracePro for different beta angles and different slat spacing. The efficiency was defined as the ratio of redirected rays divided by the number of incident rays. For each beta value, the optimum spacing ratio, *W*, was found by changing the distance between slats and measuring efficiency. The summary of these simulations is provided in Table 2. For the solar altitude $\alpha = 70°$, $\beta = 22°$ and W= $d/w = 1.7$ gave the best overall efficiency for the redirector.

Beta	$\boldsymbol{W_{opt.} = (\frac{d}{w})_{opt.}}$	Efficiency
15	1.50	0.166
18	1.60	0.312
20	1.60	0.350
21	1.56	0.400
22	1.68	**0.464**
23	1.88	0.415
24	1.96	0.387
24	2.00	0.360
25	2.00	0.352

Table 2. The efficiency of the light redirector at the double reflection mode versus different beta angle and spacing ratio for solar altitude of $\boldsymbol{\alpha = 70°}$

Since the slat spacing is a fixed value for the redirector, the same W has to be used for other solar altitude angles as well. To calculate the optimum value of beta, β_{opt}, as a function of solar altitude, a series of automated simulations was carried out in Tracepro using a macro tool that adjusted the elevation of the source and the orientation of slats appropriately to redirect light to the proper angle. The optimization was done for solar altitudes ranging from 30° to 90° with 3° increments. This range represents the typical operation window of the double reflection mode. To improve the performance of the redirector further, the value of W was optimized considering the performance of system both in single reflection and double reflection mode, for all solar altitude angles. The next section describes this in more detail.

4.3.2 Optimizing the slat spacing

The slat spacing impacts the efficiency of the redirector. To study the impact of the spacing on the efficiency, a number of slat pairs with equal length were modeled in TracePro and the amount of redirected light was measured as a function of solar altitude for different spacing values. The performance of the system was studied for both single reflection mode and double reflection mode to find the optimum value of W.

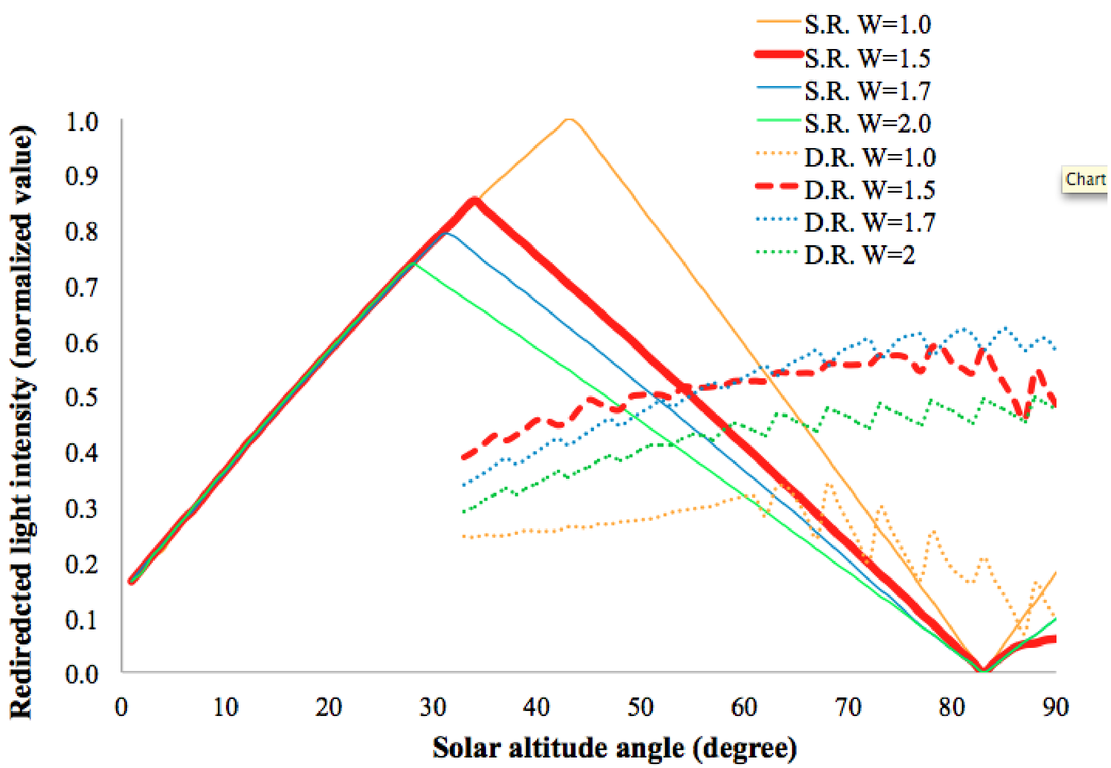

Figure 22. The intensity of redirected light versus solar azimuth angle for different slat spacing (S.R. stands for single reflection mode, D.R. stands for double reflection mode)

Figure 22 shows the result of this calculation for three values of *W*. As illustrated in Figure 22, the amount of redirected light decreases as *W* increases for the single reflection mode. However, there is an optimum value of *W* for the double reflection mode. To optimize the performance of the system over the whole solar altitude range and for both modes, W=1.5 was chosen.

4.3.3 Optimizing the number of slats

The number of slat pairs is another criterion that impacts the efficiency of the system. For a given slat spacing to width ratio, to first order, increasing the number of slats does not change the overall area of the redirector mirrors. However increasing the number of slats adds cost and complexity to the redirector assembly. Conversely, if the number is too small, the circular frame is not efficiently filled. Thus, an optimal number of slats needs to be determined.

The performance of the redirector was studied through the whole range of the solar altitude for different numbers of slats. The intensity of redirected light was measured for the single and double reflection modes and the average value was calculated. Figure 23 shows the average intensity, where values were normalized to one for simplicity. As shown in Figure 23, the performance of the redirector improved as the number of slats increases, however after a point increasing the number of slats doesn't make a noticeable improvement to the performance, whereas adding more slats adds complexity to the manufacturing process and would probably increase the cost. It was decided that 12 slat pairs in a 1 m diameter redirector unit, with each slat 50 mm wide, is reasonable and practical.

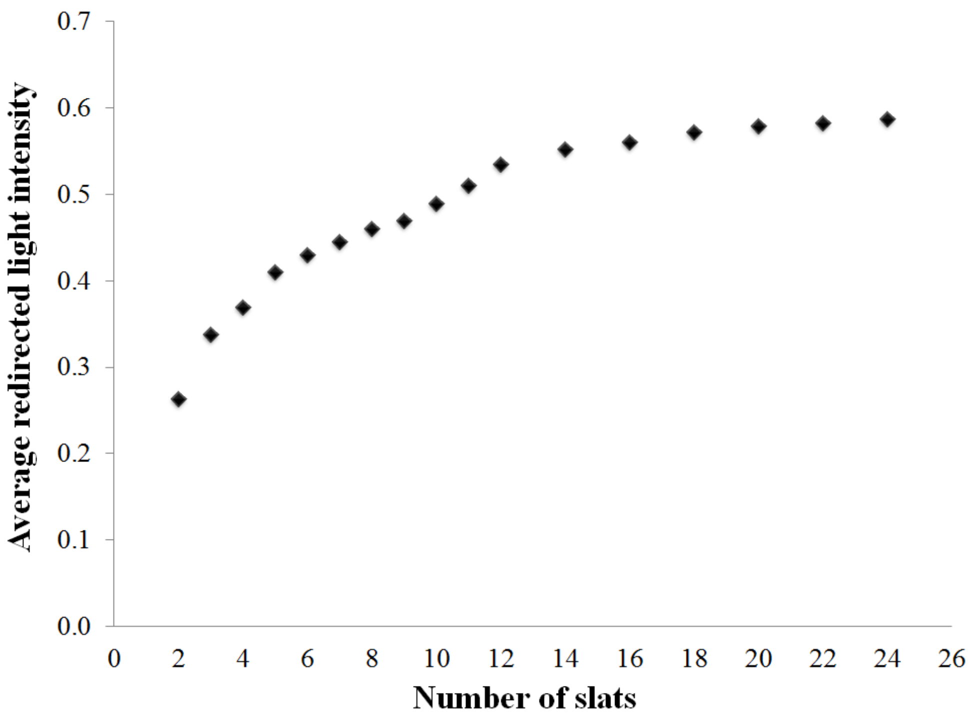

Figure 23. Normalized averaged redirected light intensity versus number of slats

4.3.4 Optimizing the configuration of the slats

The configuration of the slats in the circular frame is another factor that impacts the efficiency of the redirector. The slats are located equally spaced in the frame; however the distance between slats, *d*, can slightly change for a given number of slats and width ratio, *W*. As the distance between slats decreases, the length of the slats increases, illustrated in Figure 24. Thus the effective reflective area occupied by the slats increases as well.

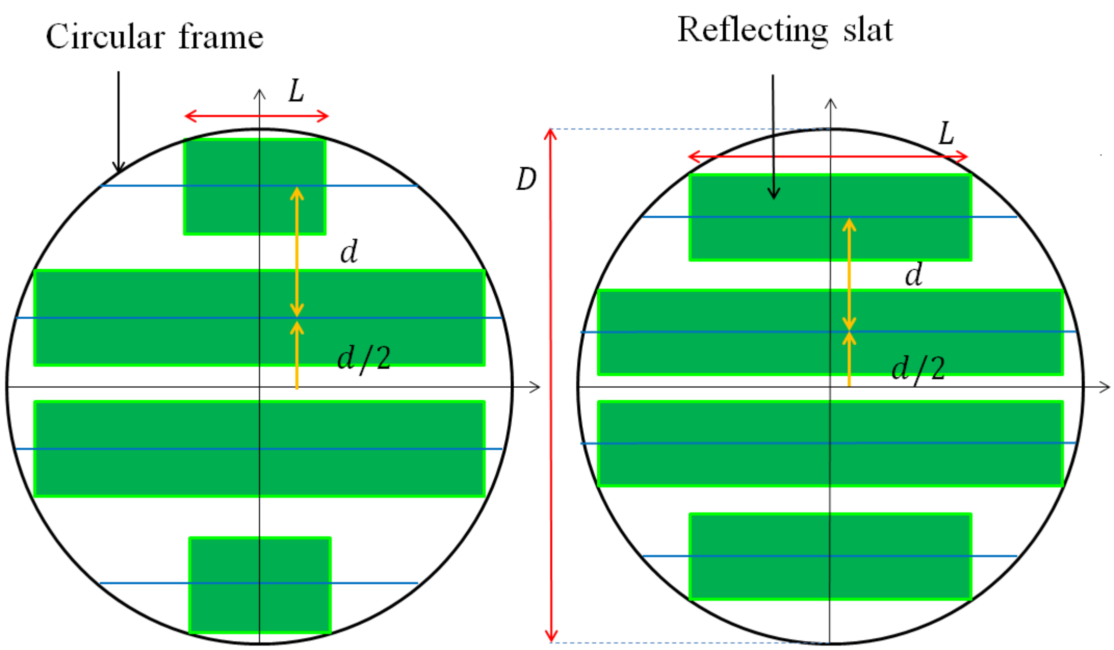

Figure 24. Light redirector with two different slat configurations

To find the optimum spacing configuration, the effective reflective area was calculated as a function of the spacing ratio for different number of slats. The spacing ratio, *Z*, is the ratio of distance between slats, *d*, divided by diameter of the redirector, *D*. The summary of this calculation is illustrated in Figure 25. As the spacing ratio decreases, more slat pairs can fit into the redirector unit. This calculation shows that for a given number of slat, the optimum value for slat spacing can be approximated as $d = D/(N + 1)$. The dashed lines in Figure 25 represent this value for each number of slats.

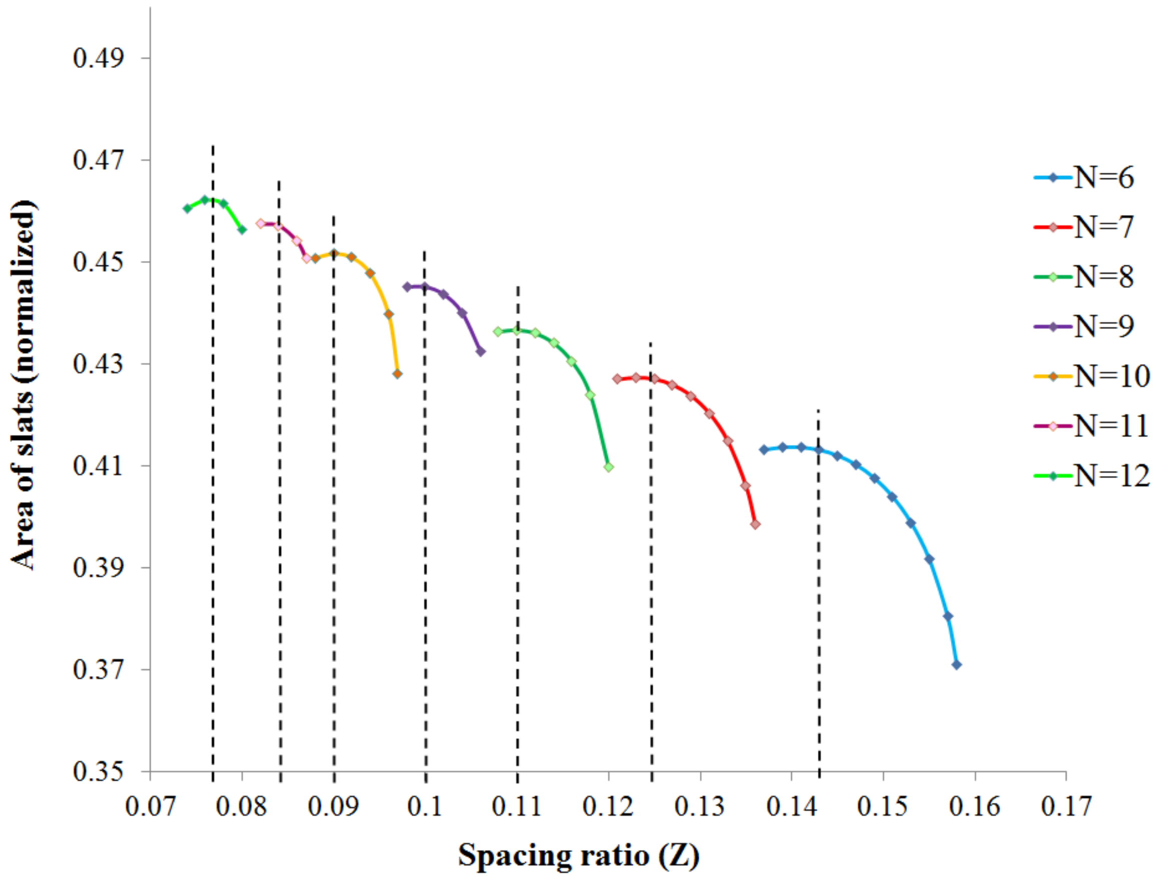

Figure 25. Overall area of the reflective slats versus spacing ratio

4.4 Efficiency and performance measurement

After all the variables in the redirector were optimized, the performance and efficiency were estimated using TracePro as raytracing software simulations. The efficiency of the redirector (E_R) is the ratio of captured light by the redirector (L_R) divided by light striking the top surface of the redirector (L_0), Figure 26.

$$E_R = \frac{L_R}{L_0} \tag{4-19}$$

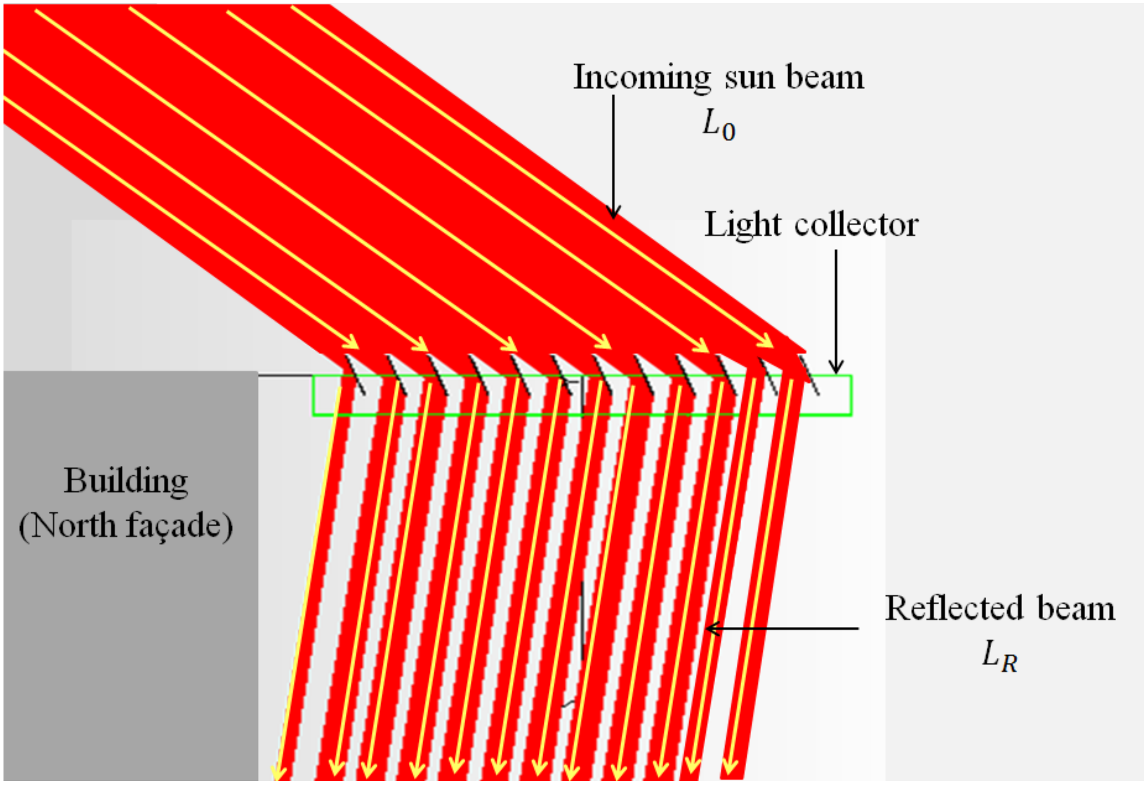

Figure 26. Light collector reflects sunlight toward the building (side view)

If the illuminance of a light source is I_0 , the luminous flux of the light that strikes the surface of the redirector, L_0 , is:

$$L_0 = I_0 \times A_{eff} \times \sin(\alpha) \qquad \textbf{(4-20)}$$

where A_{eff} is the effective area of the surface and α is the incident angle of the light. For one unit of redirector with the diameter of 1 m, the effective area is 0.785 m^2, and the incident angle is the solar altitude angle.

Using the macro scripts in TracePro Appendix B and Appendix E, the performance of redirector was simulated for the complete range of solar azimuth and altitude angles in 3° increment, and the efficiency was measured. The efficiency of the redirector in the single reflection mode steadily drops from 85% to less than 10% for solar altitude of 35° to 90°. This can especially affect performance of the system in places located at low latitudes. In these locations, the solar altitude is larger than 60° during a large portion of the days in spring and summer. On the other hand, the efficiency of the double reflection mode is relatively constant and around 40% for solar altitudes larger than 40°, as illustrated in Figure 27. When solar altitude exceeds 60°, the redirector switches to double reflection mode to capture more light. However, for solar altitude smaller than 40°, the efficiency of single reflection mode has almost twice the efficiency of the double reflection mode. The transition of the system between the two operating modes based on the sun position maximizes the amount of sunlight that is captured by the assembly.

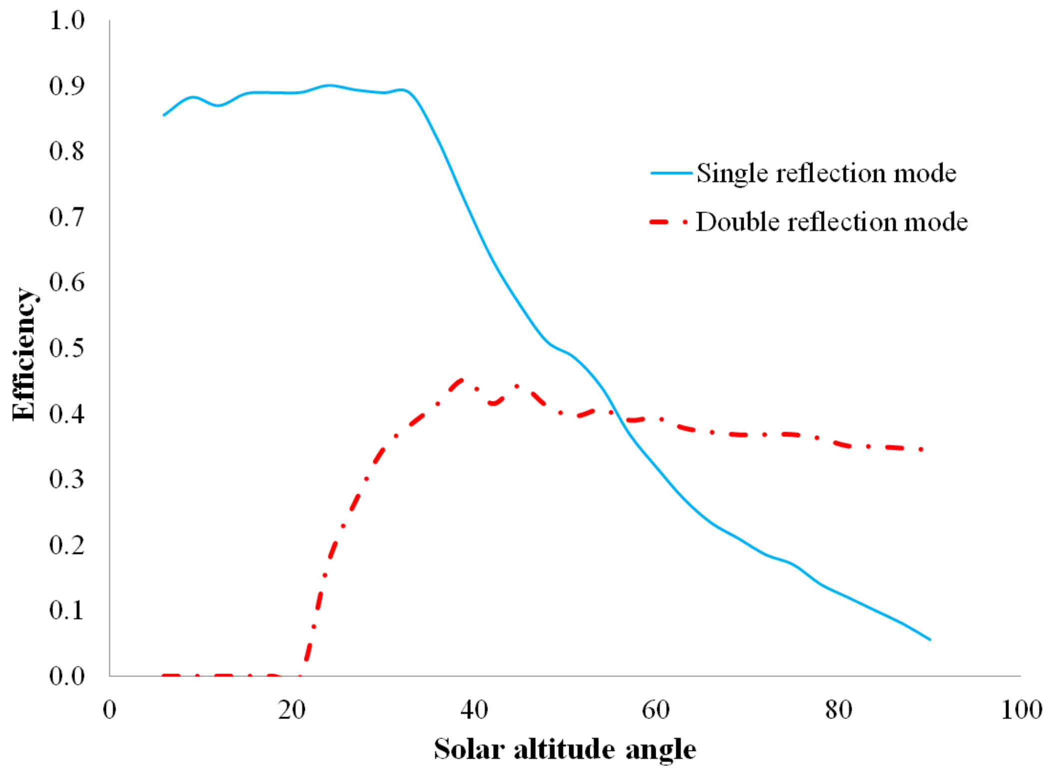

Figure 27. Efficiency of the light collector redirector versus solar altitude angle

Raytracing simulations show that the variation in efficiency over the solar azimuth angle movement is less than 15% for each mode throughout their operation window. Figure 28 represents the efficiency of the redirector in the two modes versus azimuthal angle for two example altitude angles. As illustrated in Figure 28, the single reflection mode at solar altitude of $\alpha = 30°$ and the double reflection mode at solar altitude of $\alpha = 70°$ have a relatively uniform efficiency with less than 20% variation over different solar azimuthal angles.

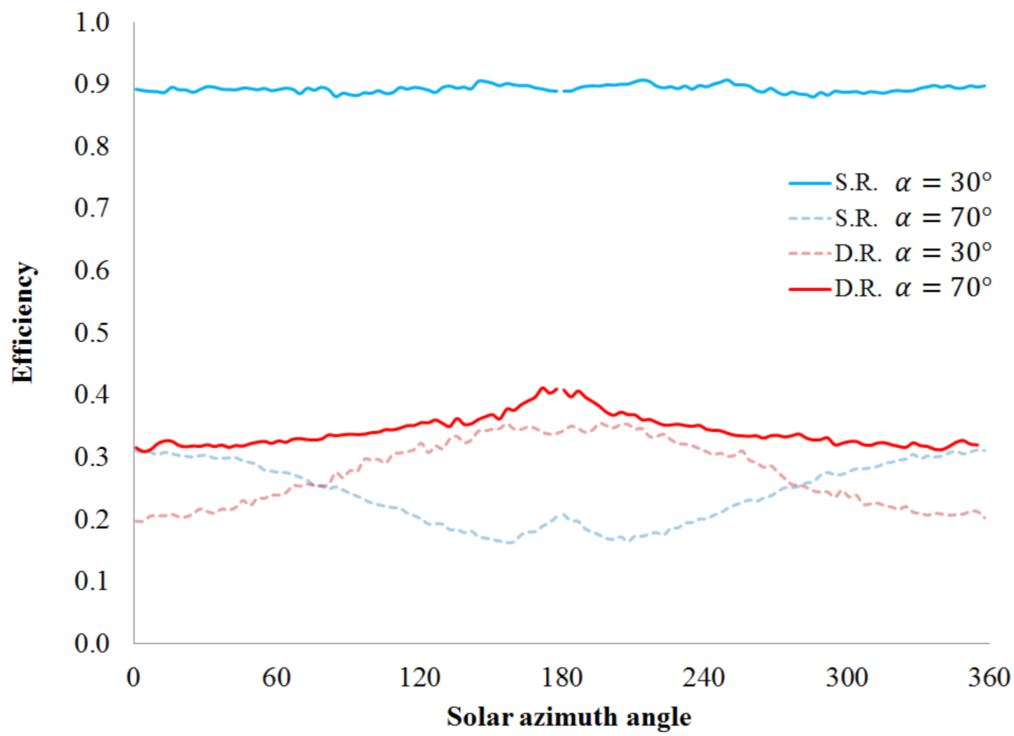

Figure 28. Efficiency of the light collector redirector versus solar azimuth angle for two altitude angles, (S.R. stands for Single reflection mode and D.R. stands for double reflection mode)

These results were for a light collector located on the south façade of building in the Northern hemisphere. Similar calculations carried out for other façades as well. Since the variation of efficiency versus azimuth angle is subtle, the amount of light captured by the light collectors is almost identical for all four facades. In the further calculations, the average efficiency for all sides of building was used to estimate the overall performance of the system.

The efficiency of the redirector for each of the two modes was combined in a look-up table in the form of a matrix for different solar altitude and azimuth angle. Part of this matrix is shown in the Table 3. Using the standard sun position calculation described in Appendix A, the solar altitude and azimuth angle can easily be calculated for a given location at any time. Thus, using the efficiency chart, it is possible to predict the efficiency of the light collector at each of the two modes for any given location throughout the year and day.

Altitude(°) / **Azimuth** (°)	………	**60**	**63**	**66**	**69**	………
.	.	.	.	.	.	.
.	.	.	.	.	.	.
.	.	.	.	.	.	.
208	………	0.371746	0.284663	0.242309	0.207377	………
211	………	0.380248	0.291681	0.248219	0.209915	………
214	………	0.380656	0.294737	0.248605	0.203705	………
217	………	0.372969	0.292756	0.254571	0.211265	………
.	.	.	.	.	.	.
.	.	.	.	.	.	.
.	.	.	.	.	.	.

Table 3. A portion of the efficiency matrix

Using the efficiency matrix, the amount of light that can be captured by the light collector can be estimated. Figure 29 represents the luminous flux of captured light by the redirector in a bright sunlight with solar illuminance of 100,000 lux. As illustrated in the graph, combining the single and double reflection modes allows maintaining the captured luminous flux at 25,000 lumens for a 1m diameter redirector, which is enough to illuminate 45 m^2 of office area at 500 lux, for a longer portion of day.

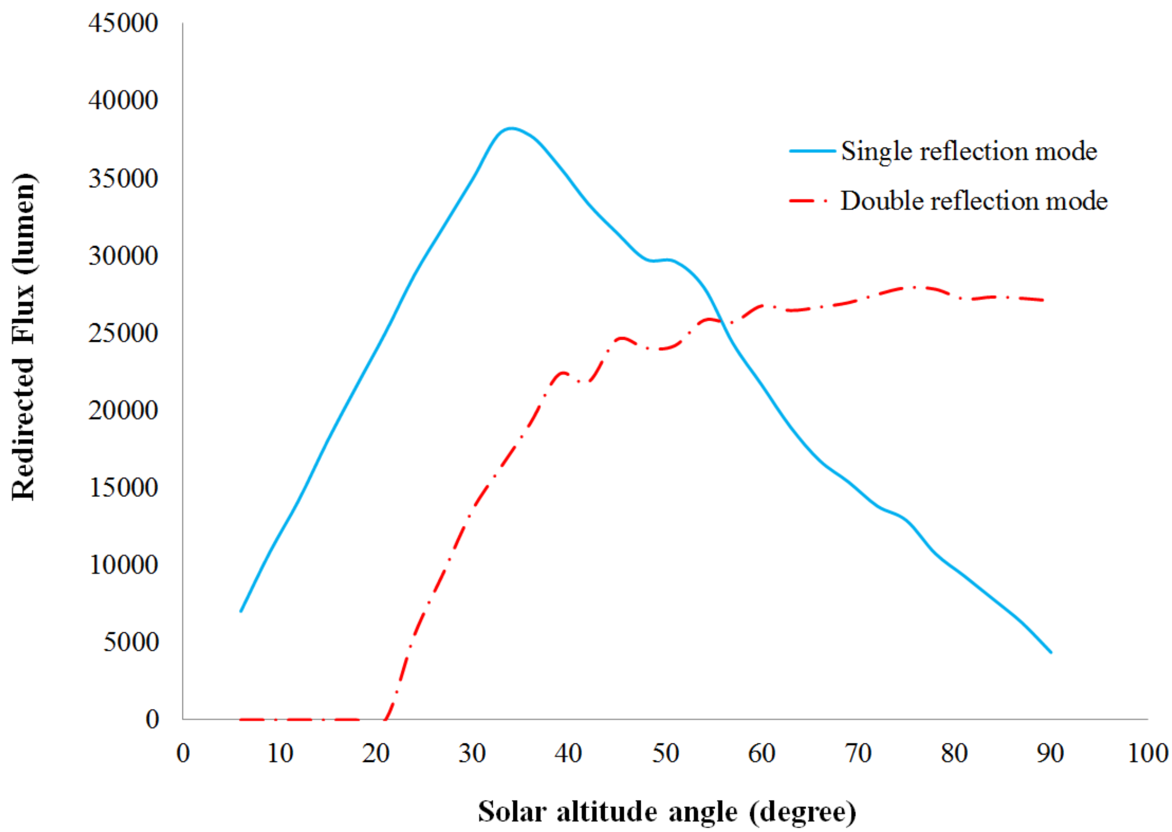

Figure 29. The luminous flux captured by one unit of redirector versus solar altitude angel

The next chapter describes how the reflected beam is captured by the light concentrator component to be delivered to the proper location in the building.

Chapter 5: The passive light collector component: the light concentrator

Once solar radiation is captured by the rooftop collectors and redirected towards the building facades, it is then concentrated into a collimated beam so that it can be fed into the light guide and distributed uniformly throughout the building. This is done by a concentrator assembly, which is installed at the façade of the building at each floor in the space between the windows, as previously described in Section 3.1.3. An innovative concentrator is proposed in this research project to meet the requirements for this system. In this chapter the optical design of the concentrator is described in detail and the performance is analyzed.

5.1 Optical concentrators

In general, a concentrator is an optical device that receives light at a first aperture surface and efficiently transfers it to a second, smaller surface, shown in Figure 30. The resultant concentration of flux is described by concentration ratio and denoted by *CR*. It is defined as the ratio of input aperture area divided by the output aperture area [41]:

$$CR = \frac{A_{in}}{A_{out}} \tag{5-1}$$

The efficiency of the flux transfer is denoted as η. It is defined as the ratio of the output flux to the input flux [42].

$$\eta = \frac{I_{out}}{I_{in}} \tag{5-2}$$

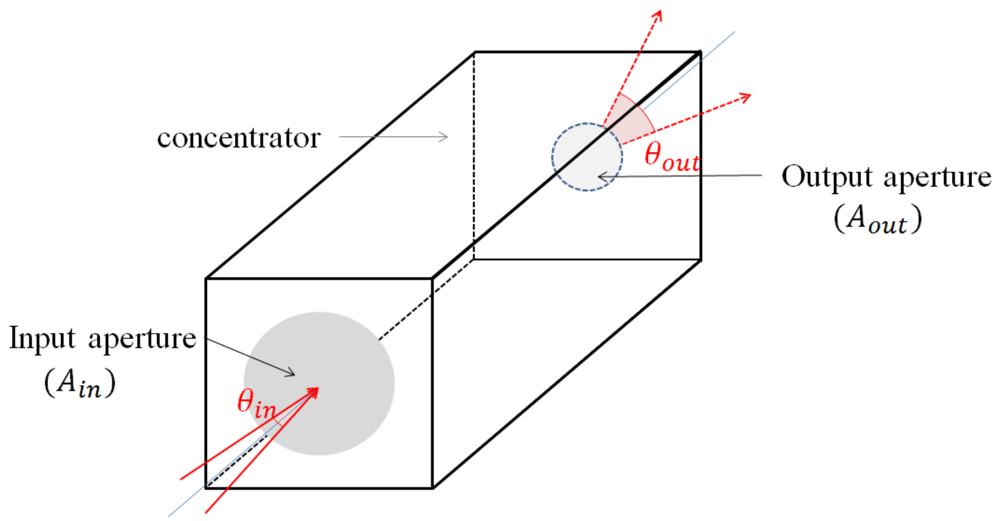

Figure 30. General concept of a light concentrator

An important measure used in the field of optical concentrators is the concept of etendue, which is the product of the area and solid angle of a light beam [41]. It is easily shown that no optical process can reduce the etendue of a light beam [41]; the best that is possible is to avoid increasing it. This concept has a direct parallel to the concept of the entropy of a thermodynamic system, in which no process can decrease the entropy of a closed thermodynamic system; the best that is possible is to have it not increase.

Returning to the concept of etendue, as shown in Figure 31, a light beam can be characterized by two parameters, the beam diameter, 2a, and the angular extent, 2θ. The combined product of the two variables, θa describes how spread out the light beam is in area and angle and is called étendue. In an ideal 2D optical system where there is no loss and scattering. If there is no obstruction in the light beam, the étendue is expected to be invariant along a ray path throughout the system [41]. In a 3D system, the étendue is described as the square of the quantity:

$$É = (\theta a)^2 \tag{5-3}$$

Analogous to entropy in thermodynamics, the étendue of an optical system can only increase. Étendue efficiency, ε, is a quantity that describes the performance of the concentrator on maintaining the étendue of the light beam. It is defined as the ratio of the étendue of the input beam to the étendue of output beam:

$$\varepsilon = \frac{É_{in}}{É_{out}} \tag{5-4}$$

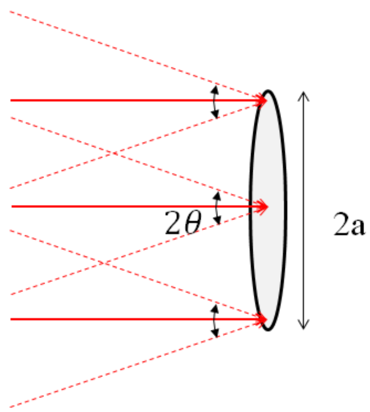

Figure 31. A light beam is characterized by its angular extent and beam diameter

As mentioned earlier, all optical systems can only increase etendue. Thus, as the spatial distribution of light is reduced the angular distribution automatically increases. In some applications, like the case of interest here, the angular distribution of the output light is very important, thus the concentrator should maintain the collimation of the output light beam as much as possible. The collimation factor, c, is defined here as the ratio of the angular divergence of the input light divided by the angular divergence of the output light, Figure 31.

$$c = \frac{\theta_{in}}{\theta_{out}} \tag{5-5}$$

This value is restricted by the étendue of the input light beam. In an ideal system where étendue does not increase, ε is expected to be one. Thus in any concentrator system, the angular divergence of light will increase at least by factor of the concentration ratio.

$$(\theta_{out})_{min} = CR \times \theta_{in} \tag{5-6}$$

Solar concentrators can generally be classified as imaging or non-imaging, depending on the design and optical elements used [42]. Conventional imaging concentrators use lenses and mirrors to concentrate light by forming an image of the light source using the principles of geometrical optics. These systems may require high accuracy in the optical design, perfectly manufactured optical elements, and need to be precisely assembled to perform well.

Non-imaging systems are only intended to optimize transfer and concentration of light at the output aperture, using multiple reflections in an optimized reflector shape. These systems can have a larger acceptance angle and often are more tolerant of imperfections in the optical elements and the installation process as well as the movement accuracy of the system. However, maintaining étendue and achieving low collimation factor are often as challenging in non-imaging systems as they are in imaging systems.

In the Two-Stage Core Sunlighting System designed in this research project, the angular divergence of light plays an important role, thus an imaging concentrator system was designed to maximize collimated light output in order to maintain the étendue. In the next section the details of the two proposed designs are described.

5.2 Combined Fresnel lens and fibre optics concentrator design

The preliminary proposed design included arrays of thin plastic Fresnel lenses and a bundle of optical fibres. As illustrated in Figure 32, five rows of 10 cm wide acrylic sheets, embossed with an array of small circular Fresnel lens, are used to capture light at different position and concentrate it to a focal point. A 2 mm diameter optical fibre is located at the focal point of each lens to transfer the concentrated light into the light guide while smoothly changing its direction from vertical to horizontal. The whole assembly protrudes 20-30 cm away from the building façade and is mounted at the building façade at each floor above the window intercept.

Although the proposed design can concentrate light and deliver it into the light guide, its performance is limited by the characteristics of the Fresnel lens and optical fibres. The angular divergence of the output light is restricted by the diameter of lens and the focal distance:

$$\theta_{min} = \tan^{-1}(\frac{R}{f}) \tag{5-7}$$

where R is the radius of the Fresnel lens and f is the focal distance of the lens. The two parameters need to be chosen to achieve the required angular divergence of the light guide, which is minimum of $28°$ for the light guide with acrylic prismatic microstructural film (explained in Section 6.1.1).

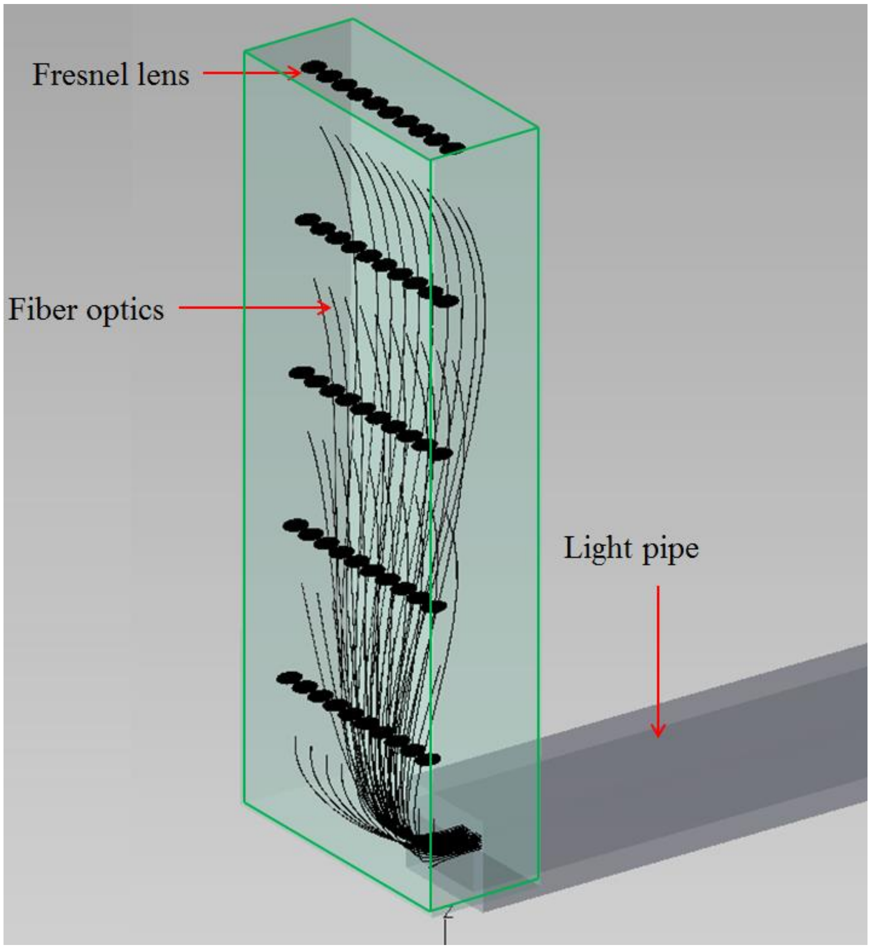

Figure 32. Fresnel lens and fibre optics concentrator

This concentrator design requires a high level of accuracy to function efficiently. The optical fibre has to be precisely located at the focal point of the lens within mm level of accuracy. This makes the manufacturing process complicated and costly. In addition, the solar energy is concentrated into a very small area in the optical fibre, which can damage the fibre permanently. To avoid this problem, a large number of smaller lenses and fibres were used, which adds to the complexity of the system.

Substantial energy loss due to optical imperfections and absorption is another limitation of the concentrator design. Fused silica glass fibre optics have the lowest absorption, about 20 dB/km for the visible range [43], which is equivalent to 0.5% loss per m, however, glass fibre is prohibitively more expensive and less flexible. Plastic fibres are more flexible and thus easier to manage and position. It is also less expensive, however they usually have a higher attenuation coefficient, around 200 dB/km.

The concentrator assembly is only 30 cm thick, however the enclosure contains a lot of lenses and fibres optics and this may have a negative impact on the aesthetics of the building. The proposed concentrator design was impractical, thus another concentrator was designed. This new design is explained in the next section.

5.3 Folded path concentrator design

To meet all the requirements of the concentrator, a new design was studied, which consists of a Fresnel lens assembly that protrudes 40 cm from the building façade and looks like a canopy and a thin glass covered concentrator enclosure as shown in Figure 14. Two thin flat Fresnel lenses mounted in the lens assembly concentrate light gradually over the focal distance and the reflective and refractive optical element in the concentrator enclosure collimate the light. The concentrated and collimated light feed eventually into a light guide located at the bottom of the collimator box.

To make the light guide resemble the actual luminaires in a big office area, it was decided to position them equally spaced at 1.5 m distance. Thus each concentrator unit that feeds one light guide is 1.5 m wide. Moreover, it was estimated that the light from each redirector unit, which is 1 m diameter, is sufficient to illuminate more than two floors. Thus, each concentrator unit should capture almost half of the redirected light. This means that the concentration ratio of the concentrator should be of the order of 5 to concentrate this light beam, ~1.5 m by 0.4 m, to fit into a small light guide, ~ 30 cm by 7 cm. Moreover, to make sure that the concentrator enclosure can always fit between windows, it was designed to be 1m tall, Figure 9.

To be able to transfer the sunlight across the building via the light guide, the angular divergence of the output beam should not exceed 28°. However, reducing the divergent angle would minimize the number of interactions of light rays with the light guide and hence reduce the loss (see Section 6.1.1). Thus it is desirable to have a more collimated light source to be able to transfer light deeper into the building core. The goal of this research project was achieving a collimation angle smaller than 10°.

It is also important to achieve high optical efficiency for the concentrator. In addition to the loss due to the absorption and the optical imperfection, the efficiency of a Fresnel lens also depends on its optical power. As the power of a Fresnel lens increases, the optical aberration increases, which also decreases the étendue efficiency. Thus to achieve high efficiency, it is necessary to use weaker lenses with longer focal distances and correspondingly larger *f*-number, where the *f*-number is defined as focal distance of the lens divided by the lens diameter.

$$f\# = \frac{f}{D} \tag{5-8}$$

Fresnel lenses with *f*-number larger than 1.5 usually have acceptable efficiency, ~0.9, and reasonably low aberration. However, the concentrator is required to focus a 1.5m wide beam over 1 m length (the height of the concentrator), which require a stronger lens with *f*-number ≅ 0.7. This problem was addressed by adding multiple reflectors in the concentrator enclosure, which effectively increases the optical path of light along a vertical folded path inside the enclosure. As illustrated in the Figure 33, multiple bounces between the top mirrors and bottom mirrors increase the optical path of light by factor of 3, thus the Fresnel lens can gradually concentrate light over a distance which is effectively three times longer.

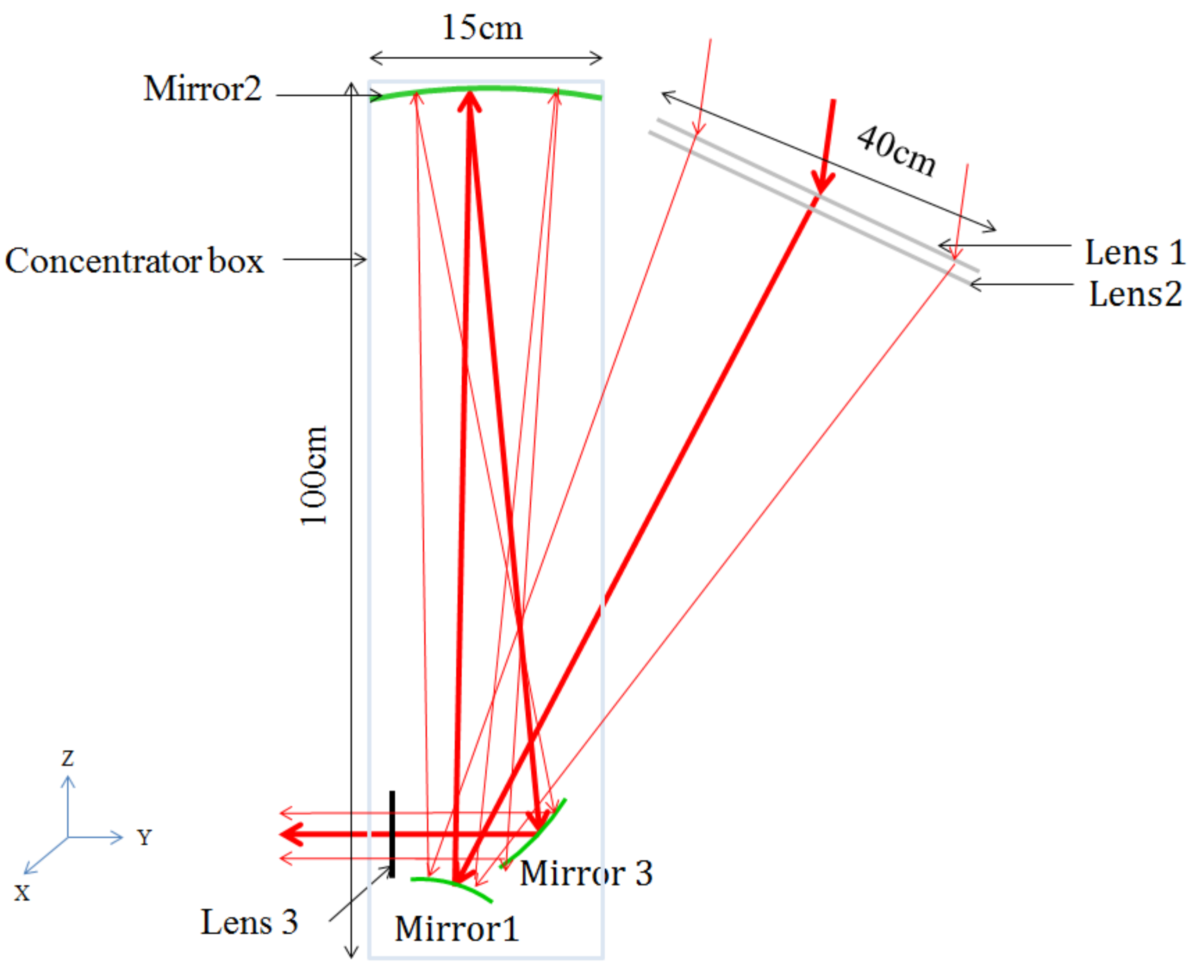

Figure 33. The folded path concentrator design, side view, not shown to scale

To minimize the system's visual impact on the appearance of the building, it is desirable to make the enclosure thin in the y direction, whereas in the x direction, the enclosure can be as wide as the Fresnel lens. This allows the use of two linear Fresnel lenses with different powers in the x and y directions. All other optical elements are linear or cylindrical as well, which allows independent concentration in two directions. The main advantage of this design is concentrating light separately in two lines rather than at a point which avoids hot spot with intensely focused sunlight, which otherwise can be a safety concern.

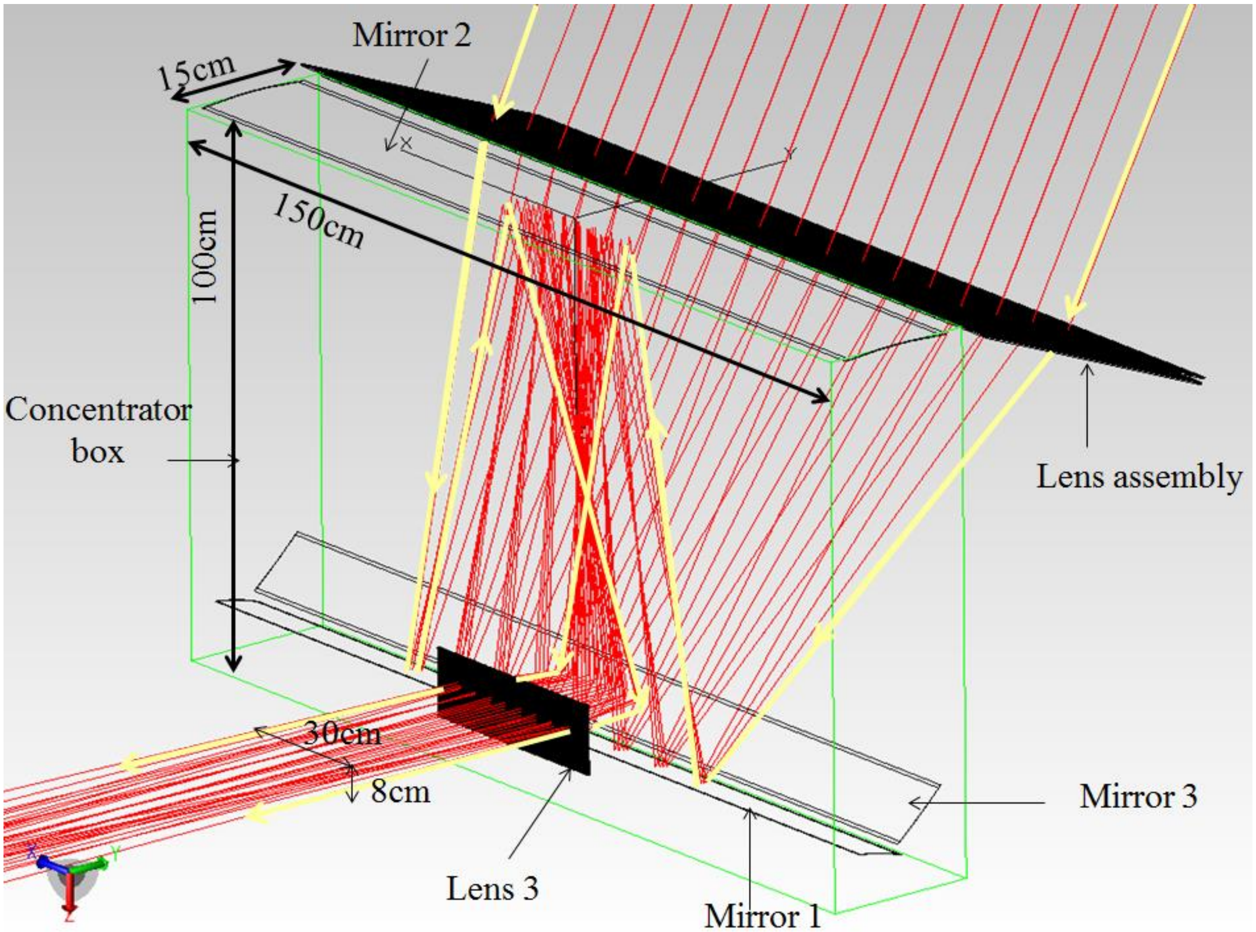

Figure 34.The folded path concentrator design, isometric view

Lens 1, which is a linear Fresnel lens active in the x direction, concentrates light in the x direction. As illustrated in Figure 33 and Figure 34, the light is slowly concentrated as it is bouncing up and down between mirrors 1, 2 and 3. These mirrors have no curvature along the x axis and are only used to increase the light path within the enclosure. The light is focused at some point before Mirror 3. Mirror 3 changes the direction of light to horizontal and redirects it towards Lens 3, a linear Fresnel lens that collimates the concentrated light in the x direction.

Since the enclosure needs to be thin in the y direction, a higher optical power lens must be used in this direction to narrow the beam diameter enough so that all the light strikes mirror 1. Lens 2, which is a linear Fresnel lens in y direction, concentrates light at a short distance after Mirror 1. However, the light needs to travel all the way to Mirror 2 and Mirror 3 before being concentrated. Thus, a diverging mirror in the y direction was used to slow down the concentration, Mirror 1. The diverging lens makes the rays almost parallel before striking mirror 2, which is converging mirror in the y direction. This mirror causes the light to be focused at the focal point of Mirror 3 which is another converging mirror. Mirror 3 eventually collimates light in the y direction and redirects it to the proper angle to be fed to the light guide. Since Lens 3 is a linear lens in the x direction, it does not affect the optical pathway of light in the y direction. The combination of all these components allows independent concentration of light in both directions.

It is also important to keep the efficiency of the system as high as possible. The light is redirected toward the building at a glancing angle, around 7°. However, the sunlight has to strike Mirror 1 inside the enclosure, which is 1 m below the lens assembly, thus the light must be further redirected to a steeper angle, for example 25° in this design. In order to achieve that, the whole lens assembly is positioned at 25° from the horizontal direction, as shown in Figure 33. As a result, the light that strikes the Fresnel lens is not perpendicular to the surface. This causes an aberration effect called Petzval field curvature. When off-axial light rays that are not perpendicular to the lens surface strike the converging lens, it is focused on a parabolic Petzval surface instead of the focal point, Figure 35 [44].

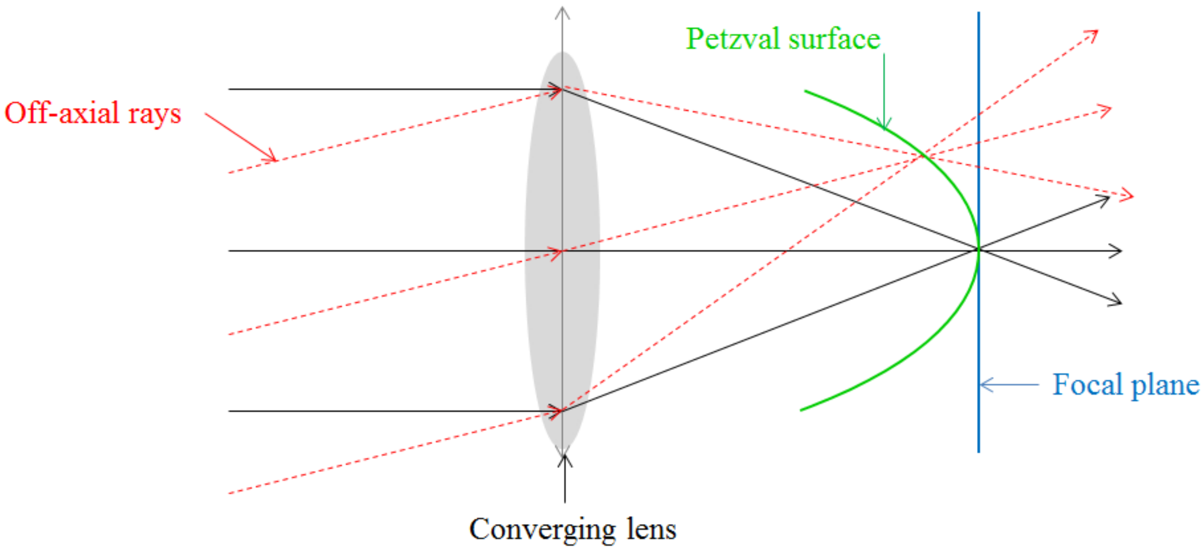

Figure 35. The converging lens focus light in the Petzval surface

To avoid this problem, a customized prism film, placed on top of the lens assembly, changes the angle of incident light and makes it perpendicular to the surface of lenses, as illustrated in Figure 36. In the next section, the detailed calculation of the prism film is explained in more detail.

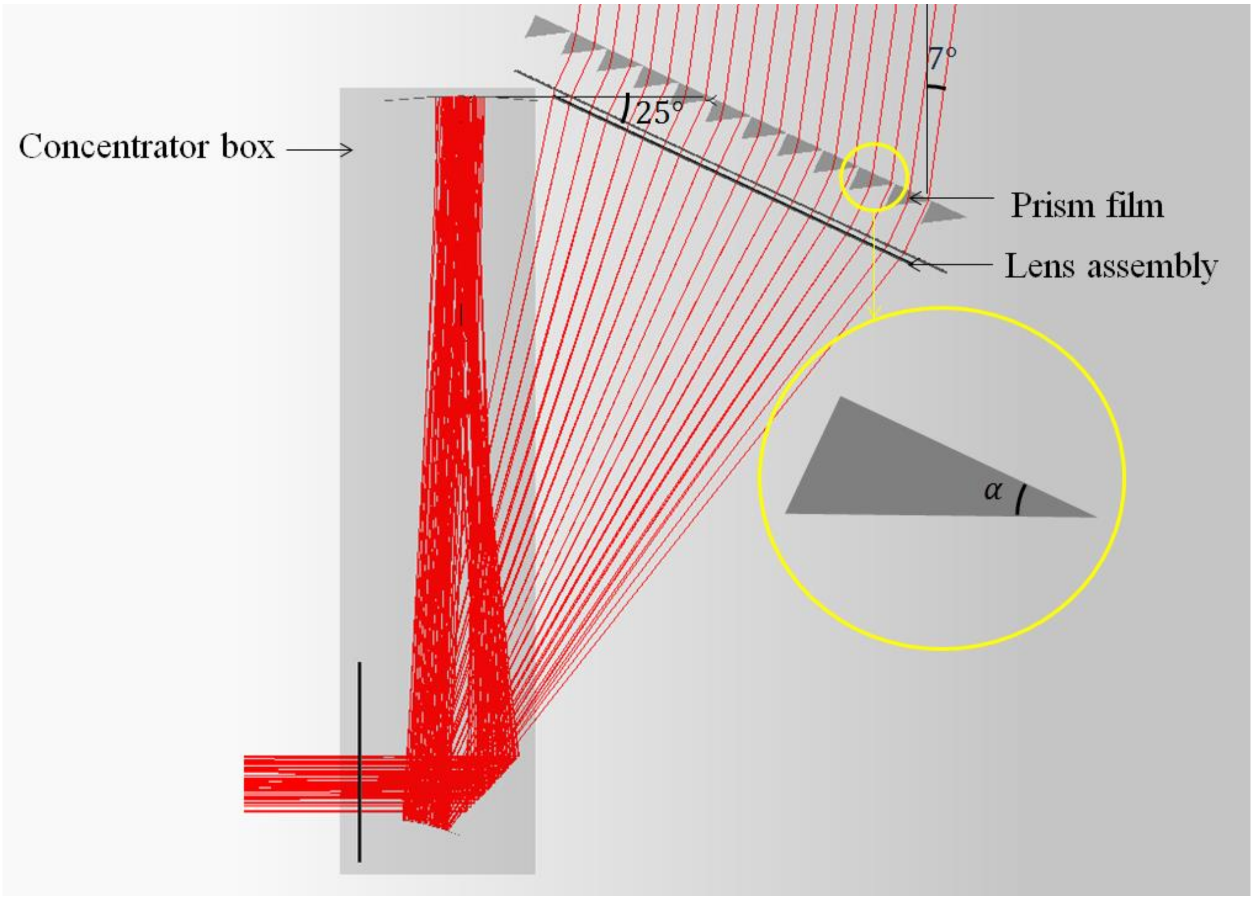

Figure 36. A prismatic film changes the direction of the incoming light and makes it perpendicular to the surface of Fresnel lens (picture of prism film is out of scale, and otherwise this figure is drawn to scale)

5.4 Optimizing the performance of the concentrator

To achieve the maximum efficiency for the concentrator, the optical characteristics of all elements in the concentrator needed to be calculated. Since the concentrator has a complex optical design, all elements are correlated. A series of iterated simulations were carried out to achieve the optimized state of the system. However, this problem does not have a unique solution and hence there may be other states that improve the efficiency even further. As the first order of approximation, optimization was done separately in two directions.

The Fresnel lens is a 150 by 40 cm flat plastic sheet and is oriented 25° from the horizontal to make sure that the light will strike Mirror 1, which is located roughly 1 m below the lens assembly. To make sure both Mirror 1 and Mirror 3 fit in the 15 cm thick enclosure, they should be 7 cm in y direction. (These dimensions are chosen arbitrarily and the whole system can be modified based on the desired dimensions).

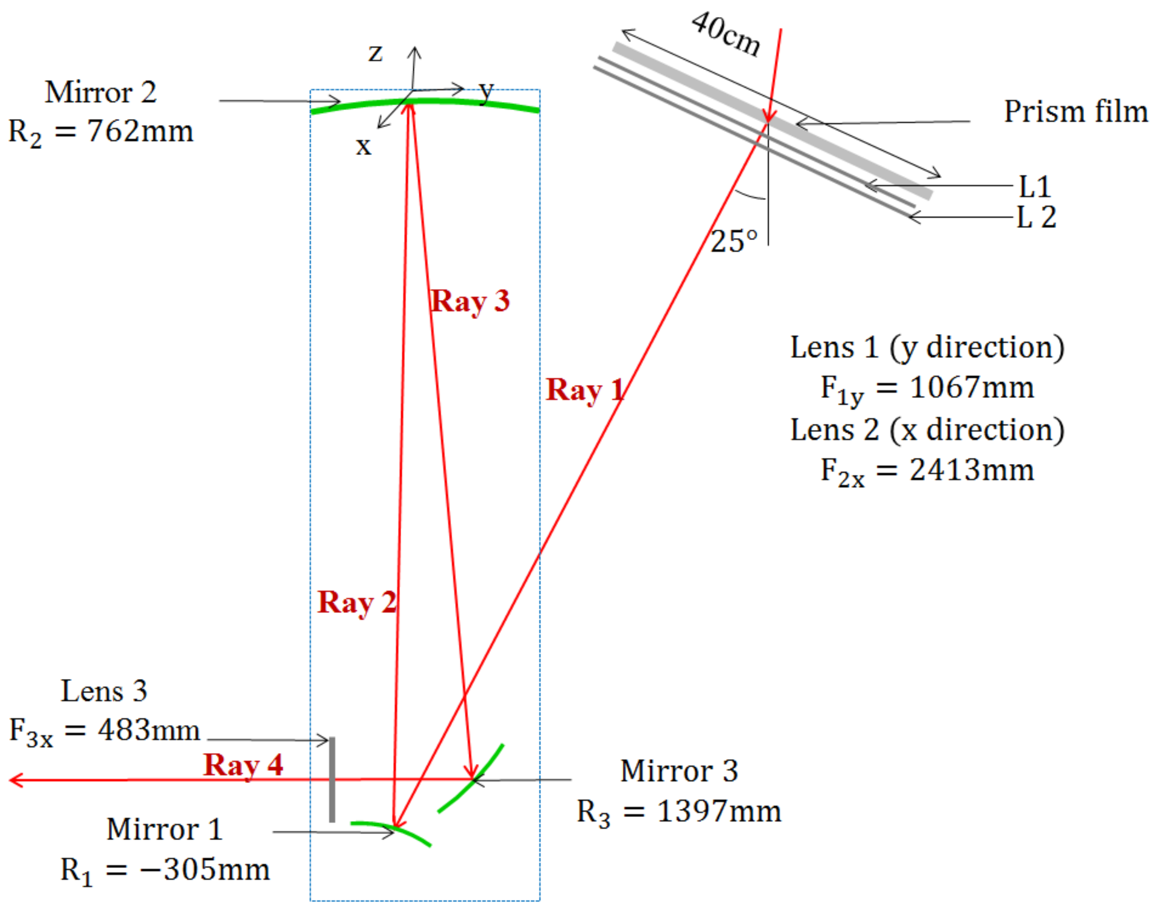

Figure 37. The schematic cross-section of the concentrator, viewed from the side

The orientation of each mirror was calculated such that the central ray of the beam strikes the center of each optical element and exits the concentrator in horizontal direction. Ray 1 originates from the center of the Fresnel lens and strikes the center of Mirror 1, thus Ray 1 deviates 25° from the vertical direction. To minimize the optical aberration of the lens, the lens assembly is rotated 25° to be perpendicular to Ray1. To reflect Ray 2 to the center of Mirror 2 Mirror 1 should be tilted 14.75°. Mirror 2 is horizontal and reflects ray 3 to the center of mirror 3, which is tilted $-46.2°$ and redirects ray 4 to the horizontal direction, Figure 37.

Each concentrator unit delivers light into one light guide, thus the concentrator needs to concentrate a 150 cm by 40 cm beam into a 30 cm by 7 cm (the cross-sectional area of the light guide), which means the concentration ratio of the system is 5. To achieve high collimation angle for the output beam, smaller than 10°, the focal length of all lenses and mirrors was precisely calculated. The concentrator can be simplified as a compound lens system, Figure 38. For a system that consists of two lenses with different powers separated by a distance *d*, the overall focal distance is calculated as follows:

$$\frac{1}{f} = \frac{1}{f_1} + \frac{1}{f_2} - \frac{d}{f_1 f_2} \tag{5-9}$$

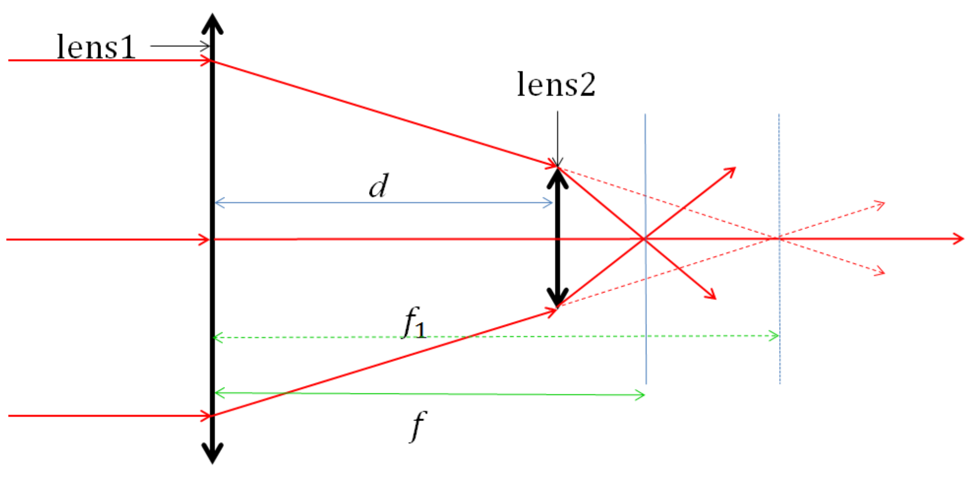

Figure 38. A compound optical system consists of two converging lens

For $d = f_1 + f_2$, $f = \infty$, which means the compound lens assembly makes a collimating lens, Figure 39. The mirrors have no curvature in the x direction and they have no influence on the effect on the beam except increasing the optical path. The optical path can be simplified and unfolded as illustrated in Figure 39. Lens 2 converges the light in the x direction and Lens 3, which is at approximate distance of 3 m in respect to the first lens, collimates the light rays, as shown in Figure 33. The *f*-number of each lens is calculated as follow:

$$f\# = \frac{f}{D} = 2\cot\theta \tag{5-10}$$

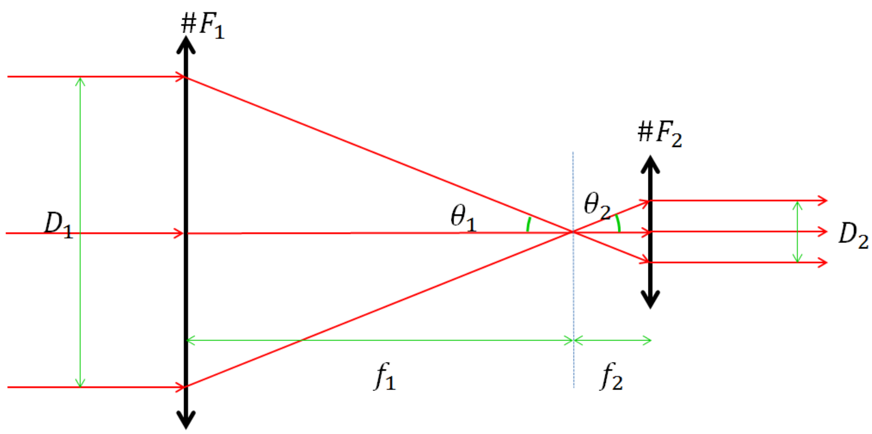

Figure 39. Tow converging lens make a collimating lens

Since $\theta_1 = \theta_2$, both lenses have the same *f*-number. Since the concentration ratio in this plane, $\frac{D_1}{D_2}$, is required to be 5. Thus Equation (5-10) leads to:

$$f_1 = 5\, f_2 \tag{5-11}$$

Since the second lens is located 1 m below the lens assembly, the effective optical path between the two lenses is equal to:

$$f_1 + f_2 \sim 3000 \text{ mm} \tag{5-12}$$

Using the calculated value as first estimate, the concentrator was modeled in TracePro using completely collimated light source. The focal distance of the lenses was modified to minimize the angular divergence of the output beam. For $f_2 = 2413$ mm and $f_3 = 483$ mm, the angular divergence of the light output was measured to be less than 1°, which is far less than the target of the project. This angular divergence is a result of optical aberration caused at the edge of the Fresnel lens and is inevitable.

The concentrator is a bit more complicated in the y direction as it consists of 4 lenses and mirrors. Lens 1 is required to be strong enough to decrease the size of the beam from 400 mm to 70 mm at an approximate distance of 900 mm. thus the focal distance of the lens set to be 1000 mm as first estimate. If Mirror 1 was a flat mirror, light would be focused shortly after reflecting from the surface and the beam waist would increases as it reaches Mirror 2 and 3. However, since Mirror 1 is a convex mirror it causes the beam to diverge so that all rays strike Mirror 2. The light beam is focused at the focal point of the Mirror 3, a concave mirror, which collimates the light beam and redirects it into the light guide.

A series of iterative simulations were carried out to determine the focal length of each of the lenses and mirrors to minimize the angular divergence of the incoming light as much as possible. As illustrated by the raytracing result, the focal length of $f_1 = 1067$ mm, and the radius of curvature of $R_1 = -35$ mm, $R_2 = 762$ mm, and $R_3 = 1397$ mm for the mirrors, leads to the most collimated light output in the y direction, less than 1°.

For this design process, the raytracing modeling was carried out using a collimated light source that is perpendicular to the lens assembly. However, the light redirected by the rooftop light collectors is not normal to the surface of the lens assembly. Thus a prismatic film is required to change the angle of incoming rays, 7° inclined from vertical direction, and make it perpendicular to the Fresnel lens which is tilted 25° from horizontal axis, Figure 40.

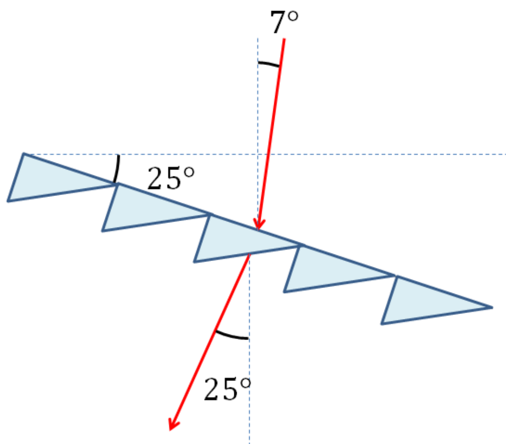

Figure 40. The prismatic film changes the direction of the incident light to the desired direction

The incoming light strikes the surface of film at an incident angle of $\theta_i = 25° - 7° = 18°$. The refracted angle can be calculated using the refraction law:

$$\sin\theta_i = n \sin\theta_r \tag{5-13}$$

Thus for an acrylic film with index of $n = 1.49$, the refracted angle is $\theta_r = 11.94°$, Figure 41. For a prismatic film comprised of right-angle triangle, the incident angle at which light strikes the wedge surface of film is $\theta_{i'} = \alpha - \theta_r$, where $\theta_r = \alpha$. Substituting these into the Equation (5-13) would lead to:

$$1.49 \times \sin(\alpha - 11.94\ \text{degrees}) = \sin\alpha \tag{5-14}$$

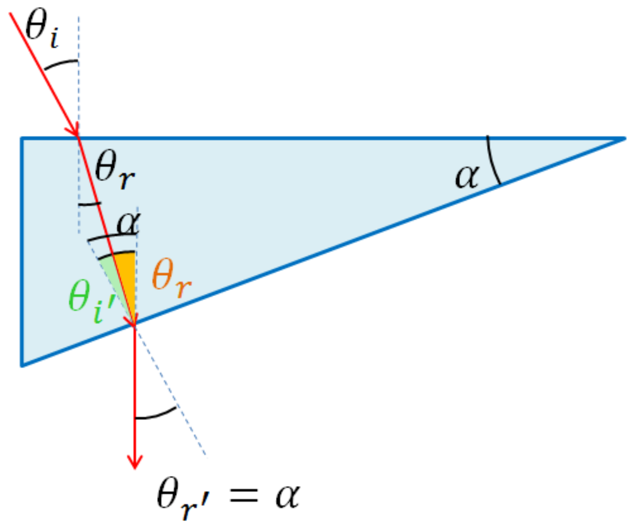

Figure 41. One single prism refract the light such that the incident angle is along the desired direction

Thus, a prismatic microstructure with prism angle of $\alpha = 33.85°$, can change the angle of incident light and make it perpendicular to the lens assembly.

5.5 Optical performance of the concentrator

The performance of the concentrator was studied initially with a uniform light source with zero degree divergence in order to measure the intrinsic error caused by the concentrator. The simulation was carried out also for a light source with $0.25°$ divergence, which represents the solar light beam [45]. The efficiency of the concentrator, which is the ratio of input light to the output light, was measured to be 95% for a completely collimated light source. The angular divergence of the output light beam was about 1.5°. For an ideal optical system, the angular divergence would be expected to be zero, since the angular divergence of the input light was also zero. This non-zero divergence is caused by the optical aberration of Fresnel lens, which increases for the light rays that strike close to the edge of the lens and is inevitable for a broadband light source.

The concentrator was modeled using the sun as the light source with an intrinsic angular divergence of $\pm 0.25°$, and the efficiency of the concentrator was measured to be about 93%. Figure 42 is the polar candela plot of the concentrator output, which illustrates the angular divergence of the concentrator output at two directions for solar light source. The polar angle represents the angle at which rays strike the detector plane measured from the normal direction of the plane and the azimuthal angle is the angle of the projected vector on the detector plane. According the Equation (5-6) the minimum expected angular divergence for this concentrator design is 1.25°. As illustrated in the following graph, about 93% of the light has an angular divergence of less than 2° which is very close to that of an ideal system. This largely maintains the etendue of the light beam.

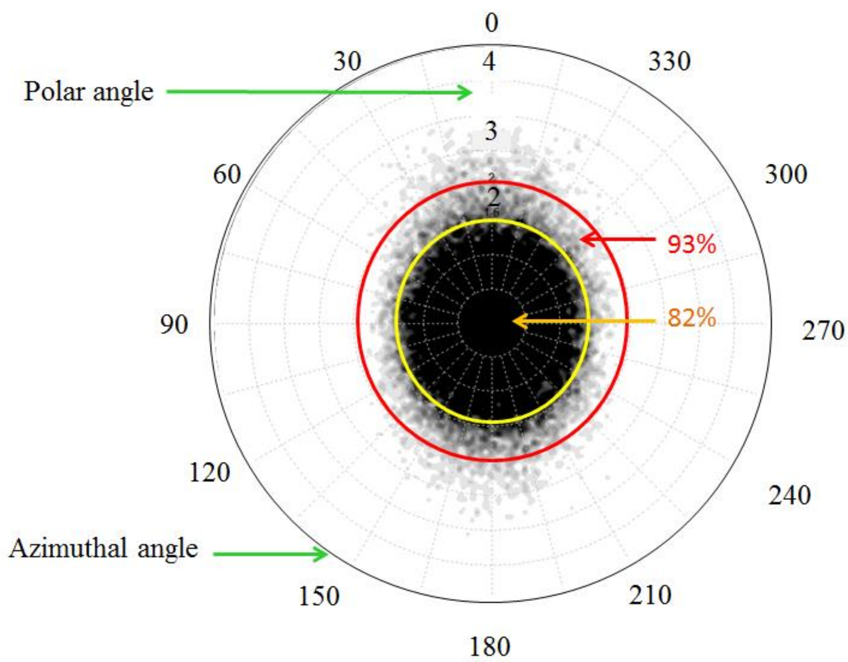

Figure 42. Polar Candela plot of the concentrator output for monochromatic solar light source

All simulations were done using a monochromatic light source and the concentrator was optimized for the central wavelength of the visible spectrum, $\lambda = 550\, nm$. However, the effect of the other wavelengths needed to be considered as well, since the refractive index of the lens material, and therefore the focal distance of the lens, depends on the wavelength. For a thin lens with identical curvature on both sides, the focal distance can be calculated as:

$$\frac{1}{f} = \frac{2(n-1)}{R} \qquad \textbf{(5-15)}$$

where R is the curvature of the lens and n is the index of refraction, which depends on the wavelength. Thus the focal length of the lens would slightly vary for different wavelengths:

$$\frac{\Delta f}{f} = \frac{(\frac{\Delta n}{n-1})}{(1 + \frac{\Delta n}{n-1})} \tag{5-16}$$

This well-known effect, termed chromatic aberration, is inevitable for a broad spectrum light source and a single element lens. Figure 43 shows how a slight change in the index of refraction of acrylic for two wavelengths can cause chromatic aberration in an optical system. As illustrated in Figure 43, a light source with two different wavelengths was used, λ =400nm and λ =500nm. The difference between indices of refraction is about $\Delta n = 0.012$ for acrylic lens, which would lead to $\Delta f = 0.023$ in the focal distance.

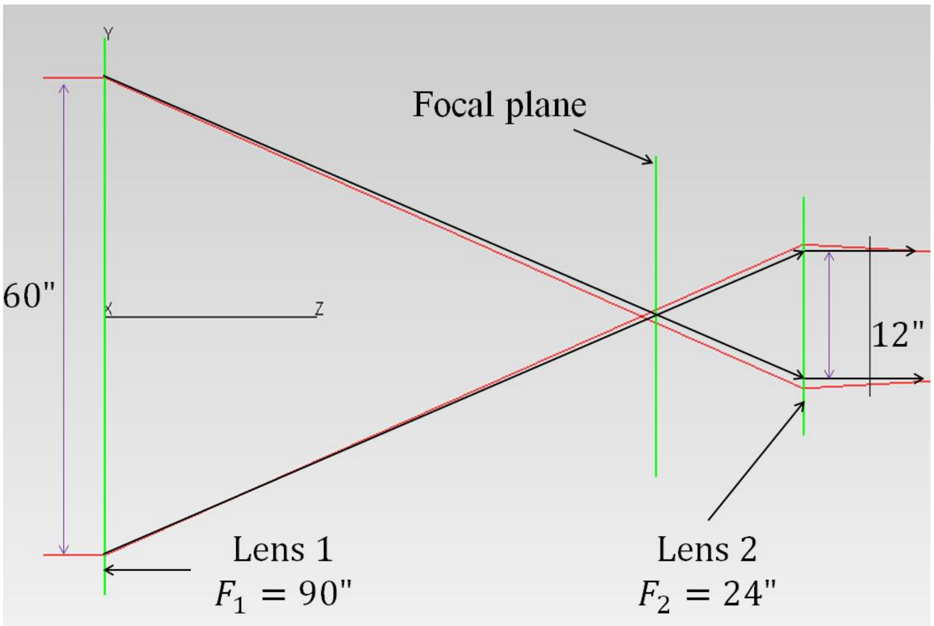

Figure 43. Chromatic aberration in an optical system caused by a bi-chromatic light source (Red rays: λ =400 nm, black rays: λ = 550 nm)

The solar light source is a broadband spectrum light source and hence the concentrator was modeled for a multi-wavelength light source, ranging from 400 nm to 700 nm. The efficiency of the system was measured to be 92%. More than 96% of the output light is within ±2.5° divergence. Figure 44 represents the angular divergence of the concentrator output for a broad-spectrum solar light source.

After the sunlight is captured and concentrated, it must be transferred to the proper location and distributed uniformly across the building floor plate. This is done via the light guide that is explained in the next chapter.

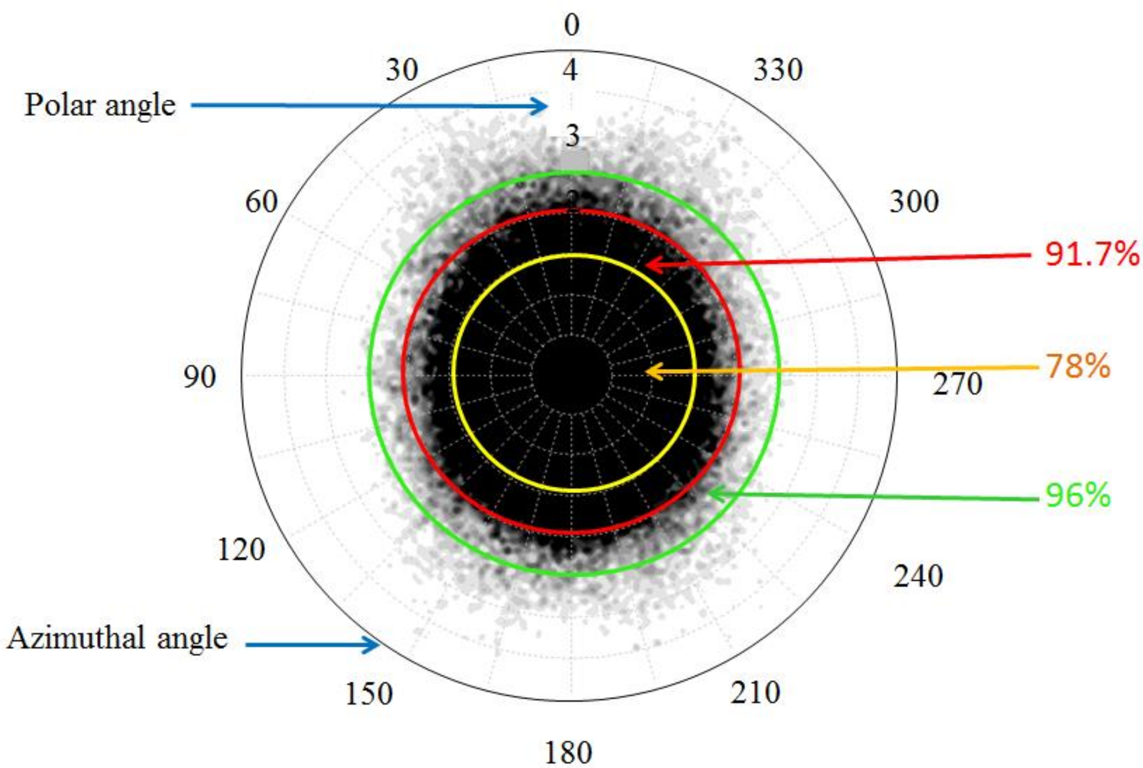

Figure 44.Angular divergence of the concentrator output for broad spectrum solar light source

Chapter 6: Light distribution system

Once sunlight was captured and concentrated, it can then be delivered to the proper location in the building using light guides, as briefly described in Section 3.1.4. This chapter includes a detailed study of the light guide, including the characteristics of the optical elements, the performance of the light guide and the light distribution of the output light inside the building. It is followed by an analysis of the Two-Stage Core Sunlighting System with all components combined and studied via raytracing. It also includes a comparison of the simulation results with photometric measurements of a light guide equipped with electrical lighting, as a verification of the simulation results.

6.1 Elements in the light guide

The light guide is a hollow linear structure, the inner surface of which is covered with highly specularly reflective material, Figure 45. Often the cross-section is rectangular, as is the case in all of the work described here. The bottom of light guide is lined with a special optical material know as prismatic microstructured film, which has the dual functionality of reflection and light transmission described in Section 6.1.1. Sunlight exits the light guide and illuminates the office area similar to an overhead luminaire. To control the level of output light, an extractor is applied to the light guide (see Section 6.1.3). To maintain a constant level of illumination over time, the light guide is also equipped with electric lighting that supplements sunlight as necessary. The electric lighting also illuminates the building during the night when no sunlight is available.

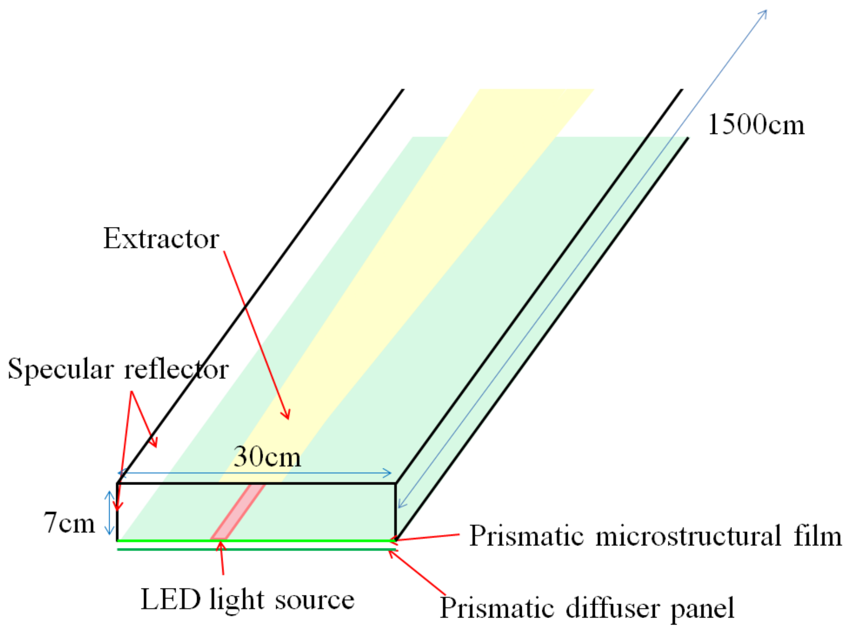

Figure 45. Cross sectional view of a light guide

As light travels down the guide, it reflects from the interior surfaces multiple times. Although the materials used in the light guide are more than 95% reflective, many interactions leads to substantial energy loss of light over a long light guide. Therefore, it is desirable to minimize the number of reflections as light travels down the guide.

For any particular guide with specific geometry, the approximate number of times an average light ray reflects off the wall of the light guide before reaching the end, in the absence of any extractor, can be estimated as follows [46]:

$$N \cong \frac{\theta_{1/2}}{50}\frac{L}{W} \tag{6-1}$$

where L is the length of the guide and W is the cross section width. To minimize the number of interactions, it is desired to have a light guide with a smaller aspect ratio, where aspect ratio is the ratio of length to the effective diameter. Thus, to efficiently deliver light greater distances, a greater diameter is required. This in turn would occupy a larger volume inside the room which is not desirable from an interior design perspective and can sometimes be impractical.

It is important to keep the number of interaction smaller than 30, otherwise the overall loss would be prohibitively large [46]. Ideally it should be less than 10. This may only be possible by reducing the angular divergence of the light to $\sim 5°$. In most of the mentioned design in chapter 2, including the Solar Canopy Illumination System, this degree of collimation was not achieved. However, in the Two-Stage Core Sunlighting System designed in this research project, a high level of collimation was achieved using a more sophisticated optical concentrator. This allows further transportation of sunlight down to the building core, while using a relatively thin light guide. In this particular design, we aim to send light 15m down to the core of the building using a light guide with cross sectional dimensions of 7 cm by 30 cm.

To understand the concept of the light guide better, each element of the light guide, including the relevant properties and characteristics, is described in more detail in the next section.

6.1.1 Prismatic microstructured film

The prismatic microstructured film has a linear right angle prismatic structure running parallel to the light guide axis. The film, depicted in Figure 46, is about 0.5 mm thick and is made out of either polycarbonate or acrylic. There are several different types of prismatic film commercially available. The one that we used in our model has a prism width, δ, of 300 microns. This is the most common prism width among commercially available films.

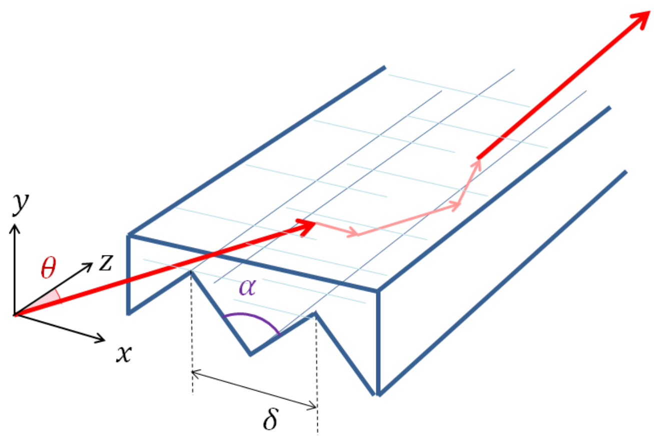

Figure 46. A cross sectional view of the prismatic microstructured film, showing a light ray coming from above the film, entering the film through the top surface, reflecting off the two bottom prismatic surfaces and exiting the top surface

If the angular deviation of incident light from the axial direction of the guide θ, is less than a critical angle, θ_{max}, it undergoes total internal reflection and is reflected such that it continues to propagate along the guide. For values of $\theta > \theta_{max}$, most rays transmit through the prismatic film, although for certain angles, total internal reflection may still occur. The value of this critical angle depends on the refractive index of the prismatic film and is given by this formula [47].

$$\theta_{max} = \cos^{-1}\left[\frac{1 - n^2 \sin^2(\pi/8)}{1 - \sin^2(\pi/8)}\right]^{1/2} \tag{6-2}$$

Thus, most of the rays sent into the guide must be less than this maximum angle. For the polycarbonate prismatic film that we used in our model, n=1.59 and the critical angle is around 28°, which is much greater than the angular divergence of concentrator output. Thus, any light ray that strikes the surface of the prismatic film undergoes total internal reflection and is bounced back along the light guide.

The prismatic microstructured film is a very efficient reflector. The loss due to absorption is very small since the attenuation factor, α, of polycarbonate is only $4m^{-1}$ [48] and the thickness of the film is 0.5 mm [49]. (For a light ray that undergoes total internal reflection, the effective thickness is twice this, or about 1 mm.) The intensity drop due to absorption is [39]:

$$I = I_0 e^{-\alpha x} \tag{6-3}$$

Thus the absorption loss in each interaction is around 0.4%. Optical imperfection also causes around 1.5% energy loss in the prismatic film in each interaction, which is discussed further in Chapter 8.

6.1.2 Specular reflector

The sidewalls of the guide and the top surface are covered with a highly specular reflective material. In this model, Enhanced Specular Reflector Film (ESR), which is an efficient specular reflector and is commercially available, was used. ESR is a flexible thin reflective film based on multilayers of dielectric, coated by a protective liner [50]. The reflectance of the ESR is about 98% [50]; it is known to be one of the most reflective materials commercially available.

6.1.3 Extractor

The concentrated sunlight entering the light guide is highly collimated, so for most light rays that strike the prismatic film surface, the angular divergence does not exceed the critical angle of the prismatic film and hence, cannot exit the light guide. As a result, most of the light will be inside the light guide for an excessively long time, which increases the overall loss in the light guide. Thus, an extractor mechanism is introduced in order to extract light uniformly along the light guide. The extractor is a diffusely reflective sheet that is positioned inside the light guide on the top surface. When a light ray strikes the surface of diffuser, it reflects over a wide range of directions. Much of this reflected light exceeds the critical angle of the prismatic film and therefore can escape from the light guide.

The probability of interaction of the ray with the diffuser sheet increases with the size of the extractor, thus it is important to adjust the shape of the extractor to achieve an efficient and uniform distribution of light. In particular, it is important to extract light uniformly along the guide; however, as light being extracted along the guide, the intensity of the light within the guide correspondingly drops. To maintain a uniform level of illumination, the size of the extractor must to increase along the light guide, to compensate for the decreasing internal flux.

To extract most of the light inside the light guide, the end of the guide is equipped with a perpendicular flat end-mirror which reflects the remaining light backward, to be extracted on its way toward the entrance. To optimize the light extraction along the guide, it is usually recommended to design the extractor such that approximately 25% of light reaches the end of the pipe [46].

To determine the optimum shape for the extractor, the light guide and concentrator were combined in the ray tracing simulation and the output of light guide was measured along the light guide for various diffuser dimensions and shapes. It was possible to produce a relatively uniform light distribution by a specific design, which is plotted in Figure 47. Almost 22% of the input light reaches the end of the light guide and 3% was lost by return to the entrance aperture. As the simulation result shows, the fractional variation of light intensity below the light guide is small, about ±15%, and the fluctuations happen gradually over a long distance. This degree of variation in light level is not apparent to most people, so it is acceptable.

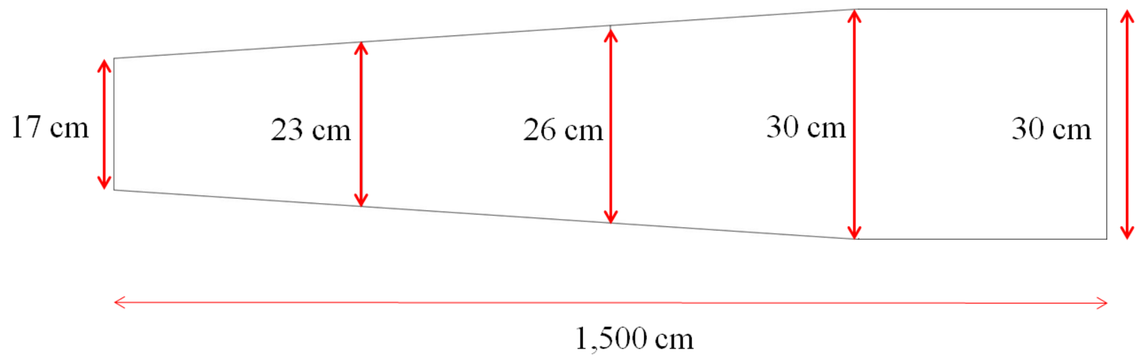

Figure 47. The variation of the extractor shape over the length of the light guide (the picture is compressed in the direction of length by a factor of 10)

Tyvek® sheet was used as the reflective diffuser, as it has high reflectivity, 95%, and also it is commercially available [51]. The Tyvek sheet has some absorption (about 5%). However, the light rays that strike the diffuser surface exit the light guide immediately with high probability and thus the interaction of light rays with the diffuser is limited and it does not cause a large loss in the light guide.

6.1.4 K12 prismatic diffuser sheet

One of the important factors in the lighting quality is the nature of the angular distribution of the output light. To improve lighting efficiency, luminaires are often designed to direct more of their light closer to vertically downward than would be the case for a Lambertian (i.e. totally random) diffuser. It is also important to diffuse the light output to avoid bright spots, which may cause visual discomfort. Thus, luminaires are usually equipped with a diffuser panel, which changes the light output to the desired profile. One of the products that is commercially available and was used in the light guide is K12-prismatic diffuser panel [52]. It is a semi-flexible acrylic or polycarbonate sheet, 2.5 to 4 mm thick, made out of approximately 5 mm diameter conical prisms moulded in the sheet in a two-dimensional array. The prism half angle is 54° and its depth is 1.8 mm. The repeating structure has a square based configuration rotated 45° [52], Figure 48. The K12 prismatic diffuser is made out of clear acrylic with very low absorption. The attenuation factor α, of the acrylic is only 0.5 m^{-1} [53]. For the film that was modeled in this design, with the thickness of 4 mm, the absorption loss in each reflection is around 0.2%, which is essentially negligible.

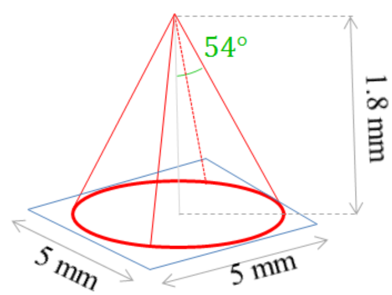

(a)

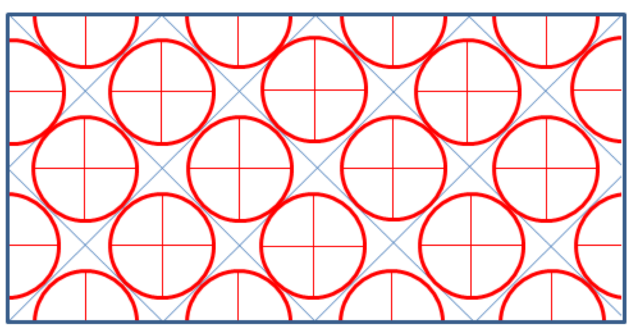

(b)

Figure 48. The K12 conical prismatic sheet

((a) is a single conical structure which was replicated, (b) top view of the film)

The light profile of the K12 sheet output was measured both in simulation and in a physical experiment. In a simple experimental set up, the light output angular distribution of a Lambertian light source was generated by an aperture in an illuminated integrating sphere. The illuminance was measured along a line at a plane spaced away from and parallel to the aperture. The measurement was then repeated with the aperture covered with K12 sheet. The results were then compared with a ray trace simulation of the same set-up. As illustrated in Figure 49, the light distribution of the Lambertian light source in the experimental and simulation measurement matched very well with the coefficient of determination or R-squared value of 99.8%, which indicates the two data points highly match. The uncertainty in the simulation result is due to numerical error that depends on the number of rays. The error calculation is explained in more detail in Section 6.1.5.

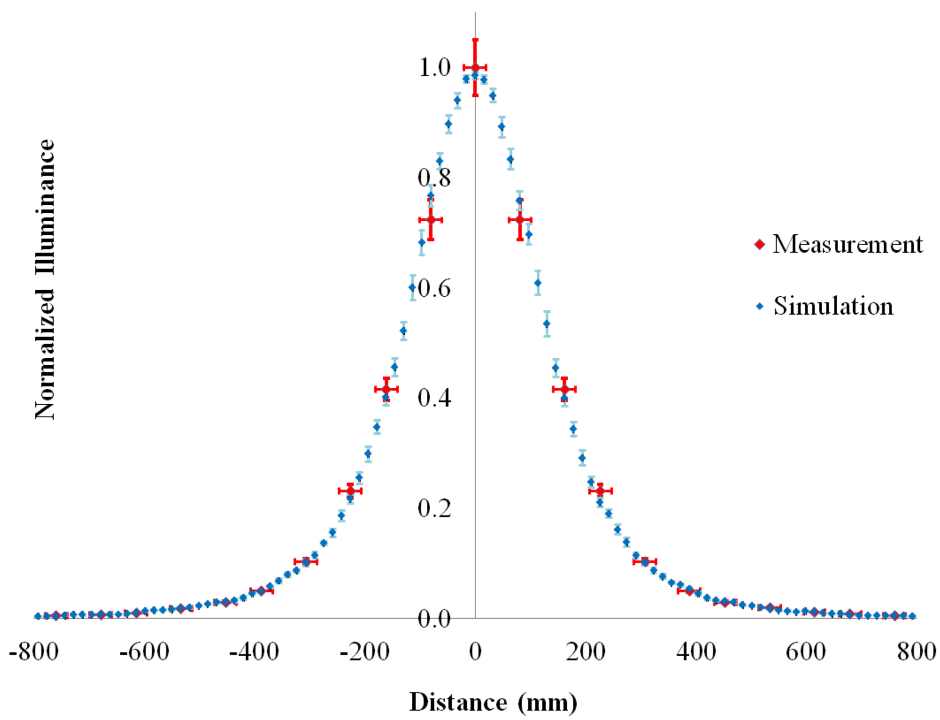

Figure 49. Comparison of experimental measurement and simulation result for a Lambertian light source

As mentioned, the procedure was repeated with a panel of K12 sheet covering the Lambertian light source. The result of the physical experiment and the simulation were compared as presented in Figure 50. As illustrated in the graph, the light profile of the modeled K12, which is used in the simulations, is similar but not identical to the light profile of the actual material (K12 is a commercially-available product, but the data sheet for the product does not provide highly detailed information regarding the expected light distribution). Even though the R-squared value of 98.8% indicates that the two data sets match to a high level, it was interesting to investigate the source of this discrepancy.

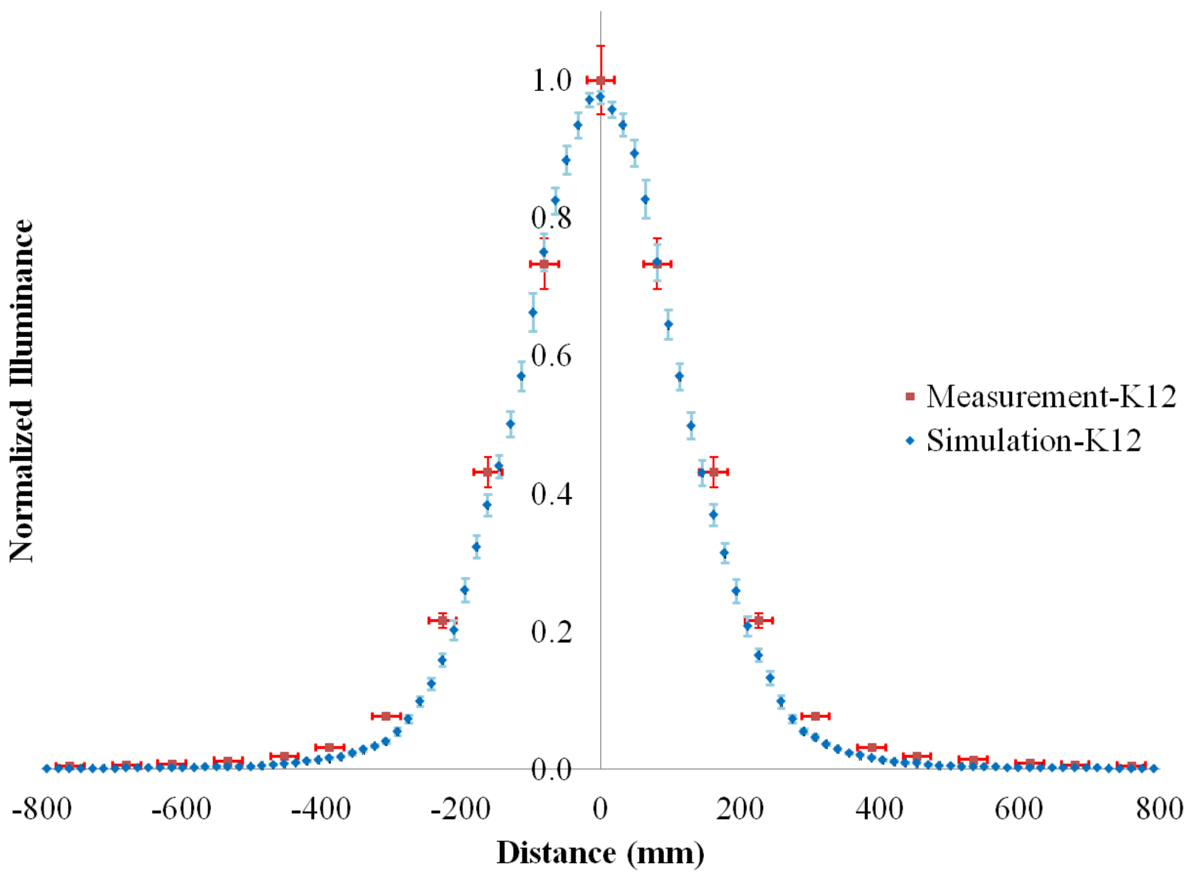

Figure 50. Comparison of experimental measurement and simulation result for a Lambertian light source with K12 prismatic panel

The diffuser panel is designed to change the light profile and increases the energy concentration of light at the centre; however, as illustrated in Figure 50, the actual K12 prismatic sheet does not change the light distribution as well as it is supposed to. When the K12 sheet was investigated under a microscope, it was found that the faces of the prismatic structure are slightly curved and the tip of the prism is chamfered, which was different from the conical prism in the datasheet for the film. Also, the back surface of K12 is slightly wavy. This could be due to some imperfections in the manufacturing process. Although K12 diffuser sheet is largely used in luminaires, there may be other products that have a better performance from this perspective. However, studying the performance of these other diffuser sheets was out of scope of this research project and so no other diffuser sheets were tested.

To compensate for these optical imperfections, we added in the ray trace model a small amount of bulk scattering within the K12 sheet. In Tracepro, when light passes through such a scattering material, it may be scattered at any angle. The probability of light not being scattered at all after traveling a unit distance in the material depends on the scattering coefficient and the distance as follows [54]:

$$P_T = \exp(-\mu_s L) \tag{6-4}$$

where μ_s is a scattering coefficient. The scattered light can be deflected at any angle with a probability distribution that is approximated by the Henyey-Greenstein phase function [55] [56]:

$$P(\varphi) = \frac{(1 - g^2)}{4\pi(1 + g^2 - 2g\cos(\varphi))^{3/2}} \tag{6-5}$$

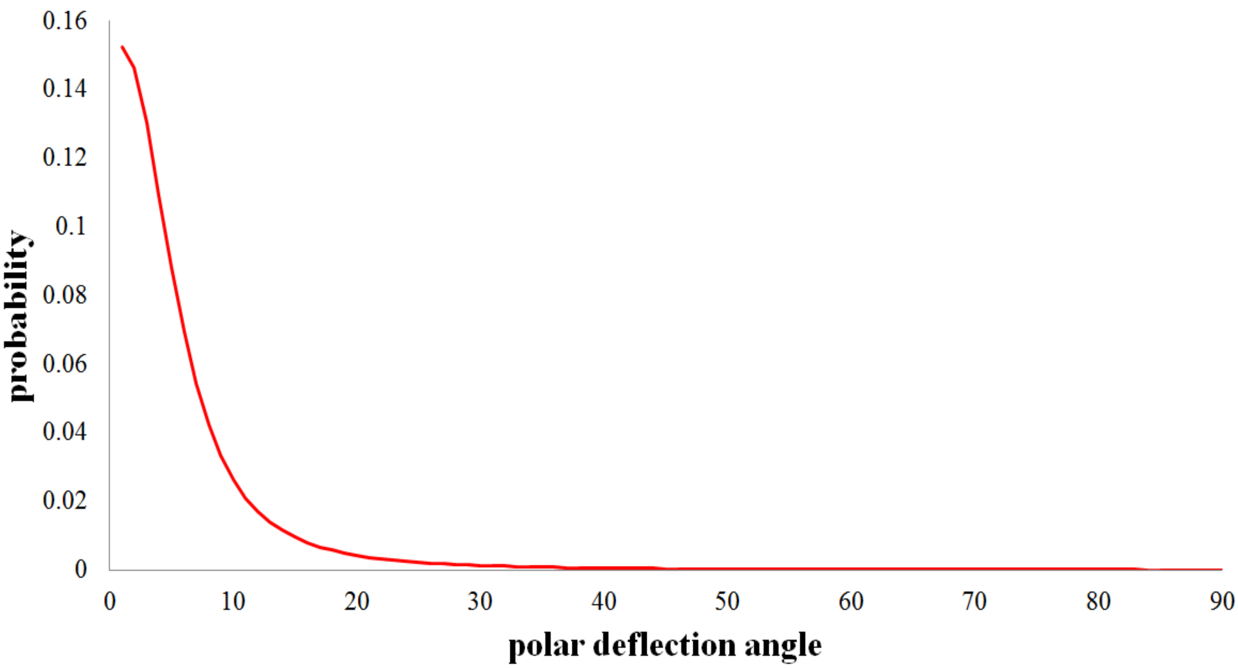

Figure 51. The Henyey-Greenstein phase function for anisotropy coefficient of 0.9

where g is the anisotropy coefficient, ranging from -1 to 1. When g=1, light is only deflected at $0°$ and the probability of light getting deflected at any other angle is zero, in other words, no light is scattered. For g=-1, all light deflected at 180° and g=0 represents an isotropic material that diffuses light in all directions equally. To avoid back reflection, the anisotropic factor should be close to 1 and it was set to g=0.9. The probability of scattering versus polar deflection angle is shown in the Figure 51.

The scattering properties were chosen such that the light distribution from the simulation and the measurement matches closely. We set the scattering coefficient to be $0.5/\mathrm{mm}$. Since the thickness of the K12 is 4 mm, light would be scattered with the probability of 86.46%.

$$P_s = 1 - \exp(-0.5 \times 4) = 86.46\% \qquad \textbf{(6-6)}$$

Hence, about 87% of the light rays would be scattering as they go through the sheet. However, as illustrated in Figure 51, the angular distribution of the scattered light is small. For g= 0.9, the average scattering angle is approximately 7°. This is analogous to a bulge with diameter of 5 mm and height of 0.4 mm, which is equivalent to the average surface angle of 10°. This estimated value is also in agreement with the previously mentioned microscope observations. The light profile of the Lambertian light source that passes a K12 diffuser panel with bulk scattering was measured in the TracePro simulation. As it is illustrated in Figure 52, light distribution of modified K12 model with bulk scattering matches well with the experimental measurement and the R-squared value increased to 99.6%. This bulk scattering was used with the K12 sheet in all subsequent ray trace simulations.

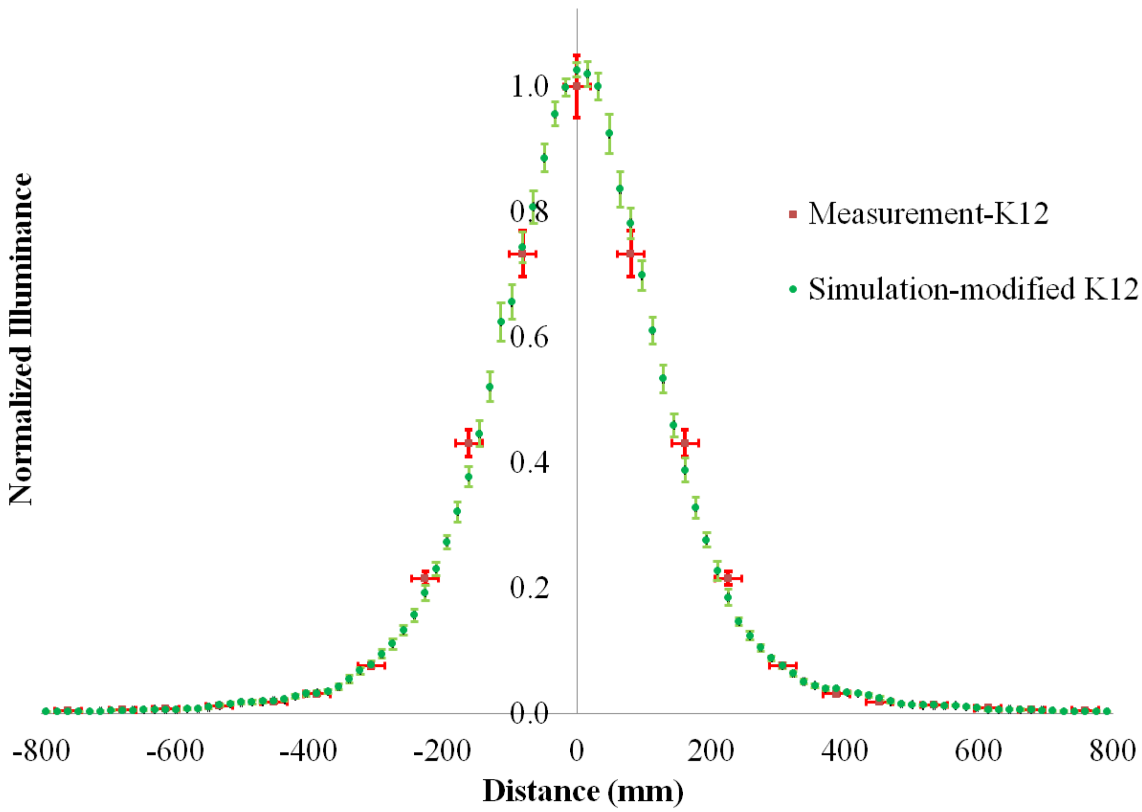

Figure 52. Comparison of experimental measurement and simulation result with modified K12

6.1.5 Error analysis in the simulation

As explained before, the TracePro modeling used in this project used the Monte Carlo method for which the number of simulated rays determines the accuracy of the measurements. To measure the light distribution across a plane, the detector plane was divided into a grid and the light intensity, illuminance, was measured at each pixel. Thus the total illuminance was given by a sum:

$$I = \frac{\sum_{r=1}^{n} E_r}{A} \quad (\mathrm{lux} = \frac{\mathrm{lm}}{\mathrm{m}^2}) \tag{6-7}$$

where E_r is the luminous flux of each ray that strikes the detector and A is the area of the pixel. The error in the measurement is affected by the size of the pixel. If the intensity varies largely across the pixel, the uncertainty in the measurement increases. This argues for decreasing the size of pixels to an extent that the intensity in one pixel varies only negligibly from its neighbour. However, the uncertainty also depends on the number of rays in each pixel. To decrease the random fractional error, the area of each pixel should receive a significant number of rays. Clearly, a compromise is required.

Satisfying the two conditions at the same time requires a large computation space and time, thus one must carefully choose the number of rays and size of pixels to get a reasonable uncertainty. To reduce the noisy fluctuation in the light profile function in Figure 49 to Figure 52, pixels with a width of 16 mm by 16 mm were chosen. To calculate the uncertainty, the variation of intensity across each pixel was studied. To do so, each pixel was sub-divided into 16 smaller pixels, Figure 53.

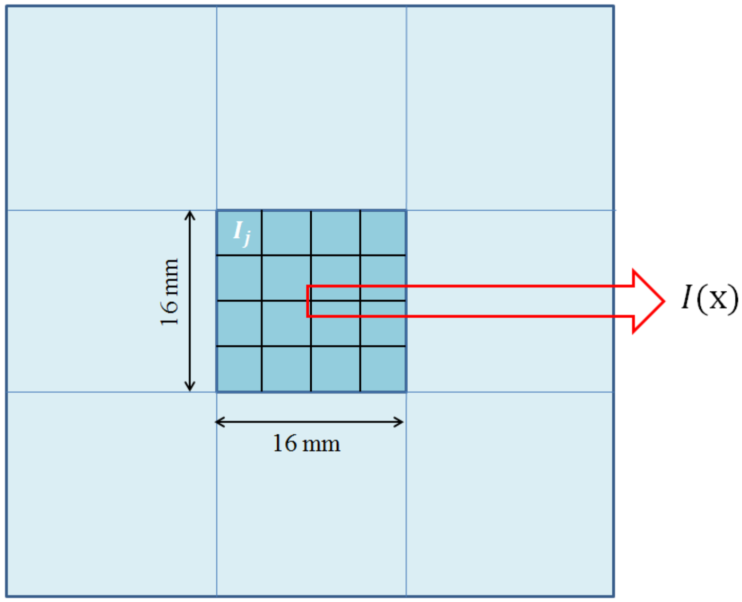

Figure 53. Each small detector is pixelated into smaller pixels

The intensity at each pixel is calculated as the average of intensity in the smaller pixels:

$$I = ave\,(I_j) = \frac{\sum_{j=1}^{n} I_j}{n} \qquad (6\text{-}8)$$

The uncertainty in the measurement is calculated as follow:

$$\Delta I = \frac{\sigma}{\sqrt{n}} = \sqrt{\frac{\sum_{j=1}^{n}(I - I_j)^2}{n^2}} \qquad (6\text{-}9)$$

where σ is the standard deviation of illuminance at each sub-pixel and describes the variation of I_j from the average value. The fractional error at each pixel is defined as $\Delta I/I$. The amount of fractional error depends on the uniformity of light distribution at each small detector, which depends on the number of rays that strike each pixel. For a Lambertian light distribution, where the intensity drops over the distance, the number of rays and the fractional error increase at further pixels, as illustrated in Figure 52. To obtain an accurate light distribution where the variation occurs smoothly over distance, an adequate number of rays must be chosen in the modeling. The simulation was repeated for different number of rays up to a point where the average fractional error of all pixels across the detector was about 5%, which is less than the contrast sensitivity range of the human eye, typically 20% for most people. In this particular measurement, the fractional error for the central pixel was less than 0.6% and around 14% for the pixels at the tail of the distribution.

As the optical performance of each element in the light guide was measured separately, the performance of the light guide was studied using the output light of the concentrator. The efficiency of the light guide was measured as the ratio of the output light to the input light and was determined to be around 77%. The simulation result showed that almost 20% of the energy is absorbed in the light guide by different materials such as the reflective walls, the prismatic microstructured film and the diffusers. Also 3% of the energy returns to the entrance and exits the pipe and is lost there. The next section briefly describes the error analysis in the simulations. The light distribution of the light guide inside the building was also studied and is described in the next section.

6.2 The light distribution in the building

One of the limitations of previous sunlighting systems was their inability to both distribute sunlight deep within the building and illuminate the work plane uniformly. This is an important factor in lighting quality and therefore it was studied for the Two-Stage Core Sunlighting System. Sunlight is distributed via the light guides in the building and thus they should resemble the luminaire which are commonly used in the office area. In order to simulate an office environment, the light guides in the simulation were spaced 1.5 m apart and the light distribution was measured inside a virtual office.

The size and shape of the offices vary from one building to another, thus a standard module, which resembles a slice of the building, was chosen to simulate the light distribution. Each lighting module is 1.5 m wide and is illuminated with one light guide. The module is 15 m long, which is the maximum distance that the CSLS is typically expected to provide sunlight within the building. The module parameters are set such that it represents a portion of the building, and side-by-side modules simulate the light distribution in a larger area, Figure 54.

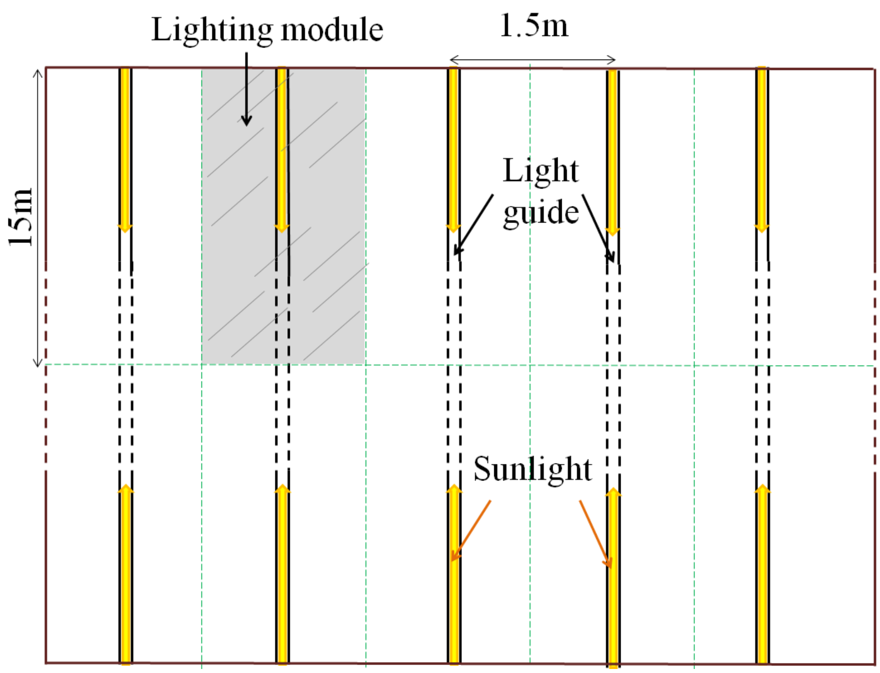

Figure 54. A simulated open office area is divided into imaginary smaller lighting modules; light guides are fed with sunlight from both sides of building

To make this module a realistic simulation of a larger office area in the building, an appropriate reflectance characteristic was applied to the surfaces. The side walls in the lighting module are imaginary and transparent, thus the light from neighbour light guides contributes to the light distribution at each module. This is optically identical to having mirror walls with 100% specular reflectance. However, the actual offices have some side walls that have to be taken into account. Thus, the walls of the module have to have the characteristics of both transparent wall (100% specular reflectance) and a typical white wall (70% diffused reflectance and 30% absorption). A reasonable middle ground was assumed and the side walls of the module were assigned 85% of the properties of the transparent walls and 15% of properties of the white wall. Thus the specular reflectance of the wall is 85%, diffusely reflectance is 10.5% and the absorption is around 1.5%. The ceiling is assumed to be 80% diffused reflective and 20% absorptive, similar to a ceiling in a typical office, and the floor is 20% diffuse reflectance and 80% absorptive, again similar to typical real-world conditions.

To model the light distribution inside the module, it was coupled with a redirector, concentrator and light guide, as shown in Figure 55, and the light distribution was measured at the work plane, which is 1 m above the ground. The ratio of light that can be delivered to the work plane over the light output of a luminaire is defined as the coefficient of utilization, CU, and it depends on the angular distribution of the light source, properties of surfaces and the geometry of the room [18]. For a room with large absorption in the walls, CU is smaller than 1. However in a room with highly reflective walls, light undergoes many reflections before being absorbed, thus the CU may become larger than 1, as in the described module where the coefficient of utilization was determined to be 1.16.

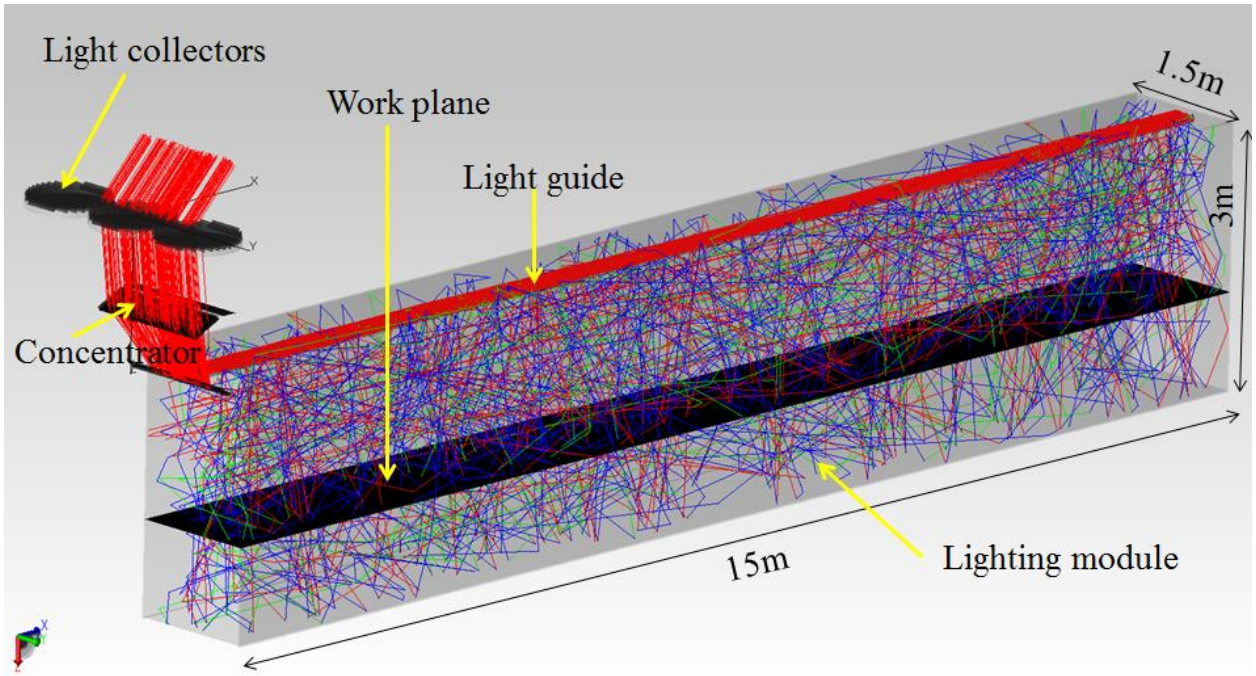

Figure 55. Two-Stage Core Sunlighting System captures sunlight at rooftop and delivers it to the building core

The uniformity of light distribution at the work plane is another important factor in the lighting quality. Large variations of light intensity over a short distance can cause visual discomfort and are unpleasant. The simulation results showed that the variation of light intensity is less than 17.6% across the module and less than 12.6% along the module. Depending on the task which is done at each space, a certain level of uniformity is required. The uniformity is defined as the ratio of the lowest illuminance over the mean illuminance at the evaluated surface. According to the Illumination Engineering Society standard, for an offices space where people carry out computer and paper based tasks, uniformity of 0.6 is required, whereas the uniformity of light in the lighting module is measured to be greater than 0.8 [57]. The illuminance distribution along the module at the work plane in the module is shown in Figure 56 for 30°N during summer solstice at both 9:00am and noon (the illuminance map at 3:00pm is identical to

9:00am, so it is not shown here). The light distribution within the module remains quite uniform during the course of the day, and the only thing that changes slowly is the average illuminance level.

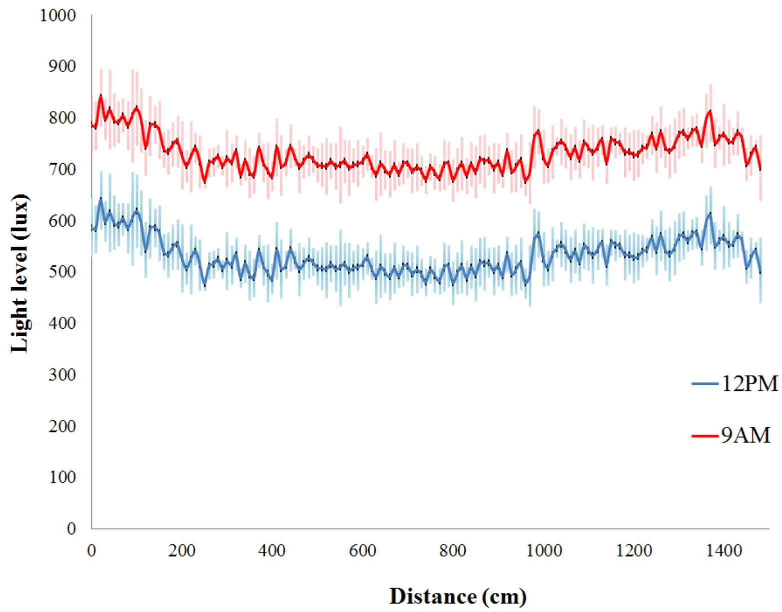

Figure 56. Light distribution along the module for 30° N at 9 AM and 12 PM of Jun 21st

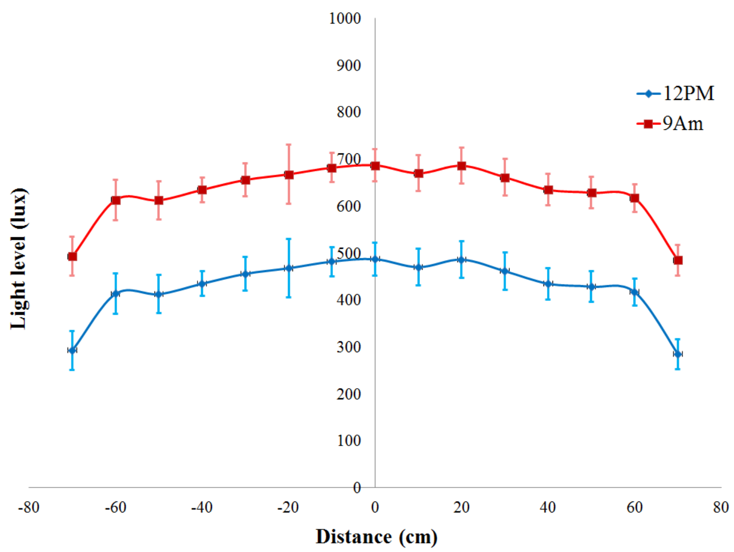

Figure 57. Light distribution across the module for 30° N at 9 AM and 12 PM of Jun 21st

Figure 57 shows the light distribution across the module. The small fluctuations in the graph are due to insufficient number of rays. (It would take excessively long time and large processing memory to increase the number of rays further, and this would not substantially change the overall result). The lighting module represents a slice of the building, thus repeating the light distribution of one module side by side represents the light distribution over a larger area.

6.3 The overall efficiency of the two-stage core sunlighting system

Once the efficiency of each component was evaluated separately, the overall efficiency of the system can be calculated, which is the fraction of the light captured by the redirector that can be delivered to the room. The expected efficiency of the system is the multiplication of efficiency of each component:

$$Eff = A_C \times E_c \times E_P \times CU \tag{6-10}$$

where A_C is the ratio of light that strikes each unit of the concentrator, I_1, to the light that is redirected by the redirector, I. The efficiency of the concentrator is E_c ($E_c = \frac{I_2}{I_1}$), and E_P is the efficiency of light guide ($E_P = \frac{I_3}{I_2}$), and CU is the coefficient of utilization, ($CU = \frac{I_4}{I_3}$). Multiplying all these values from previous measurements, the overall efficiency of the system is approximately 30%. The overall efficiency of the system was also measured by simulating the whole system together for a few chosen sun positions, as shown in Figure 58, and the result was in agreement with the expected value of 30% that was achieved using Equation (6-10). As illustrated in Figure 59, the light that is captured by 1 unit of redirector (1 m-diameter) is distributed equally between two floors.

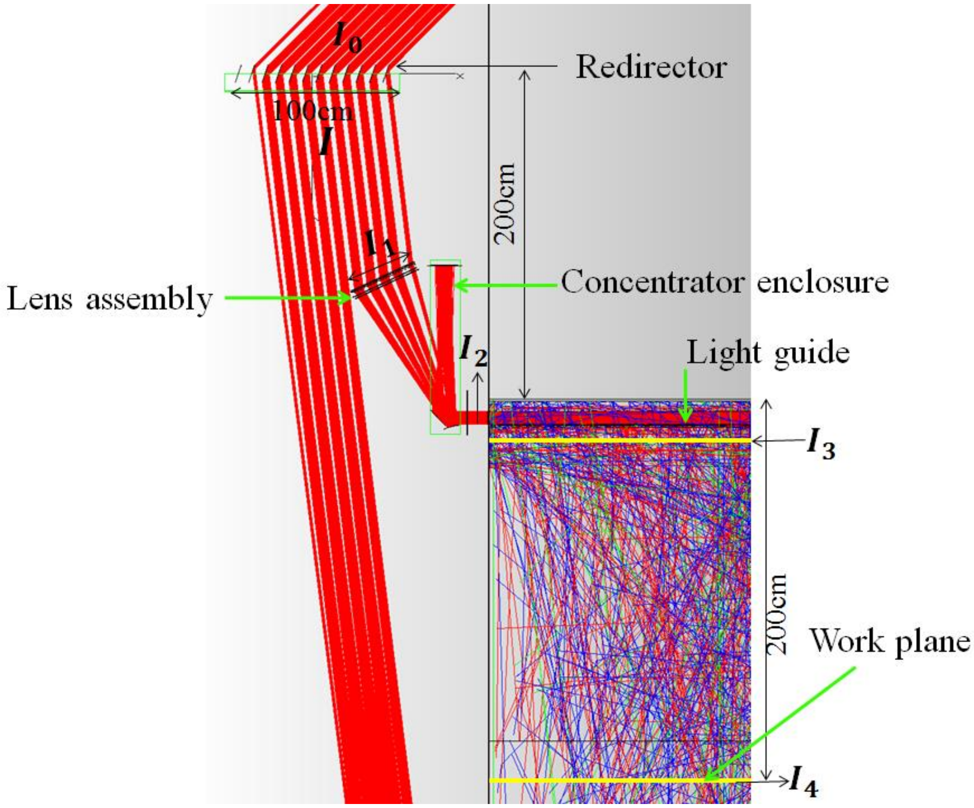

Figure 58. Two-Stage Core Sunlighting System captures sunlight and delivers it to the work plane

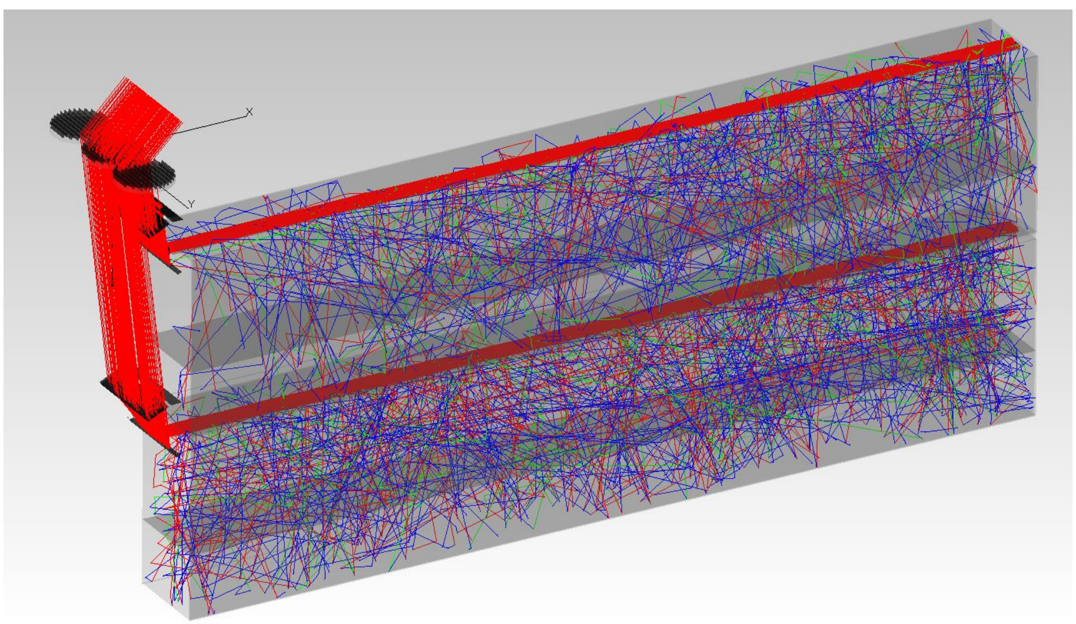

Figure 59. The Two-Stage Core Sunlighting System illuminates two floors with sunlight

6.4 Electrical lighting supplement

To make sure that the lighting level does not drop below the required level, the light guide is equipped with dimmable electrical lighting that can supplement sunlight when necessary. To provide a uniform light distribution along the light guide, different types of electrical light sources may be used. In this modeling, a 2.5 cm wide LED strip was used. The LED strip was equipped with 4 rows of LEDs side by side with 24 LEDs in each segment (each segment is 55 mm long). The output of the LED strip provided 2125 lm/m. To avoid visual discomfort caused by glare, the LED strip was placed on the bottom surface of the light guide, pointing upward. The LED strip was powered by a dimmable power supply that could set the output of the LED to an appropriate value depending on the available daylight level.

To ensure that the electrical lighting reproduces a light distribution similar to daylighting, the light guide was modeled in TracePro using a light source that resembles the LED strip. The LED that was used has a Lambertian light distribution with the maximum output of 2600 lm/m. This is equivalent to a surface light source with the same dimensions and the same light distribution. It was established in the simulation result that this lighting module provides an illuminance of 500 lux purely with electrical light source. As the light distribution was measured in a module that is purely illuminated with the electrical light source, the light distribution was determined to be similar to Figure 56 and Figure 57 along and across the module at the work plane.

6.5 Experimental verification of the simulation result

Construction of all optical components of the Two-Stage Core Sunlighting System and testing the performance with sunlight was beyond the scope of the research project. However, it was decided to compare some simulation results with experimental observations to help establish greater confidence in the ray trace model. Thus as a complementary project, we set up and conducted an experiment to study the light distribution of the output of an already existing light guide using an electrical light source and the results were compared with simulation results. The light guide, which was already installed in the laboratory, was equipped with an LED strip and the light distribution was measured both along and across the light guide at the work plane. A similar setup was modeled in TracePro and the light distribution of the simulated system was compared with photometric measurements.

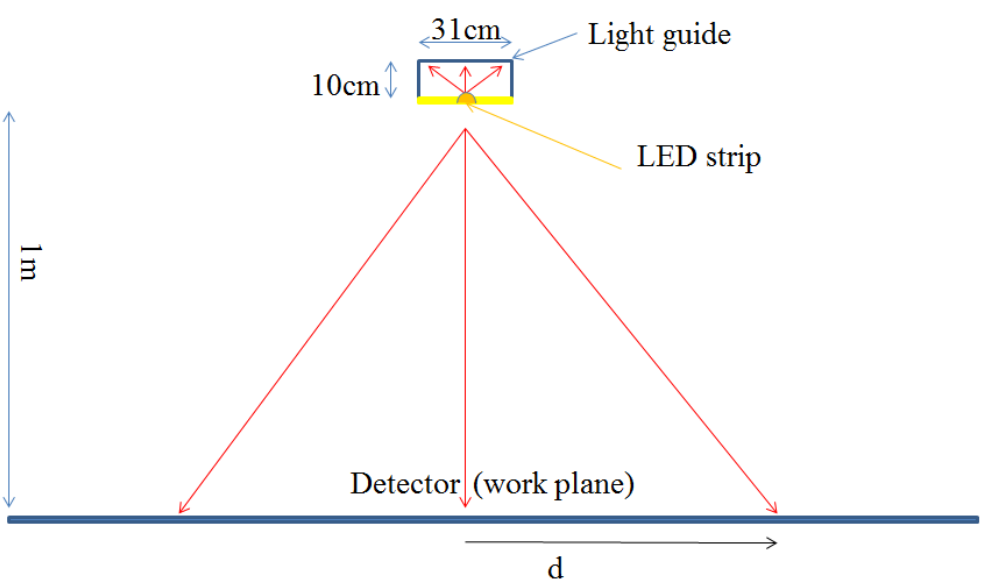

Figure 60. The experimental set up to measure the light distribution (cross sectional view)

Two LED strips with the maximum output of 2600 lm/m, each 4m long, were mounted in the 8 m long light guide. This dimensions of this light guide slightly vary from the one implemented in the Two-Stage Core Sunlighting System; it has 31 cm by 10 cm cross section. These dimensions were modeled in TracePro. The illuminance distribution was measured below the light guide at the work plane, as shown in Figure 60. The work plane is usually considered 1.5 m below the luminaire but due to some spatial limitations in the lab, the light intensity was measured at plane 1 m below the light guide.

The light guide was installed approximately in the middle of a 13 m by 8 m laboratory. This situation was also modeled in TracePro, with 50% diffusely reflective walls and 20% diffusely reflective flooring. Figure 61 represents the normalized illuminance distribution across the work plane, in a direction perpendicular to the guide, as it was measured and simulated. As illustrated in Figure 61, the light distribution of the simulation and measurement agree well with the R-squared value of 99.7%, which indicates high precision.

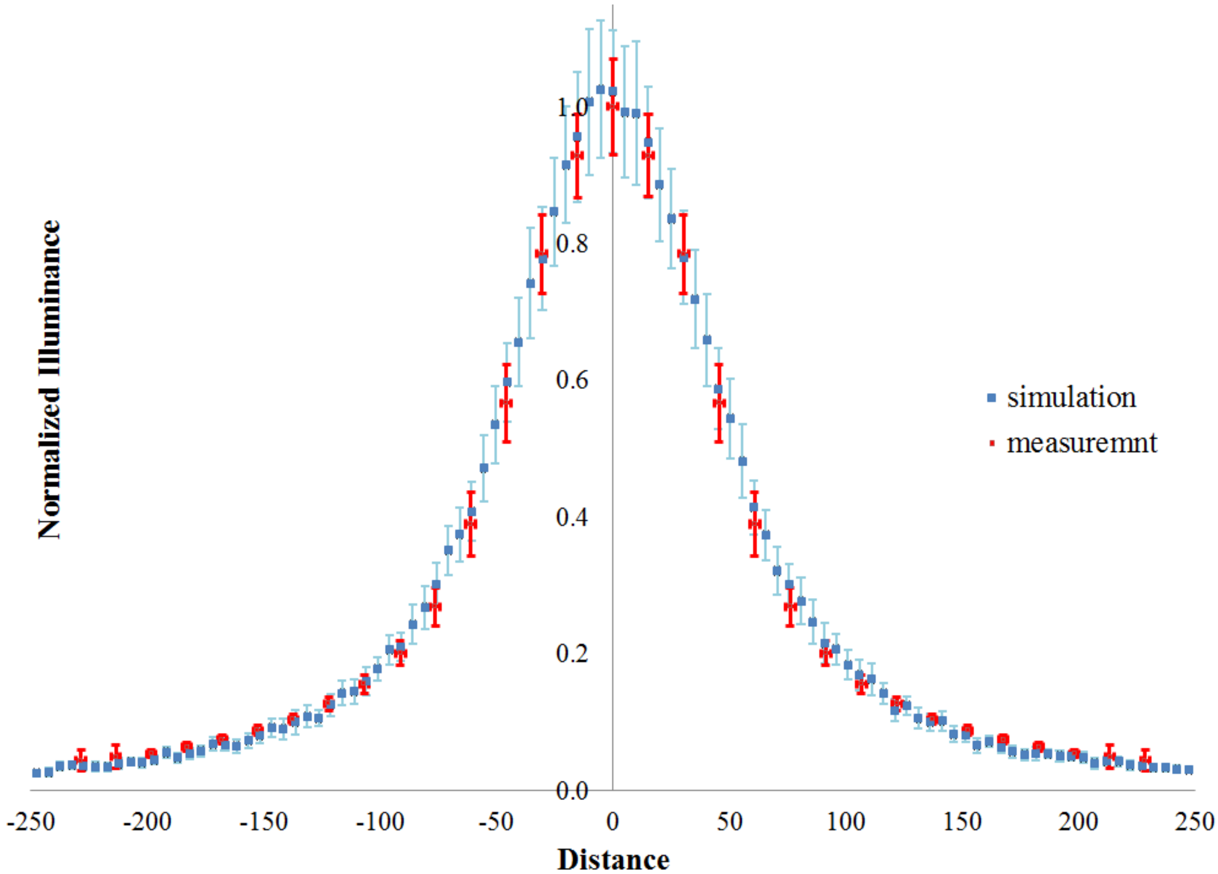

Figure 61. Comparison of light distribution at the work plane in simulation and experimental measurement

The simulation results provided in this chapter and the previous one showed that the Two-Stage Core Sunlighting System can effectively capture enough light to illuminate a multistory building with 30 m wide building plate at 500 lux. The simulation also shows that a uniform light distribution can be achieved using light guides equipped with an electrical light source, as shown in Figure 56 and Figure 57. However, it is important to know if the annual energy saving of the system can approximately compensate for the upfront cost and embodied energy of this system. The next chapter discusses these questions.

Chapter 7: Energy savings calculation

One important consideration in the field of sustainability is the energy saving of one product in comparison to alternative technologies. Although sustainable technologies focus on the use of energy efficient resources, they sometimes fail to save enough energy to compensate for their embodied energy and upfront cost. For this reason, an energy saving analysis was carried out for the Two-Stage Core Sunlighting System, in order to assess the total amount of sunlight that the system can provide for the building throughout the year, thus replacing electrical lighting and the value of the associated energy savings. The availability of sunlight varies considerably by latitude and geographical location, and therefore the result of the energy saving analysis is different for different locations. The previous chapter described the calculated efficiency of the redirector for different solar altitudes and azimuthal angles. In this chapter the amount of sunlight that can be delivered by the Two-Stage Core Sunlighting System is calculated for different locations throughout the year. This analysis helps us to determine where and when the Two-Stage Core Sunlighting System can provide enough sunlight for the building to justify its use, both economically and with respect to overall energy savings.

7.1 Sun position calculation

Using an excel document from the National Ocean and Atmospheric Administration Research Centre [58], the solar altitude and azimuthal angles were calculated for a few typical places throughout the year. Combining these calculations with the efficiency matrix of the redirector, Table 3, it is possible to calculate the efficiency of the Two-Stage Core Sunlighting System throughout the year for these locations.

The maximum elevation of the sun depends on the latitude. For latitudes between 0° to $\pm 23.5°$ the sun reaches the maximum solar altitude of 90° two times a year, once in the spring and once in the summer. For latitudes larger than $23.5°$ the maximum solar altitude is reached at summer solstice and can be calculated as followed:

$$\alpha_{max} = 90° - (latitude - 23.5)° \tag{7-1}$$

The redirector type is also defined based on the solar calculation. When the solar altitude angle is larger than 55°, the efficiency of double reflection mode exceeds the efficiency of the single reflection mode. However, for locations with latitude higher than $40°$, the solar elevation barely reaches that angle and the double reflection mode cannot significantly improve the performance of the redirector. Thus the less complicated single stage redirector should be used in those locations.

7.2 Sunlight captured by a unit of redirector

To calculate the amount of sunlight that can be delivered to the building throughout the year, the amount of light that each unit of redirector can capture was estimated at different locations and different time of the year, assuming that the illuminance of bright sunshine is about 100,000 lux. As an example, Figure 62 to Figure 64 represent the luminous flux of the captured light by a 1 m diameter redirector both for single reflection mode and double reflection mode. The graphs show luminous flux during the spring equinox[2], summer solstice and winter solstice respectively for a typical place at 30°N, for example Phoenix.

[2] Autumn equinox is identical to spring equinox

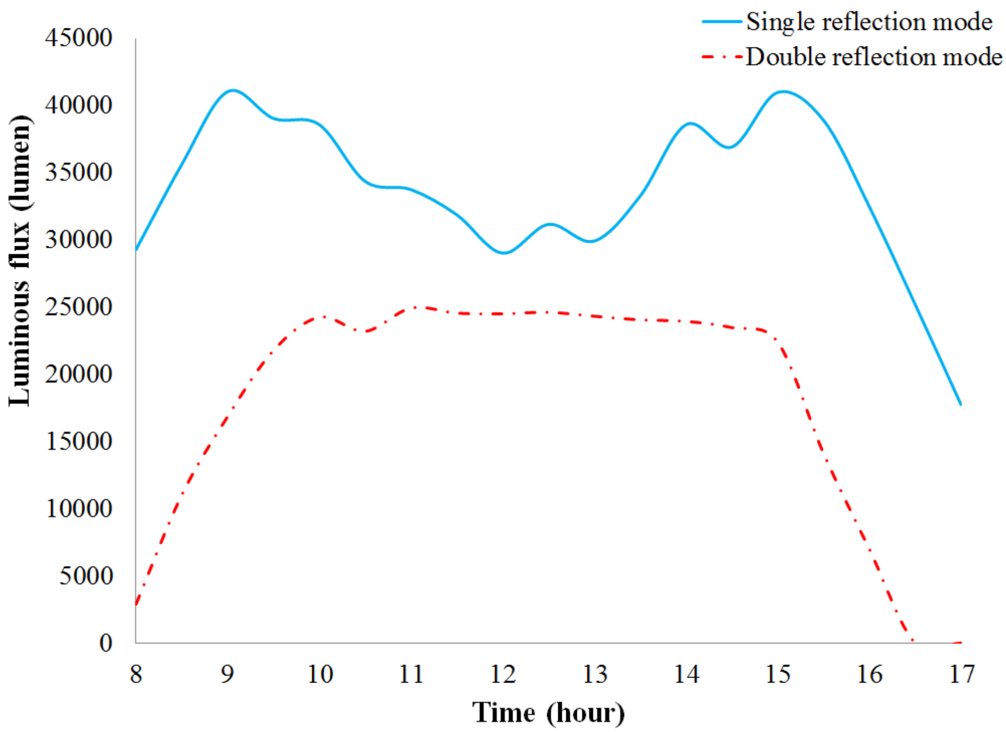

Figure 62. Luminous flux of light captured by one redirector unit during spring equinox at 30° N (identical to autumn equinox)

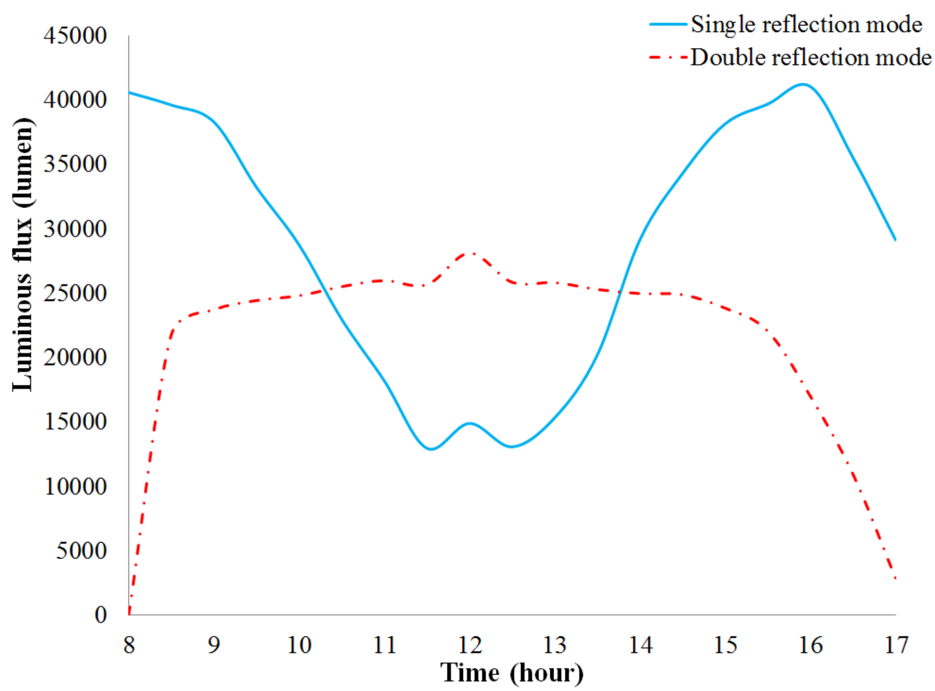

Figure 63. Luminous flux of light captured by one redirector unit during summer solstice at 30°N

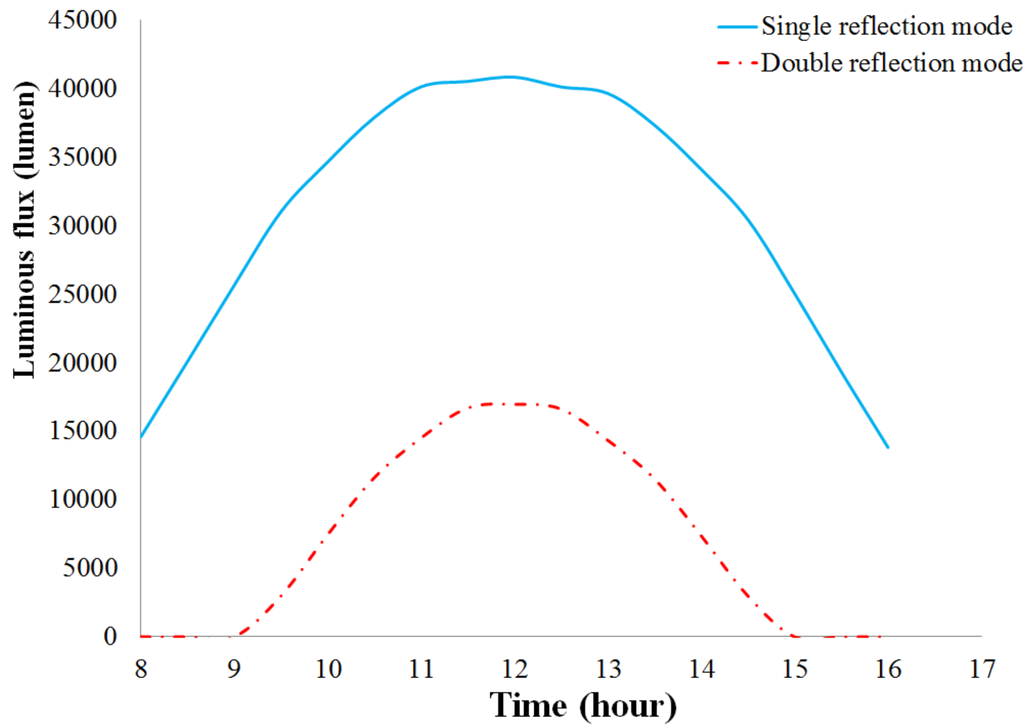

Figure 64. Luminous flux of light captured by one redirector unit during winter solstice at 30° N

Based on the Illuminating Engineering Society standard, it is required to provide on average 500 lux for offices where people carry out computer and paper based tasks [59]. According to the previous calculation, 30% of the light that is captured by the redirector is delivered into the 22.5 m^2 module. This means that each redirector unit needs to capture at least 22,500 lumens to illuminate the lighting module purely with sunlight.

As illustrated in Figure 62 and Figure 63, the light captured by the single reflection mode is sometimes below 25,000 lm. Switching to the double reflection mode during that time boosts the performance of the system and almost doubles the daylighting level. For a typical location at 30° N, this mainly happens during spring and summer days.

7.3 Luminous flux delivered to the office

To assess the practicality of the Two-Stage Core Sunlighting System, it is important to know how much light can be delivered into the building and what fraction of the building can be illuminated purely with sunlight. The amount of light that can be delivered to the work plane, which is the total luminous flux delivered to the module divided by the area of the module, was calculated for different places throughout the year.

Figure 65 represents the average illuminance level for a typical place at 30° N during equinox and solstices. During sunny spring and summer days, the Two-Stage Core Sunlighting System can provide enough sunlight to illuminate the building. However, during small portions of autumn and winter days, some electrical lighting is required to supplement daylight. As shown in Figure 65, for some portion of the day, the delivered illuminance level may exceed the required 500 lux. It is likely that most occupants will find this higher light level pleasant, provided that it does not cause glare and that the transition between different light level occurs gradually. However, if requested, a few of the light redirectors can be turned off for that portion of the day to maintain the 500 lux light level.

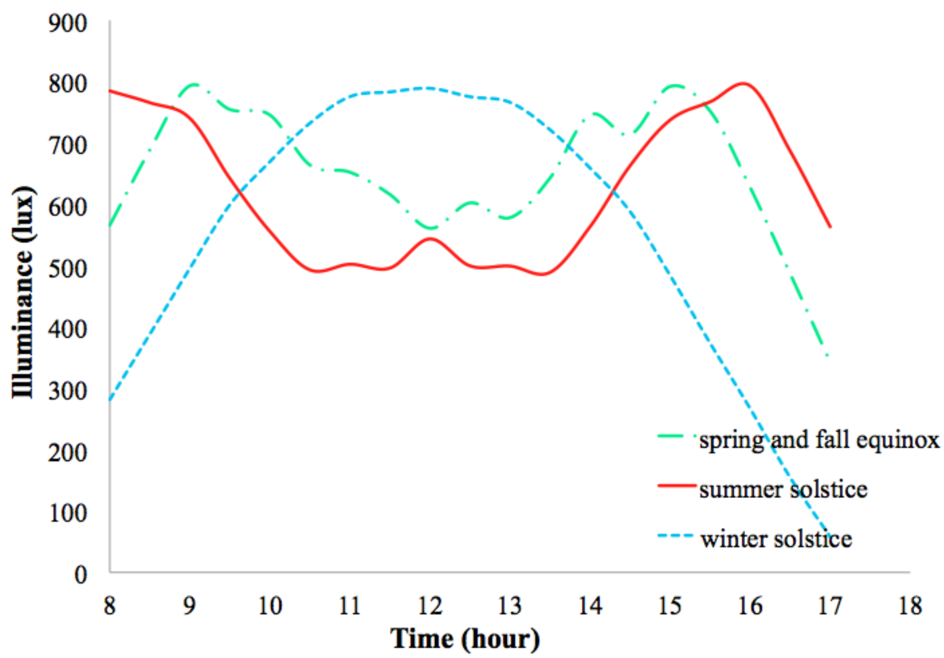

Figure 65. Average available sunlight at the work plane during the day at 30°N

The light captured by the redirectors is distributed uniformly between multiple floors. In this specific design, the redirector unit, 1 m diameter, provides at least 500 lux for two floors, 30 m^2. In many installations it would be practical to have a 3 m wide redirector positioned at the roof edge, which would provide light for six floors of the building. Considering the fact that about 50% of commercial buildings in the US have between two and nine floors [60], the Two-Stage Core Sunlighting System can serve a sizeable fraction of the existing commercial building stock.

The Two-Stage Core Sunlighting System can deliver sunlight 15 m deep into the building core. As illustrated in Figure 54, the light collectors of the Two-Stage Core Sunlighting System are installed along the building perimeter and captures light from two sides of the building, thus the Two-Stage Core Sunlighting System can potentially illuminate a 30 m wide building with any length. The ability of the Two-Stage Core Sunlighting System to illuminate a large multi floor building is one of its main advantages over previous daylighting technologies.

7.4 Energy savings for selected cities

All the calculations in the previous section are for unobstructed sunlight, and of course weather conditions and sunshine probability must also be taken into account. The Two-Stage Core Sunlighting System cannot concentrate diffused light and electrical lighting is required under overcast conditions.

The electrical lighting energy load for a typical office area, which is illuminated with fluorescent lamps at 500 lux, is $11\ \mathrm{W/m^2}$. Considering the average of nine working hours per day, the daily electrical load of lighting for a building that is mainly illuminated with electrical lighting is about $99\ \mathrm{Wh/m^2}$. For a building that also uses daylighting for illumination, the electrical load of the building can also be calculated, based on the amount of sunlight that can be provided for the building throughout the day. The daily electrical energy load per square meter was calculated for 3 days throughout each month and then averaged to estimate the electrical energy load during the month, EL_{ave}. Thus, the average energy savings per day at each month, E_{day}, is calculated as:

$$E_{day} = 99 - EL_{ave}\ (\frac{\mathrm{Wh}}{\mathrm{m^2}}) \tag{7-2}$$

Accordingly, the average energy savings per month is derived as follows:

$$E_{month} = E_{day} \times days\ \times sunshine\ probability \tag{7-3}$$

Equation (7-3) does not take into account variations in the sunshine probability throughout the day. Data regarding these variations in sunshine probability were not readily available for the selected locations studied here. However, these variations would have a comparatively small effect and would not substantially change the overall conclusions based on the reasonable approximations presented here.

The sunshine probability of each city was determined from data provided by the National Climate Data Centre at the National Oceanic and Atmospheric Administration [61]. The average annual energy savings was estimated for five different cities: Honolulu, Chicago, Phoenix, Los Angeles and Vancouver. The annual savings were estimated for a typical 6 floor building ($3600\ \mathrm{m}^2$) in five cities in North America, where the cost of electricity varies from 0.07 $\$/\mathrm{kWh}$ in British Columbia to 0.37 $\$/\mathrm{kWh}$ in Hawaii [62] [63]. The $\mathrm{CO_2}$ reduction was also calculated using the average greenhouse gas emission factor in each region, which varies from 12 kg $\mathrm{CO_2}/\mathrm{kWh}$ in Vancouver, to 735 kg $\mathrm{CO_2}/\mathrm{kWh}$ in Hawaii from the US Environmental Protection Agency [64]. A summary of the calculation results for the selected locations is provided in Table 4.

The electrical energy saving calculation was done assuming fluorescent lamps are used for illumination. The average luminous efficacy of a fluorescent light bulb is 90 $\mathrm{lm/W}$ [10], where luminous efficacy of a light source is the amount of visible light that is produced per input power. However, the electrical energy loading for LED lighting would be less and depends on the type of the LED. The luminous efficacy of LEDs is on average 100 $\mathrm{lm/W}$ for warm LEDS and 150 $\mathrm{lm/W}$ for cool LEDs [65]. Thus the energy saving for the warm LED would be almost same as fluorescent light bulb and 40% less for cold LED.

	Chicago	Honolulu	Los Angeles	Phoenix	Vancouver
Latitude	41.8°	21.3°	34.0°	32.2°	41.8°
Annual Sunshine Probability	55%	70%	75%	85%	40%
Annual Electricity Saving $(\frac{\text{kWh}}{\text{m}^2})$	15	20	20	25	10
Total Annual Electricity Saving (MWh)	50	75	75	90	40
Electricity cost $\left(\frac{\$}{\text{kWh}}\right)$	0.10	0.37	0.16	0.11	0.07
Total Annual saving ($)	5,000	27,500	12,500	10,000	3,000
CO_2 emission factor $\left(\frac{\text{Kg Co}_2}{\text{kWh}}\right)$	681	735	277	611	12
CO_2 Reduction $(10^6\ \text{Kg Co}_2)$	40	55	20	60	0.5

Table 4. Energy saving analysis of the Two-Stage Core Sunlighting System for five selected cities

In addition to enhancing the lighting in the building, the Two-Stage Core Sunlighting System can also impact the energy performance of the building indirectly in other ways. For example, about 19% of the electrical load in the building is allocated to air conditioning [12], and this can even increase further due to electrical lighting. All electrical light sources, even the most efficient ones, have large heat loss. The fluorescent lamps and LEDs are far more efficient in comparison to the incandescent, however their efficiency typically does not exceed 25% and approximately 75% of the input energy is lost in the form of heat [65]. Thus, all electrical light sources increase the inner temperature of the building and eventually increase the air conditioning energy load of the building. (In very cold climates this would not necessary represent an overall reduction in energy use for the building, because the reduction in heat caused by turning off electric lights would have to be offset by an increase in energy required by the heating source for the building. However, in most climates buildings require air conditioning year round, and so the reduction in heating provided by electric lights reduces overall energy use year round.)

In contrast, the Two-Stage Core Sunlighting System does not transform energy from one form into the other, thus all the energy that is brought into the building is used for illumination, since the infrared part of the light that can increase the inner temperature can be filtered out in summer days. This reduces the air conditioning energy load of the building. Thus, it can be inferred that whenever air conditioning is required (which is most of the time in most climates), the actual energy saving in the building will be approximately 20% higher than those shown in Table 4.

In other daylighting methods, such as those requiring increased glazing area, the electrical energy load of building also may be reduced. A case study done for a multi-story building in Chicago shows that 80% of the electrical energy required for lighting can be replaced by daylight in a building with full height glazed envelope. However, the energy usage from other building services, such as heating and cooling, increases approximately 10% and the capital cost increases about 20% [15]. This would substantially increase the economic payback period for that building modification (to about 90 years in that particular case study [15]).

Unlike the full height glazed building, the Two-Stage Core Sunlighting System does not negatively impact the energy performance of the building and does not require more energy for heating and cooling. In addition, the upfront capital cost and the operation cost of the Two-Stage Core Sunlighting System is expected to be much less than fully glazed building, which makes the payback time of the Two-Stage Core Sunlighting System shorter.

7.5 Cost evaluation and embodied energy analysis

One important criterion that makes a technology practical and justifiable is its ability to pay off the upfront cost and the embodied energy within a reasonable time period. The embodied energy is the total energy that was used to produce a system, including primary resources, transportation, processing and manufacturing and assembly. The main source of embodied energy in the Two-Stage Core Sunlighting System is the embodied energy of the raw materials, since none of the components require considerable energy consumption in their subsequent manufacturing processes.

The Two-Stage Core Sunlighting System is at an early development stage, thus it is premature to calculate the precise cost of system in large volume production. However, since the system uses standard components, it seems plausible that it can be manufactured at a reasonable cost. The required quantity of material was used to make a rough estimate for the expected eventual cost of the system, where the major expense would be the cost of material. Table 5 presents the cost estimation and energy evaluation for one unit of the redirector with the diameter of 1m.

Elements	Quantity	Commodity price [66] [67]	Cost	Embodied energy of material [68] [69]	Embodied energy
Aluminum Rim	5 kg	2 ($/kg)	10 ($)	8.1 (MJ/kg)	40 MJ
Glass mirror	1 m^2	2-6 ($\$/m^2$)	2-6 ($)	200 (MJ/m^2) (0.5cm thick mirror)	200 MJ
Enclosure glass	2 m^2	2-6 ($\$/m^2$)	4-12 ($)	200 (MJ/m^2) (0.5cm thick glass)	400 MJ
Control system and actuator	1	20-50 $	20-50 ($)	500 (MJ)	500 MJ
Others	20% of other quantities		7-15 ($)		230 MJ
Total			40-90 ($)		1,400 MJ

Table 5. The approximate cost and embodied energy evaluation for one unit of the redirector (1 m diameter)

The final price of the system and the embodied energy was doubled as a rough estimate to include manufacturing and transportation. To provide enough daylighting for a six-floor building, a 3 rows of 1 m diameter redirector is required for two sides of the building. For a 30 m by 20 m building, 120 units of redirector are required. Thus the cost and the embodied energy of the redirector for a six floor building is estimated as followed:

$$\mathrm{Cost}_{\mathrm{LR}} = 120 \times 2 \times (40 - 90) = 10{,}000 - 21{,}500\ (\$) \tag{7-4}$$

$$\text{Embodied energy}_{\mathrm{LR}} = 2{,}800 \times 120 = 160\ (\mathrm{GJ}) \tag{7-5}$$

A similar calculation was done for one unit of the concentrator, 1.5 m wide. The result is summarized in Table 6.

Elements	Quantity	Commodity price [67] [66]	Cost	Embodied energy per unit [68] [69]	Embodied energy
Fresnel lenses	0.8 m^2	5 ($\$/m^2$)	4 ($)	500 (MJ/m^2) (0.5cm sheet)	400 MJ
Prismatic lens	0.4 m^2	5 ($\$/m^2$)	2 ($)	500 (MJ/m^2) (0.5cm sheet)	200 MJ
Aluminum mirror	4 kg	2 ($/kg)	8 ($)	8.1 (MJ/kg)	30 MJ
Shield glass	2 m^2	2-6 ($\$/m^2$)	4-12 ($)	200 (MJ/m^2) (0.5cm mirror)	400 MJ
Others	20% of other quantities		2-4 ($)		250 MJ
total			20-30 ($)		1,500 MJ

Table 6. The approximate cost and embodied energy evaluation of the concentrator

The total system cost was estimated to be twice the material cost, to approximately account for manufacturing and distribution costs. Similarly, the embodied energy of the material was doubled to approximately account for the added embodied energy associated with the manufacturing and transportation process. Each floor requires a separate concentrator that is expanded across the facade. Thus for a 6 floor building, 240 units of concentrator is required.

The cost of the concentrator for a six-floor building is estimated to be around $9,500 to $14,500 and the embodied energy to be around 700 GJ.

Table 7 represents the cost and energy calculation for a 15 m long light guide. The prismatic microstructural film is the only element that adds to the upfront cost and embodied energy of the building, since the other implemented elements, such as electric lighting system and K12 diffuser panel are used in common luminaire as well and does not add anything to the cost of the building. Thus, the prismatic film is the only element that needed to be considered for cost and embodied energy evaluation of the light guide.

Elements	Quantity	Commodity price [66]	cost	Embodied energy per unit [68]	Embodied energy
Prismatic microstructural film	4.5 m^2	5 ($\$/m^2$)	25($)	500 (MJ/m^2) (0.5 cm acrylic)	1,000 MJ

Table 7. The approximate cost and embodied energy evaluation of the light guide

The light guide replaces the ordinary luminaire system, and the cost of making a light guide is similar to that of a typical lighting fixture, hence the manufacturing and assembly process does not add anything to the cost of the building. However, the overall cost and energy was doubled to consider the cost of the light sensors and the controlling systems that are required to control the level of electric light inside the building at the desired level. The light guides are installed 1.5 m apart, thus a typical six floor building, 30 m by 20 m, requires 160 units of light guide. The upfront cost that the light guide would add to the building is estimated around $8,000 and embodied energy is estimated around 350 GJ.

Based on the previous calculation, it is possible to make the Two-Stage Core Sunlighting System at a reasonable price, for the example building, ranging from $25,000 to $45,000, which is approximately ranging from $7 to $12 per square meter. Comparing this with other common construction costs of the building, such carpet or flooring which ranges from $20 to $100 per square meter, this sounds like a reasonable value. The payback time of the Two-Stage Core Sunlighting System depends on the location, since the energy saving varies from one place to another. However, the main target of the Two-Stage Core Sunlighting System are cities with high sunshine probability, similar to Los Angeles with 12,000 $/y saving. Thus, it is reasonable to say the average payback time of the Two-Stage Core Sunlighting System is expected to be around 5 years.

In a typical environment, the Two-Stage Core Sunlighting System would require regular cleaning in order to have maximum performance. The frequency of the required cleaning depends on the air pollution in the target area and more investigation is required to have a clear understanding of how much this impacts the maintenance cost and as a result, the payback time at each location. It is important to note that this cleaning requirement would be the approximately the same for other similar daylighting systems and so this does not represent a limitation for this particular system.

Also, the embodied energy that the system would add to the building is negligible compared to the energy that is spent over structure, envelope, service, construction and etc. of the building,

$4.82\ (\mathrm{GJ/m^2})$ on average [69]. The Two-Stage Core Sunlighting System adds 1,200 (GJ) to the embodied energy of a typical 6 floor building, which is about $0.3\ (\mathrm{GJ/m^2})$ The annual energy savings only from electrical lighting sector in a place like Los Angeles is around 75 MWh which is equivalent to 270 GJ. Thus energy saving from this system can pay off the embodied energy on average in 6 years. A more detailed analysis would differentiate between primary and secondary energy sources, but this additional analysis would not meaningfully change the basic conclusions reached here.

The Two-Stage Core Sunlighting System is at an early stage of development and early product is likely to have higher costs initially. However the rough estimation of the cost and embodied energy provided in this section shows that the Two-Stage Core Sunlighting System has the potential to be widely applied in commercial buildings and provides a practical and sustainable solution to the daylighting problem.

7.6 Comparison with photovoltaic cell as an alternative to daylighting technique

Photovoltaic cells (PV) are one of the most well-known methods for generating electricity using clean, onsite energy. PVs can be provided at almost any size and can be installed on almost any building to supplement part of its electrical needs. In some special cases where a building is entirely off-grid, PV is often considered as the most convenient way to provide electricity. The generated electricity can also be used to illuminate the interior spaces; hence one may wonder if PVs can be considered as a good alternative to other daylighting technique. This is discussed in this section.

Even though PVs use a renewable free source of energy to generate electricity, there are still some concerns about them. The performance of PVs is highly limited by their poor efficiency. The efficiency of commonly used PVs is about 12% [70]. Thus at a typical place like Los Angeles with the average solar irradiance of 460 $\mathrm{W/m^2}$ [71], a 1 $\mathrm{m^2}$ panel can only provide 55 W.

To illuminate a building by solar radiation via PVs, the generated electricity needs to be transformed back to light. One example of the lamp that is commonly used for illumination in office areas is the F32 T8 HCR, which is an efficient fluorescent lamp with the efficacy of 90 lm/W. This means that 1 $\mathrm{m^2}$ of PV cells connected to this fluorescent lamp can only produce 5,000 lm. This number is slightly better for warm LEDs with efficacy of 100 $\mathrm{lm/W}$, and can be up to 65% higher for cold LEDs with efficacy of 150 $\mathrm{lm/W}$. (Note that in most LED luminaires, a combination of both cold and warm LEDs is used, so the overall efficacy would be somewhere in between these two values.) [65]. In a typical office area only 60% of the luminaire output is delivered to the work plane and the rest is absorbed by walls, flooring and other furniture. Thus 1$\mathrm{m^2}$ of PV can only provide enough electricity to illuminate 10 $\mathrm{m^2}$ of building with fluorescent lamp and 14 $\mathrm{m^2}$ with LED lamp, whereas 1 $\mathrm{m^2}$ of Two-stage Core Sunlighting System can illuminate at least 30 $\mathrm{m^2}$ with sunlight at 500 lux. A 1 $\mathrm{m^2}$ PV panel costs about ~ $50- $75 [72], thus using PV to illuminate the building would cost about $4- $7 per $\mathrm{m^2}$ of space, which is slightly less than Two-stage Core Sunlighting System.

As the manufacturing process of the PV improves, the price of PV is expected to become cheaper in the next few years, but there is still a long way to go before this PV-based approach is cost effective in general. There are some more efficient PVs available, but they are more expensive and some of them contain toxic materials that are hard to come by. In addition, the manufacturing process of the PV is highly energy intensive and thus, it is not environmentally friendly. On average the embodied energy of 1 m^2 of PV area is about 5 to 6 GJ [73]. Even though long life cycle of the PV can justify its high upfront cost, it is hard to justify its negative impact on the environment during manufacturing and demolition phase, since not all PVs are recyclable.

In summary, while using solar energy to produce electricity is in principle sustainable, transforming the generated electricity back to light to illuminate the building does not seems to be efficient or appropriate. Moreover, the interior space of the building still has to be illuminated with electrical lighting, which is not as good as natural sunlight in terms of lighting quality. Whereas the Two-stage Core Sunlighting System, provides sunlight to the core of the building for illumination. A comparison of the two approaches is summarized in the Table 8.

	PV	Core Sunlighting System
Cost	4- 7 $/m^2	7-12 $/m^2
Embodied energy	0.3-0.6 GJ/m^2	0.3 GJ/m^2
Area of illumination	10-14 m^2	30 m^2
Expected life cycle	20-30 year	20 year

Table 8. Comparison between PV and Two-stage Core Sunlighting System to illuminate the building

(This comparison is made per unit area of illuminated space within the building)

Chapter 8: Possibilities for improving the efficiency of prismatic light guide film

The Two-Stage Core Sunlighting System developed in this research project was based on currently available optical materials and its performance is therefore limited by their properties. In previous chapters, the design has been shown to have a good potential for enhancing daylighting in buildings, and it is interesting to consider if that potential could be expanded through the use of improved optical materials that might realistically become available in the future.

From this perspective, the most fundamental limitation in a system based on hollow light guides arises from imperfect reflection of light by the prismatic film. The use of prismatic film was important, because it avoided the absorption losses in conventional metallic reflectors, which typically are in the range of 5% to 10% per reflection. In contrast, the micro-prismatic film available today has about 10 times less loss per reflection, which made practical the designs developed in previous chapters. Nevertheless this loss still causes a significant design limitation, because it is difficult to achieve high efficiency of the light guide if each light ray reflects many times as it travels along the light guide. The total number of reflections is proportional to the divergence of the light and inversely proportional to the diameter of the guide. If the loss per reflection can be reduced, then it would become practical to use much smaller light guides, which is highly desirable. Since this could significantly improve the practicality of the system, it is interesting to consider whether there is any hope for this being achieved in the near future.

The causes of light loss in the prismatic film are well-known. There are several practical limitations, and there is also a fundamental efficiency limitation. The practical limitations include bulk absorption in the optical material used in the film, optical imperfections in the surfaces, and imperfections in the shape of the corners. These have been well studied in previous work [47]. The optical imperfections are likely to be reduced over time, and the absorption loss could be reduced by making the film thinner, which would require correspondingly more numerous prisms. Unfortunately that change would increase the one fundamental loss mechanism, which is diffractive energy escape from the prismatic corners. This loss has been well studied [74] and from that work it is clear that diffraction will be non-negligible as prismatic films become thinner.

It has never been proven that this lost light cannot be "recycled" back into the optical structure. In the previous modeling work, the diffractive losses seem to primarily take the form of cylindrical waves radiating from the external prism tips, so it is interesting to consider whether some kind of reflective structure could redirect that escaping energy back into the prisms and thus effectively reduce diffractive loss. For this reason, as a complement to the primary research project described in previous chapters, a very preliminary assessment was carried out to investigate whether such redirection and re-entry of the diffractively emitted light might be possible. The goal of the assessment was to provide motivation for future in-depth research in this interesting area. Although only limited time and resources were appropriate at this stage, it was possible to reach a tentative conclusion as a result of three factors. First, the work already had a strong base. [74]. Second, excellent FDTD software is now commercially available, avoiding the significant computer science challenge present in previous work. Third, the previous work [74] showed that full 3D system behaves, from a diffraction loss perspective, very similarly to the full 2D system. This justified the use of 2D modelling, which in turn made the required level of computational resources manageable for this preliminary study. The results of this preliminary assessment are presented in this chapter.

8.1 Prismatic microstructured film

As described in Section 6.1.1, the prismatic microstructured film contains a linear right angle prismatic structure running parallel to the light guide axis, as illustrated in Figure 46. The prismatic structure gives a dual functionality to the film. If the angular deviation of incident light from the axial direction of the guide θ, is less than the critical angle described in Equation (6-2), it undergoes total internal reflection and is reflected such that it continues to propagate along the guide. Otherwise, it is partially transmitted through the prismatic film and out of the guide.

Prismatic microstructured films are known to be highly efficient in transporting light. For one commonly-used prismatic film, Optical Lighting Film® manufactured by 3M Company [49], about 98% of energy is reflected back to the light guide. However, for a long light guide where light goes under large number of reflection, this small loss accumulates and causes a large energy loss.

Prismatic microstructured films are typically fabricated using a material with a low absorption coefficient, for example acrylic or polycarbonate, in order to minimize the absorption loss in the material. The Optical Lighting Film® measured bulk absorption loss of less than 0.4% for the transmitted ray [74], and in most applications this is considered to be negligibly small.

However, there are two other sources of loss in the prismatic film, which causes energy dissipation.

Ideally, the prism structures in the film should have perfectly sharp corners. However, the shape of the microstructures in commercially available films deviates from a perfect prism to some extent due to the manufacturing process. The tip of the prism is typically slightly rounded or chamfered during the moulding or extrusion process. As illustrated in Figure 66, the rays that strike the side of the prism undergo total internal reflection. However, a light ray that strikes the imperfect tip of the prism escapes the prism and is lost. The manufacturing imperfection is the cause of the major loss in the film. As measured for the commercially available film, prismatic film (with prism spaced ~0.3 mm apart), about 1.5% of light rays is lost due to the optical imperfection [74].

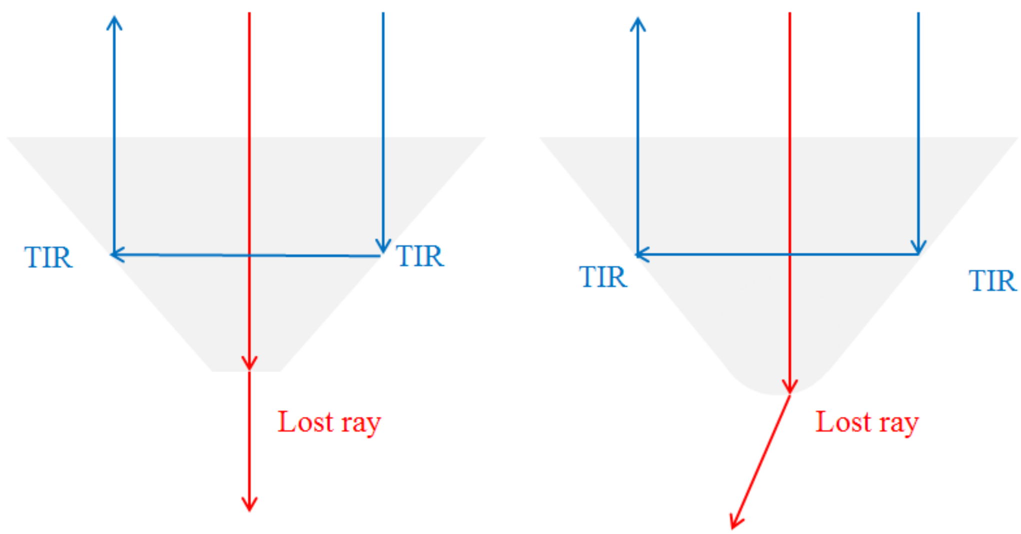

Figure 66. Light rays escape the tip of the corrupted prism

The loss due to optical imperfection can be improved to some extent by improving the manufacturing process. However, the efficiency of the prismatic film is ultimately limited by an intrinsic loss due to diffraction [74]. The diffraction loss is estimated to be much smaller than the other losses, thus it cannot be measured directly. Both the optical imperfection and the diffraction effect cause part of the light rays to exit the light guide, which is not desired. This light may be used to illuminate the building and may not be considered as being truly lost. However, in some applications where the light guide is delivering the light to be used somewhere else, the escaped rays are not used and would only cause energy loss.

Reducing the energy loss is important for the future of the light guides, where it is desired to decrease the thickness of the light guide. To decrease the thickness of the light guide, the concentrator is required to have a larger concentration ratio, which automatically increases the angular divergence of the light beam. Thus, reducing the thickness of the light guide by factor of two, increases the number of reflections at least by factor of 4, since the angular divergence of light, and therefore the average number of reflections, is also increased at least by factor of 2. This increases the energy loss over the light guide. Thus it is important to minimize the amount of the unwanted energy loss in the film. The diffraction loss is quantified in this chapter, in order to assess the possibility of modifying the film to reduce this loss.

8.2 Diffraction loss

The prismatic film is intended to interact with the visible portion of the electromagnetic wave, where the wavelength is comparable to the dimension of the microstructure in the film. Thus, as explained in Section 3.2, the interaction cannot be adequately described using geometrical optics, thus the propagation of light is described by Maxwell equations in physical optics. In this section, the interaction of light with the prismatic film is reviewed.

8.2.1 Total internal reflection

The propagation of electromagnetic waves is described by the frequency, f, and the wave vector of the wave, $\vec{k}$, where the wave vector represents the direction of propagation of light and is perpendicular to the wavefront. The magnitude of the wave number is related to the wavelength, λ as follows:

$$k = \frac{2\pi}{\lambda} \tag{8-1}$$

A point source radiates electromagnetic waves in all directions with a spherical wavefront. However, at a large enough distance from the source, the wavefront approximates a plane, and the deviation of the wave vector from rectilinear is negligible over a small portion of the wavefront, Figure 67. This form of wave is called a plane wave and the electric field propagation is described as follows [75]:

$$\vec{E} = E_0 \exp i(\omega t - i\vec{k}.\vec{r}) \tag{8-2}$$

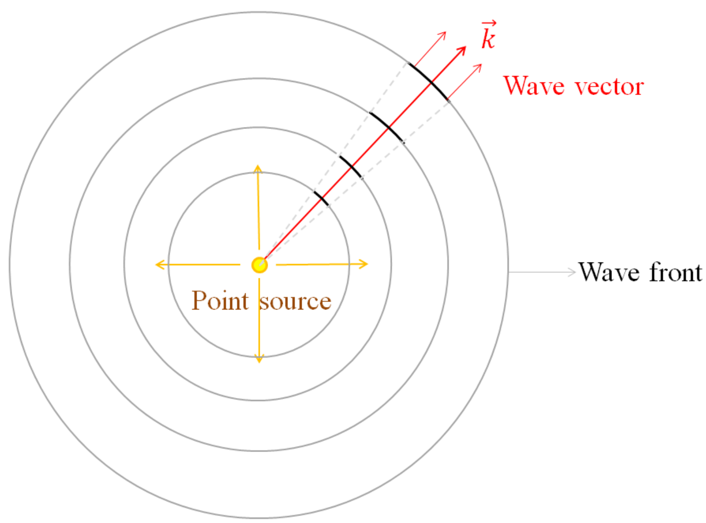

Figure 67. Small portion of point light source at a large enough distance resembles a plane wave

where E_0 is the amplitude of the electric field and $\omega = 2\pi f$. As an electromagnetic wave reaches another medium, a portion of it propagates into the new medium and the rest is reflected back. The angle of the reflected and transmitted waves is derived using Snell's law of refraction [75].

$$n_1 \sin\theta_I = n_2 \sin\theta_T \tag{8-3}$$

$$\theta_I = \theta_R \tag{8-4}$$

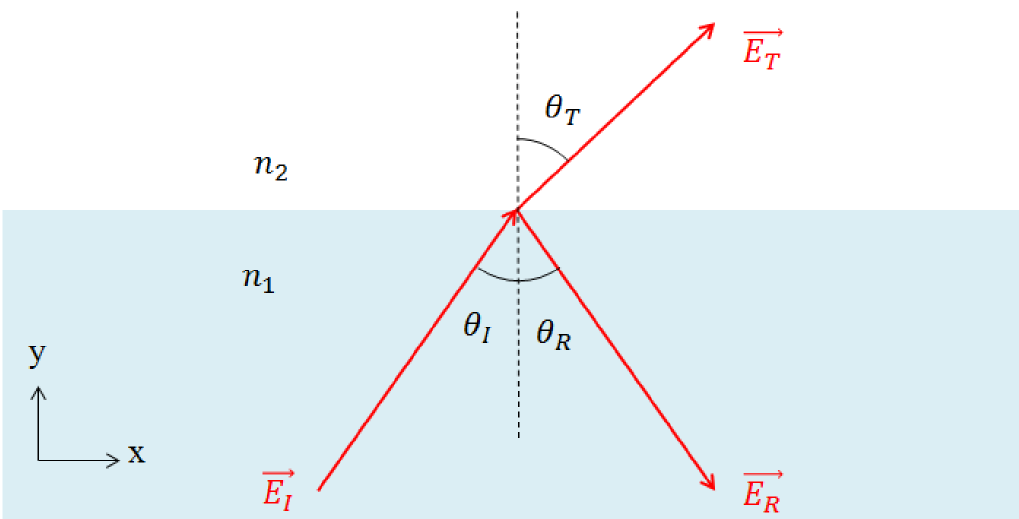

Figure 68. The refraction of light rays as it travel from one medium into another

The amplitude of the transmitted and reflected beams are calculated according the Fresnel equation for a linearly polarized wave [75]:

$$\left(\frac{E_{0R}}{E_{0I}}\right)_s = \frac{(n_1/n_2)\ \cos\theta_I - \cos\theta_T}{(n_1/n_2)\ \cos\theta_I + \cos\theta_T} \tag{8-5}$$

$$\left(\frac{E_{0R}}{E_{0I}}\right)_P = \frac{-\cos\theta_I + (n_1/n_2)\ \cos\theta_T}{\cos\theta_I + (n_1/n_2)\ \cos\theta_T} \tag{8-6}$$

where *s* represent perpendicular polarization and *p* stands for parallel polarization. The coefficient of reflection, R, is defined as ratio of the intensity of the reflected beam to the intensity of incident beam [75]:

$$R = \left(\frac{E_{0R}}{E_{0I}}\right)^2 \tag{8-7}$$

For a non-polarized wave, the coefficient of refraction is calculated as the average value of perpendicular and parallel polarized wave [75].

$$R = \frac{R_s + R_p}{2} \tag{8-8}$$

The coefficient of transmission T is the ratio of the intensity of transmitted light to the intensity of the incident ray and is calculated as follows:

$$T = 1 - R \tag{8-9}$$

When light travels from an optically dense medium to a less dense medium having a lower index of refraction, the angle of refraction is larger than the incident angle. When the incident angle exceeds the critical angle θ_c, $\sin\theta_T$ exceeds one and the transmitted angle becomes complex [76].

$$\theta_T = a + ib \tag{8-10}$$

where critical angle is $\theta_c = \sin^{-1}(\frac{n_1}{n_2})$. Thus $\sin\theta_T$ can be rewritten as:

$$\sin\theta_T = \frac{e^{-b}e^{ia} - e^{b}e^{-ia}}{2i} \qquad (8\text{-}11)$$

Since $\sin\theta_T$ is a real number, $a = \frac{\pi}{2}$ [76], which leads to:

$$\sin\theta_T = \frac{e^{-b} - e^{b}}{2} = \cosh b \qquad (8\text{-}12)$$

$$\cos\theta_T = -i(\sin^2\theta_T - 1)^{1/2} \qquad (8\text{-}13)$$

Using Equations (8-12) and (8-13), the Fresnel equation can be written as follows [76]:

$$(\frac{E_{0R}}{E_{0I}})_s = \frac{(n_1/n_2)\ \cos\theta_I + i(\sin^2\theta_T - 1)^{\frac{1}{2}}}{(n_1/n_2)\ \cos\theta_I - i(\sin^2\theta_T - 1)^{\frac{1}{2}}} = e^{i\varphi} \qquad (8\text{-}14)$$

$$(\frac{E_{0R}}{E_{0I}})_P = \frac{-\cos\theta_I + (n_1/n_2)\ i(\sin^2\theta_T - 1)^{\frac{1}{2}}}{\cos\theta_I + (n_1/n_2)\ i(\sin^2\theta_T - 1)^{\frac{1}{2}}} = e^{i\gamma} \qquad (8\text{-}15)$$

where

$$\varphi = 2\tan^{-1}\frac{(\sin^2\theta_T - 1)^{\frac{1}{2}}}{(n_1/n_2)\ \cos\theta_I} \qquad (8\text{-}16)$$

$$\gamma = 2\tan^{-1}\frac{(n_1/n_2)\,(\sin^2\theta_T - 1)^{\frac{1}{2}}}{\cos\theta_I} \qquad (8\text{-}17)$$

Thus the reflectance of the interface, $R = \left|\frac{E_{0R}}{E_{0I}}\right|^2$, is always equal to one under these conditions and all of the light is reflected back into the first medium. This effect is called total internal reflection, abbreviated TIR. The transmitted light is described as an imaginary wave and it carries no energy [76].

8.2.2 Evanescent wave

As illustrated in Figure 69, the wave vector of the transmitted wave is described as follows:

$$\overrightarrow{k_T} = k_T(\sin\theta_T\,\hat{x} - \cos\theta_T\,\hat{y}) \tag{8-18}$$

When light goes under TIR, the wave vector is rewritten as follows [76]:

$$\overrightarrow{k_T} = k_T(\sin\theta_T\,\hat{x} + i\sinh b\,\hat{y}) = \beta - i\alpha \tag{8-19}$$

The imaginary wave vector represents a non-uniform plane wave called the evanescent wave, which is similar to plane wave, except that the amplitude of the wave is not constant over the wavefront surface. The real component of the wave vector represents the direction of propagation of the wave and the amplitude decreases exponentially in the positive direction of α, as shown in Figure 69. The attenuation distance, δ, is defined as the distance over which the amplitude drops by a factor of *e* and is given by [76]:

$$\delta = \frac{1}{\alpha} = \frac{1}{k_T\sinh b} = \frac{\lambda_0}{2\pi\,n_2\sinh b} \tag{8-20}$$

Replacing Equations (8-3) and (8-12) in the previous equation, the attenuation distance can be rewritten as follows:

$$\delta = \frac{\lambda_0}{2\pi\,n_1\sinh\theta_I} \tag{8-21}$$

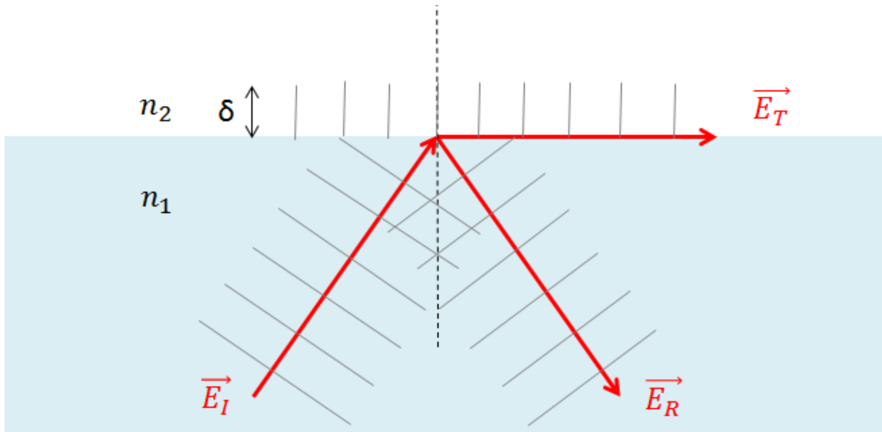

Figure 69. Total internal reflection and propagation of Evanescent wave

The real component of the evanescent wave propagates along the media interface and it does not transfer across the interface for an infinitely large interface. However, there are certain circumstances where the dimension of the interface is comparable to the wavelength and the evanescent wave escape the media and can cause energy loss in the optical systems. One of these circumstances is described in the next section.

8.2.3 Diffractive energy loss in the prismatic microstructured film

When the interface of the two media is sufficiently large and the plane wave is infinite, the evanescent wave propagates parallel to the interface plane and hence all the energy is reflected back into the first medium. However, when the area of interaction has comparable dimension to the wavelength, the evanescent wave can leave the optical structure. When this occurs for a prismatic film used in a light guiding application, it results in an energy loss. In this case, the light rays strike the sides of the prism and undergo TIR and the evanescent wave propagates along the side of the prism. However, as the evanescent wave reaches the tip of the prism, it cannot remain adjacent to the interface and exits the prism, Figure 70. The intensity of the evanescent wave is estimated to be proportional to $\frac{\lambda}{\delta}$ [74], where δ is the width of the prism and λ is the wavelength of light in that medium and is derived as follow:

$$\lambda = \frac{\lambda_0}{n} \tag{8-22}$$

where λ_0 is the wavelength in the vacuum and n is the index of refraction of the film. In the commercially available prismatic film (with $\delta = 300$ μm and n=1.5), the intensity of the evanescent wave is estimated around 0.2% (for incident angle of $20°$) [74]. Even though the diffraction loss caused by the leakage of the evanescent wave from the prism tip is negligible compared to the other optical imperfections in this particular film, it is important to know the theoretical maximum efficiency of an ideal film. Moreover, for some other applications, a film with much finer structure may be required, where the diffractive energy loss would be more significant and would perhaps even exceed the other losses. Thus, it is interesting to investigate the possibility of substantially reducing the diffractive energy loss in the prismatic film by implementing some modifications. The next section discusses a few possible solutions that can potentially reduce the diffractive energy loss.

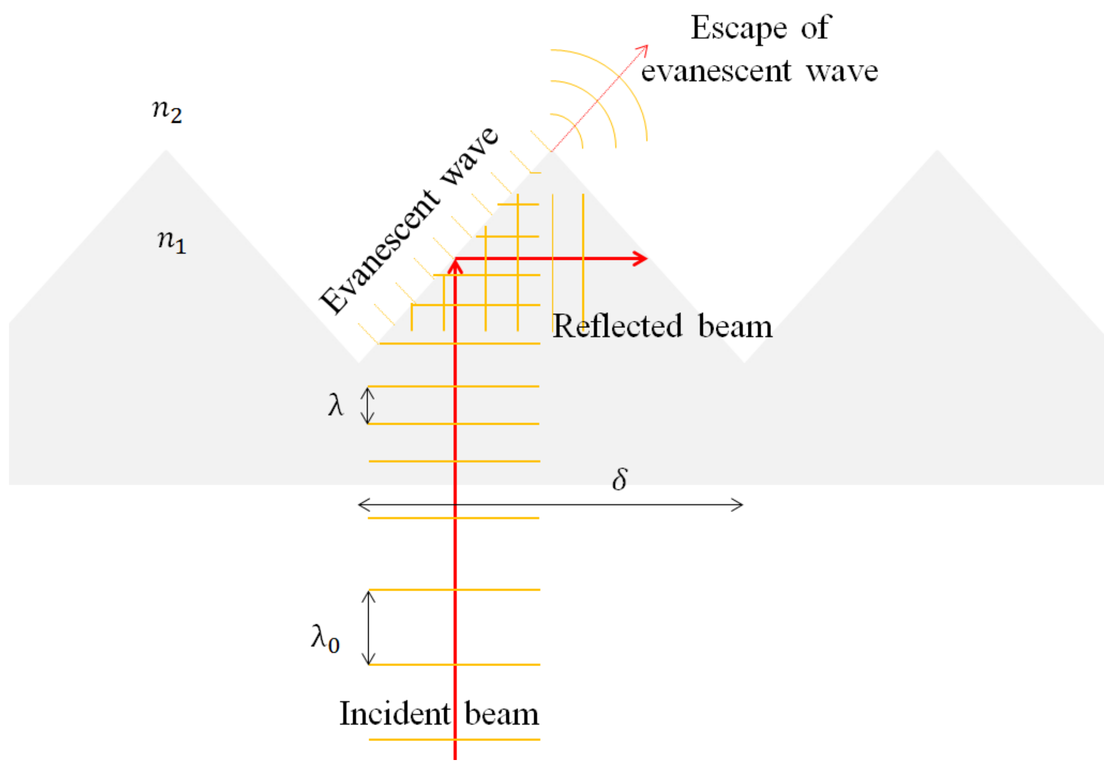

Figure 70. Escape of evanescent wave from the corner of the prism

8.3 Potential modification to eliminate the diffractive energy loss

We postulated that it is possible to modify the prismatic film to capture the lost wave energy and reflect it back toward the film. To investigate this possibility, a reflective structure was placed in front of the prism tip. Three different structures were tested, all of which are illustrated in Figure 71. They are: a flat reflector sheet spaced at a given distance from the prism tip, a flat sheet with a semi cylindrical structure in the middle, and a semi-cylindrical structure with radius *r*. The cylindrical geometry was chosen for the latter two cases because the evanescent wave energy exits the prism tip like a point source, and therefore the cylindrical reflector has a good potential of recycling part of the evanescent wave and reducing the loss.

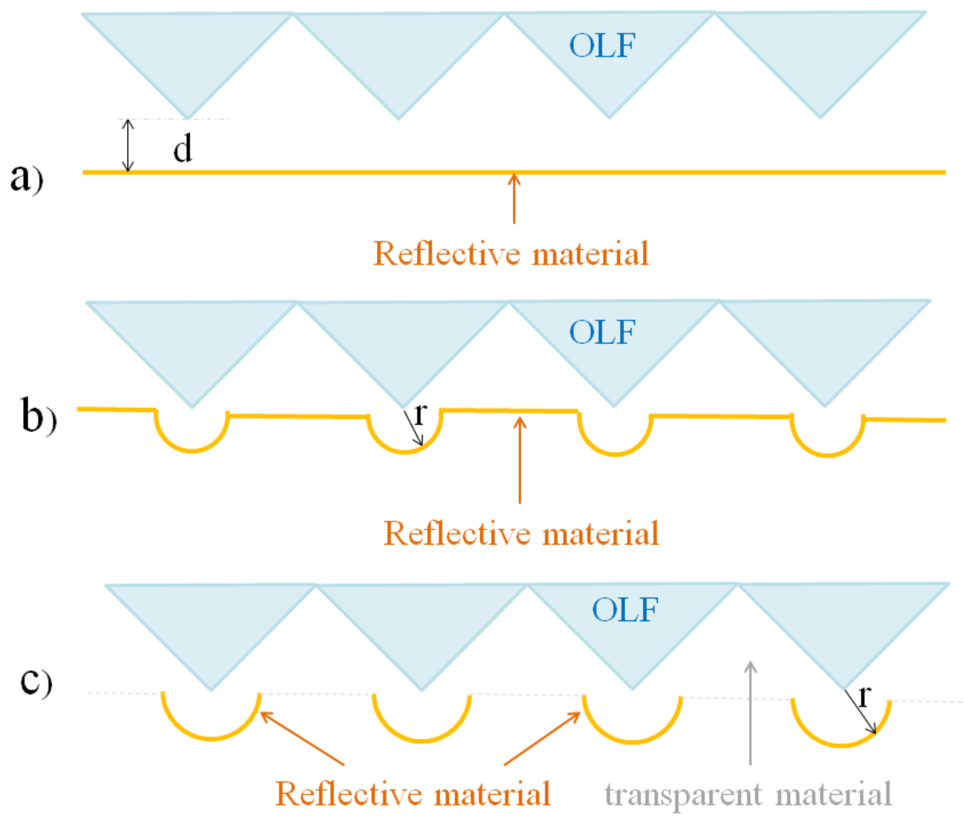

Figure 71. Reflective structure implemented to the prism film to eliminate the diffractive energy loss

All three structures were modeled, the overall energy loss was measured for each, and the results are presented in Section 8.6. The next section describes the modeling methodology.

8.4 Modeling methodology

Light is an electromagnetic wave that rapidly oscillates and propagates in space following Maxwell's equation of electrodynamics. The direction of propagation is perpendicular to the wavefront and is defined as the Poynting vector. In a simple case like a point source, the wave propagates in space with a spherical-shaped wavefront. When the wave reaches an optical system (e.g. a lens or an aperture), it enters from one medium into another. If the dimensions of the interface of the two media are much larger than the wavelength, almost all of the electromagnetic wavefront interacts with the interface of the two media and either propagates into the new medium or reflects back. Thus the wave property of the light can be neglected and light can be considered as energy that is propagating on a rectilinear path in a homogenous medium (light ray). This describes the domain of geometrical optics where optical laws can be formulated using simple geometry [77].

However, if the size of the aperture is comparable to the wavelength of the light, only a portion of the wavefront penetrates into the new medium, and thus the wave is diffracted and it would fall to the domain of physical optics [78]. Geometrical optics is the first approximation of physical optics and many optical phenomena like reflection and refraction can be explained with that.

The dimensions of the optical structure in the prismatic film is comparable to the wavelength of visible light, thus the interaction of light and the film is governed by physical optics, where the propagation of electromagnetic waves is described by the Maxwell equations [79]:

$$\nabla . E = \frac{\rho}{\varepsilon_0} \tag{8-23}$$

$$\nabla \times E = -\frac{\partial B}{\partial t} \tag{8-24}$$

$$\nabla . B = 0 \tag{8-25}$$

$$\nabla \times B = \mu_0 (J + \varepsilon_0 \frac{\partial E}{\partial t}) \tag{8-26}$$

8.4.1.1 Finite Difference Time Domain (FDTD) technique

The Maxwell equations cannot be solved in closed form for a complicated boundary condition and instead must be solved numerically, a calculation which can be computationally intensive. The Finite Difference Time Domain (FDTD) technique is a common numerical method that approximates the value of the electromagnetic wave across the desired computational domain over the course of time and does so in a computationally-efficient way.

In the FDTD method, the computational domain is broken down into a much smaller mesh in shape of cubical cells known as the Yee lattice. The electric and magnetic wave is discrete both in time and space. The time evolution of electric and magnetic field is calculated discretely at each lattice point using two of Maxwell's equations as follows [80]:

$$E(t) \rightarrow E^{n\Delta t} \tag{8-27}$$

$$H(t) \rightarrow H^{\left(n+\frac{1}{2}\right)\Delta t} \tag{8-28}$$

The updated value of the E-field in time depends on the value of the E-field that was calculated for the previous time step as well as the curl value of the local distribution of the H-field in space [80].

$$E^{n+1} = E^{n} + \alpha\nabla \times H^{\left(n+\frac{1}{2}\right)} \tag{8-29}$$

The components of the E-field vector are calculated in a volume of space at a given instant in time; then the magnetic field vector components in the same spatial volume are solved at the next instant in time [80].

$$H^{\left(n+\frac{3}{2}\right)} = H^{\left(n+\frac{1}{2}\right)} + \beta\nabla \times E^{(n+1)} \tag{8-30}$$

This process is repeated over and over again as the time step evolves, until the desired transient or steady-state electromagnetic field behaviour is fully evolved and the field in the computational domain is zero everywhere [80].

$$E^{0} \rightarrow H^{1/2} \rightarrow E^{1} \rightarrow H^{3/2} \tag{8-31}$$

The FDTD technique can solve complicated problems with arbitrary geometry and properties, thus a wide range of linear and nonlinear dielectric and magnetic material can be modeled. The electric and magnetic field intensities are calculated versus time at any point in the computational domain. Hence an animated display of the propagation of the electromagnetic field through the model can be provided, which can be very helpful in understanding the physics of the structure.

8.4.1.2 FDTD solution by Lumerical

To study the prismatic microstructured film, a software package FDTD solution by Lumerical was used. Lumerical is a numerical software package that solves the Maxwell equation in any physical domain with any optical property, using the FDTD method [81]. Figure 72 shows a snapshot of the simulation environment in the Lumerical. The propagation of the electromagnetic wave is simulated in the computational domain, which is defined by the boundary condition. The light source and the object of interest must be confined in the computational domain. The properties of the boundary condition are set based on the problem. For a physical domain where the optical structure and the light source are replicated in one direction, periodic boundary condition can be used. This makes the computational process faster and less memory intensive. Moreover, when the optical structure and the light source are invariant in one direction, the 3D problem can be simplified into 2D simulation, which requires much less processing time and memory. Using these two major simplifications, the prismatic film was modeled in a 2D domain. As illustrated in Figure 72, the boundary condition in the x direction is periodic, which represents the replication of the prism structure and an infinite light source. The Boundary condition on the y direction is absorbing which prevents any light that reaches those surfaces from returning to the computational domain.

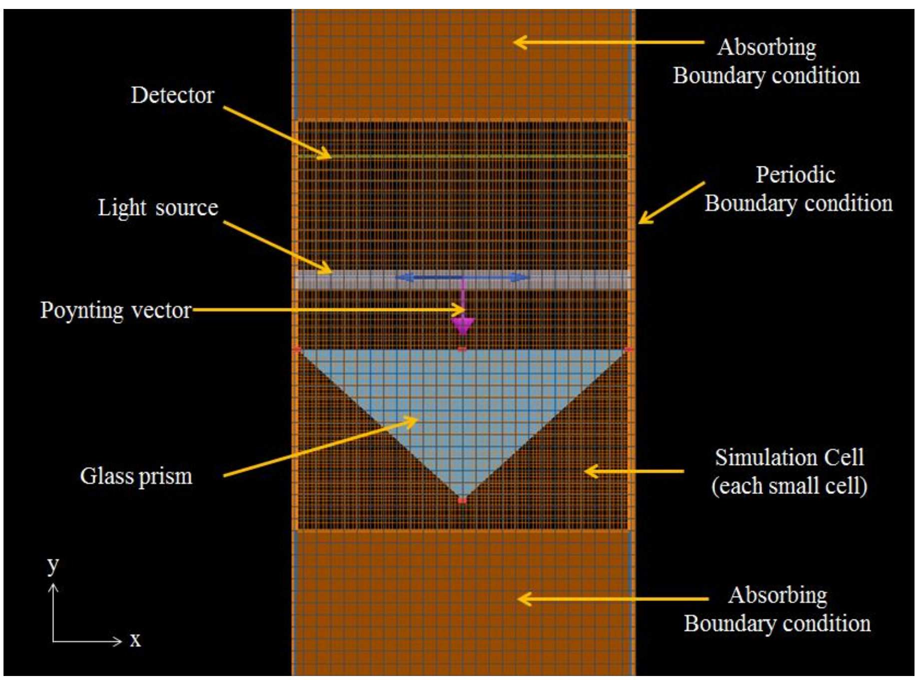

Figure 72. A snapshot of a sample computational domain with a periodic boundary condition in the x direction and an absorbing boundary condition in the y direction

To measure the diffraction loss associated with the prism, it is important to measure the reflectance and the transmittance of the prism. To determine these, a short pulse plane wave with a particular wavelength and a Poynting vector along the y direction is sent toward the prism. The pulse is a wave packet truncated by a Gaussian envelope that is much larger than the wavelength and which determines the bandwidth of the light source. The duration of the pulse is proportional to the inverse of the bandwidth and thus, it is impossible to have an infinitely short pulse. In order to make sure that the incident wave does not interfere with the reflected wave, the distances between both the light source and the prism and the light source and the detector should be much larger than the distance that light travels during the pulse.

It is also important to set the simulation time long enough so that the steady state is achieved in the system and the electromagnetic wave is zero everywhere in the computational domain. For example, for a light source with pulse length of 10 fsec, the electromagnetic field was calculated in the domain during 1000 fsec after the time-step at which the pulse was initiated.

To measure the reflectance of the prism, the intensity of the reflected wave is calculated at the imaginary detector plane by calculating the electric field and magnetic field intensity at each point of the detector throughout the simulation time. It is also possible to measure the intensity of the transmitted wave by having another detector positioned below the prism. (However, as is further described in Section 8.6, this approach would not be practical when a reflective structure is placed at the prism tip.)

The accuracy of the simulation highly depends on the dimension of each cell, dx, relative to the wavelength, λ. The cell size needs to be sufficiently small such that it resolves the wavelength and small geometrical features in the model. The number of cells per wavelength, λ/dx, can be set to different pre-selected values in Lumerical (from 6 to 34). Increasing the number of cells per wavelength increases the accuracy of the simulation as well as the time and memory required for the simulation. In this research, a mesh setting of 22 cells per wavelength was used, which is expected to have a fairly accurate result. The required time and memory also depend on the volume of the computation domain, V, (or the area, A, in 2D simulation). A summary of the required time and memory is presented in Table 9 [79]. (These simulations were carried out using a computer with a 3.5 GHz processor with Intel® TMI Core i7 2700K CPU and 16GB internal memory and the simulations took from 5 min to 1hr, depending on the wavelength and mesh setting for the proposed dimensions and indices of refraction.)

	2D	*3D*
Memory	$\propto A\,(\frac{\lambda}{dx})^2$	$\propto V\,(\frac{\lambda}{dx})^3$
Time	$\propto A\,(\frac{\lambda}{dx})^3$	$\propto A\,(\frac{\lambda}{dx})^4$

Table 9. Time and memory required for simulation in 2D and 3D

8.4.1.3 Two dimensional equivalent of a three dimensional problem

Propagation of light and analytical raytracing is a difficult problem in 3D geometry, however when the optical system has a translational symmetry in one direction, it can be simplified into a 2D problem which simplifies the calculation. When the object in the model has translational symetry along the z-axis, as is the case for the prismatic film, the shape of the object in the cross sectional plane perpendicular to $\hat{z}$ is always constant, as shown in Figure 73.

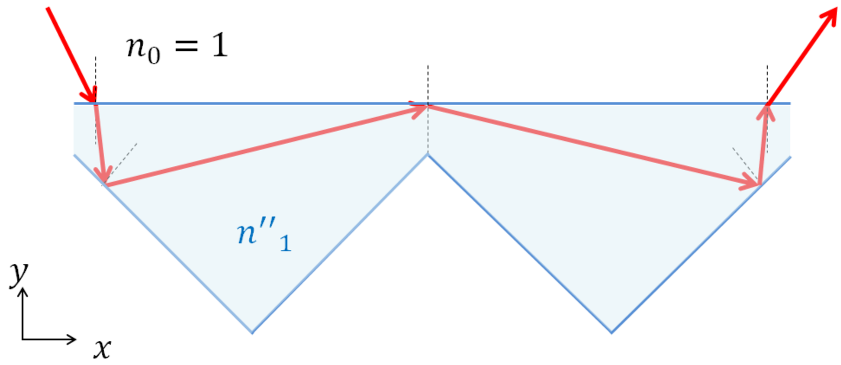

Figure 73. The path of light ray in the prismatic film as projected on the cross sectional plane

The path of the light ray in the optical structure can be projected on the cross sectional plane, as shown in Figure 73, however, the projected path and the optical interface do not obey the simplified version of Snell's law. The motion of light in the third dimension can be taken into account by replacing the indices of refraction with an effective refractive index, given by [47]:

$$n'_i = \sqrt{{n_i}^2 - {n_0}^2 \cos^2 \theta} \tag{8-32}$$

where θ is the angle of incident light with respect to $\hat{z}$ and n_0 is the index of refraction of the first medium (air, in this case). For $\theta = 25°$, the effective index of refraction of air and acrylic are calculated to be 0.4226 and 1.195 respectively. Since the minimum possible index of refraction in Lumerical is one, the index of air was kept equal to one and the effective refraction index of the prism was calculated as follows:

$$n''_{prism} = \frac{n'_{prism}}{n'_{Air}} = 2.8 \tag{8-33}$$

Using the 2D analogy for the prismatic film, the interaction of the electromagnetic wave with the film was modeled in Lumerical in 2D. This reduced the simulation time substantially and allowed more accurate simulation with a finer grid. For more accurate study on the film a 3D simulation may be required.

8.4.1.4 Error analysis

The FDTD technique is a numerical method and, as such, there are two types of errors associated with the simulation: the systematic error and the random error. The simulation result of a model, under the same initial conditions, is completely reproducible and so the simulation has no random error. However, changing the simulation parameters, such as the mesh setting, the location of boundary condition with respect to the object and source, the absorption of boundary condition, or the location of source in respect to object and detector change the simulation result. This is characterized as a random error.

The mesh setting can highly impact the accuracy of the result. However, while the finest mesh setting can lead to a more accurate simulation result, it is generally needlessly computationally intensive to run such a high resolution simulation. In this study, the appropriate mesh setting was determined by increasing the number of cells to the point where increasing the mesh setting further made no significant change in the simulation result. These simulations were carried out to measure the variation of the reflection of the prismatic film with the proposed structures. As it is described in Section 8.5, the variation in the reflectance does not exceed a few percent. However, since this research was intended to investigate the possibility of enhancing the reflectivity of the film, the 0.2% variation in the overall result was acceptable. Once the optimal mesh setting was determined, the error associated with the mesh setting was estimated by repeating the simulation numerous times at this mesh setting and comparing the difference in the results. Other factors, such as the position of the light source respect to the prism and etc. were slightly and randomly adjusted and the variation in the result was measured. Table 10 represent a summary of the sources of error in the simulation and the fractional error associated with each one of them, where the fractional error is defined as the ratio of absolute error to the measured value.

Source of error	Fractional error (e_i)
Mesh setting (Difference between the chosen setting and the finest grid)	0.2%
Bandwidth of source	0.1%
Boundary condition dimension	0.1%
Boundary condition absorption	0.05%
Source location	0.05%
Detector location	0.05%

Table 10. Sources of the error in the simulation result

The overall fractional error associated with the setting is given by:

$$E_{tot} = \sqrt[2]{\sum_{i=1}^{n} (e_i)^2} = 0.23\% \qquad \textbf{(8-34)}$$

The error analysis was carried out for one particular setting as a representative example and it was applied to all simulation result.

Using this methodology, the prism film and the reflective structure were modeled and the overall energy loss was measured for all cases. The simulation result is presented in the next sections.

8.5 Diffractive energy loss in a two-dimensional prism

As the first step, a simple prism structure was modeled in 2D and the diffractive energy loss was measured. The actual size of the prism in the prismatic film is about 300 μm and for this prism size, the diffractive energy loss for electromagnetic radiation in the visible range is estimated to be very small, around 0.2%. This amount of loss is difficult to measure, because it is comparable to the amount of error in the simulation. However, it was interesting to investigate the possibility of reducing the diffractive energy loss. Thus, it was decided to model a smaller prism with the width of 2.5 μm, which has larger loss, since the diffractive energy loss for the prism structure is proportional to λ/δ. Decreasing the prism size makes the computational domain much smaller which reduces the required computation memory and allows much faster, yet more precise simulations.

A monochromatic light source radiating a plane wave perpendicular to the prism surface was used in the simulations and the reflectance was measured at a detector plane behind the source, as shown in Figure 74. For a perfect prism without diffraction loss, the reflectance is expected to be R=1. However, the reflectance was always measured to be smaller than one, and the difference is assumed to be the diffraction loss, since there is no other source of loss in this simple case. Figure 74 represents time-domain information of the electric field component over the course of the simulation as the electromagnetic wave propagates in the computational domain. As shown in Figure 74, the evanescent wave escapes the prism tip and its energy propagates into the surrounding space as though it was a point source. The diffractive energy loss is given by:

$$Loss_{diffractive} = 1 - R \tag{8-35}$$

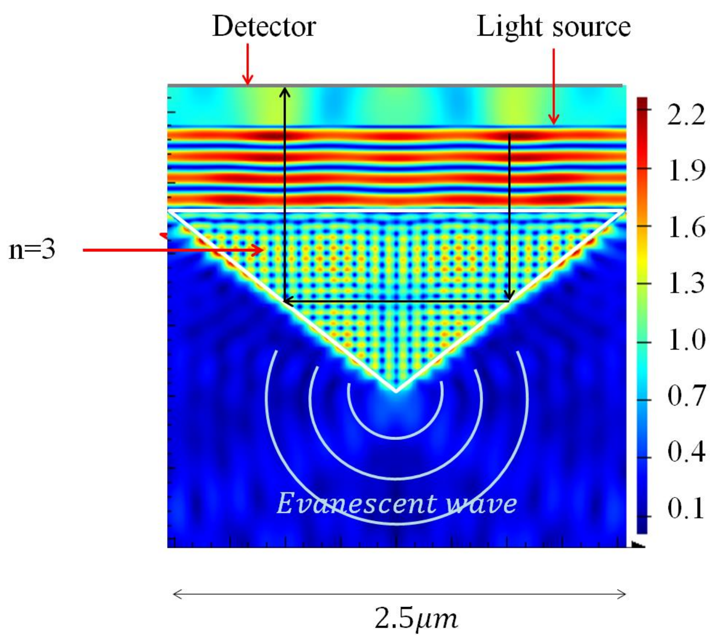

Figure 74. The prism structure reflect back the plane wave while the evanescent wave escape the prism tip (A composite snapshot image of the E-field at several different times during the simulation)

The diffractive energy loss was measured for different wavelengths, ranging from 0.05 μm to 1 µm. The measurement was also repeated for different values of the index of refraction, which represents different axial angular components of the propagating rays. For example $n = 1.5$ represents $\theta = 90°$ and $n = 3$ represents $\theta = 20°$. The overall result of the simulation is presented in the Figure 75. The diffractive energy loss increases proportional to λ/δ. When light waves strike the prism at a shallower angle, the effective index of refraction increases, and the wavelength of light in the material decreases. Thus the diffractive energy loss is smaller for higher index of refraction. In this research project, light incident on the surface at shallow angles, for which TIR occur, is of most interest. Thus the index of refraction was set to 3, which is equivalent to $\theta = 20°$. The diffractive energy loss for this case is expected to be low and the reflectance of the prism was measured to be 98.36%.

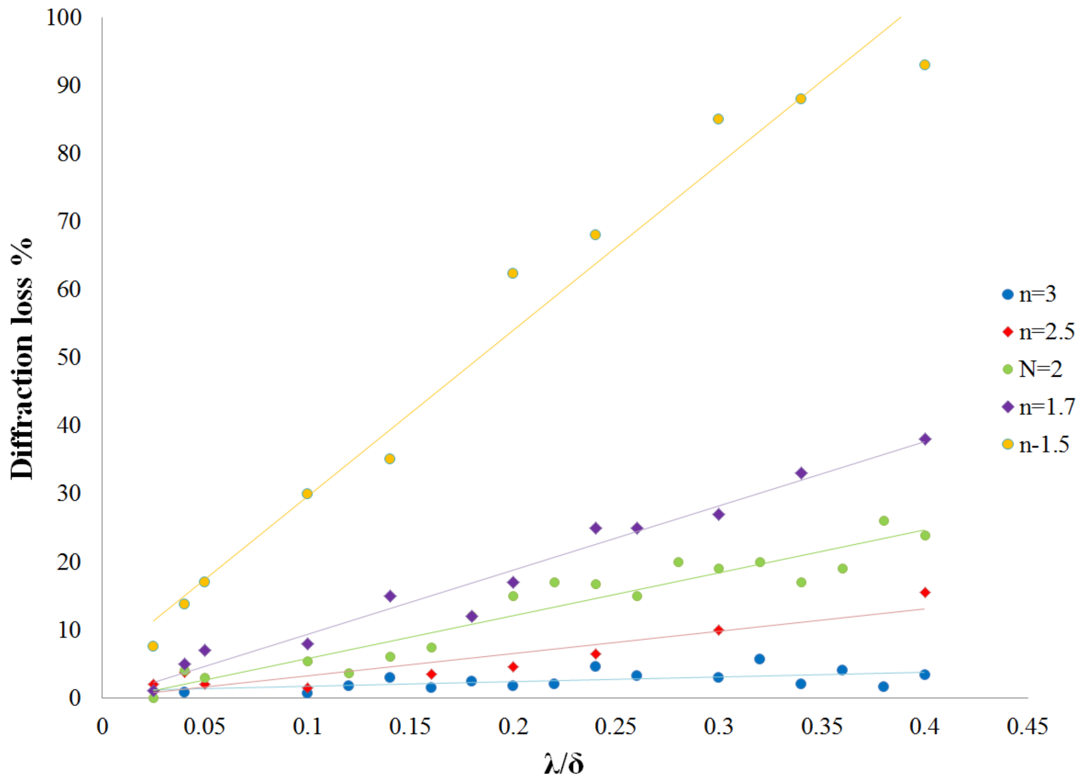

Figure 75. Diffractive energy loss versus λ_0/δ for different index of refraction

Since the index of refraction of the prism was set to *n=3*, the Fresnel reflection from the first surface is relatively high, about 25%. To avoid Fresnel reflection interfering with the TIR wave, an anti-reflective film, AR, was also added to the flat surface of the prism, which eliminates the Fresnel reflection, Figure 76. When the properties and thickness of the AR film are set properly, the Fresnel reflection from the first surface R_1, and second surface R_2, interfere destructively and cancel out each other. The thickness and index of refraction for the thin film coating are given by [82]:

$$t = \frac{\lambda_0}{4n} \tag{8-36}$$

$$n_f = \sqrt{n_0 n_1} \tag{8-37}$$

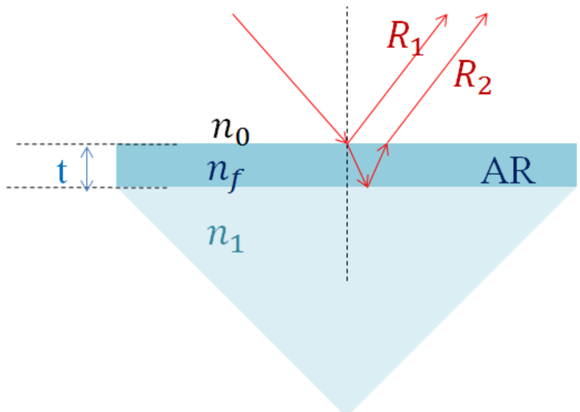

Figure 76. Anti- reflective layer eliminate the Fresnel reflection of the front surface of the prism film

Instead of using an anti-reflective layer on top surface of the prism, that top surface could have been extended up to the top absorbing boundary so that both the light source and the detector would be inside the glass and thus, the Fresnel reflection would be avoided. The difficulty with this approach is that it would have required adjusting both the source and the absorbing boundary condition to work properly within the prism material, which would have more time consuming without giving any better results.

8.6 Modifying the prismatic film

To reduce the diffraction loss, it was suggested to add a reflective structure in front of the prism, which essentially captures the evanescent wave and reflects it back into the prism. A few suggested designs were tested and the overall reflectance of the film and reflective structure was measured for each set up.

The simple modification uses a flat reflective sheet with known reflectance positioned at a certain distance from the prism tip. The reflectance of the sheet was set to a low number, 50%, in order to assess the potential effect that could be achieved with a modest reflectance increase. Figure 77 illustrates a snapshot of the FDTD simulation. The left image presents the simulation set up of a prism structure and a flat reflective sheet and the right figure represents the electric field propagation in the time domain, where colours represents the intensity of the electric field (red is the maximum and blue is zero). As it is shown in the figure, the reflector captures part of the evanescent wave and reflects it back toward the prism.

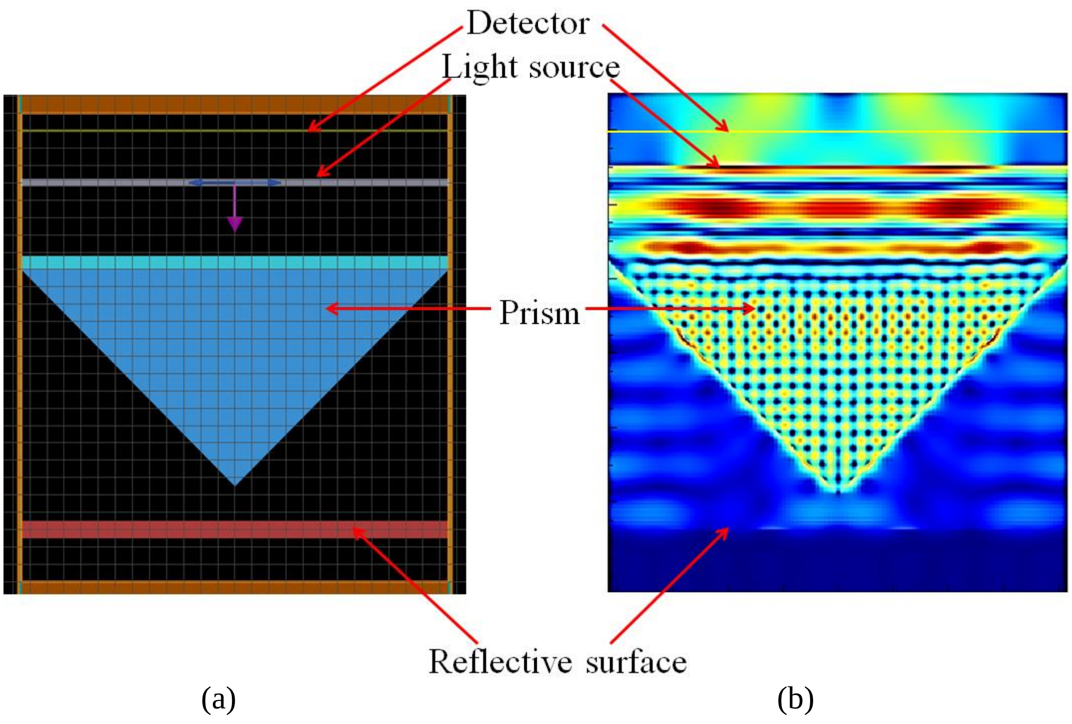

Figure 77. The prism structure and a flat surface reflect the plane wave back to the detector ((a) is the simulation set up, (b) the E-field in the time domain)

The overall reflectance of the prism and the reflector was measured for different spacing between the prism and the flat sheet for $\lambda = 0.5\mu\mathrm{m}$. As illustrated in Figure 78 the overall reflectance of the prism and the flat sheet shows an oscillatory pattern and it varies with distance. For the optimal distance, the overall reflectance exceeds the reflectance of the prism without any modifications; however, the overall reflectance may decrease for other distances in compare to the unmodified prism.

The oscillation of the intensity of the reflected wave versus distance is due to the interference of the TIR wave and the evanescent wave. As the reflector is placed at the proper distance, the optical path difference between the TIR wave and the evanescent wave is multiplication of $\frac{\lambda}{2}$, and thus two waves constructively interfere and the intensity of the reflected light increases. However, when the optical path distance is a multiple of λ, the two waves destructively interfere and this decreases the overall intensity of the reflected wave. The simulation results illustrate a periodic behavior in the overall reflectance with the period of $\frac{\lambda}{2} = 0.25\ \mu m$ that confirms this theory.

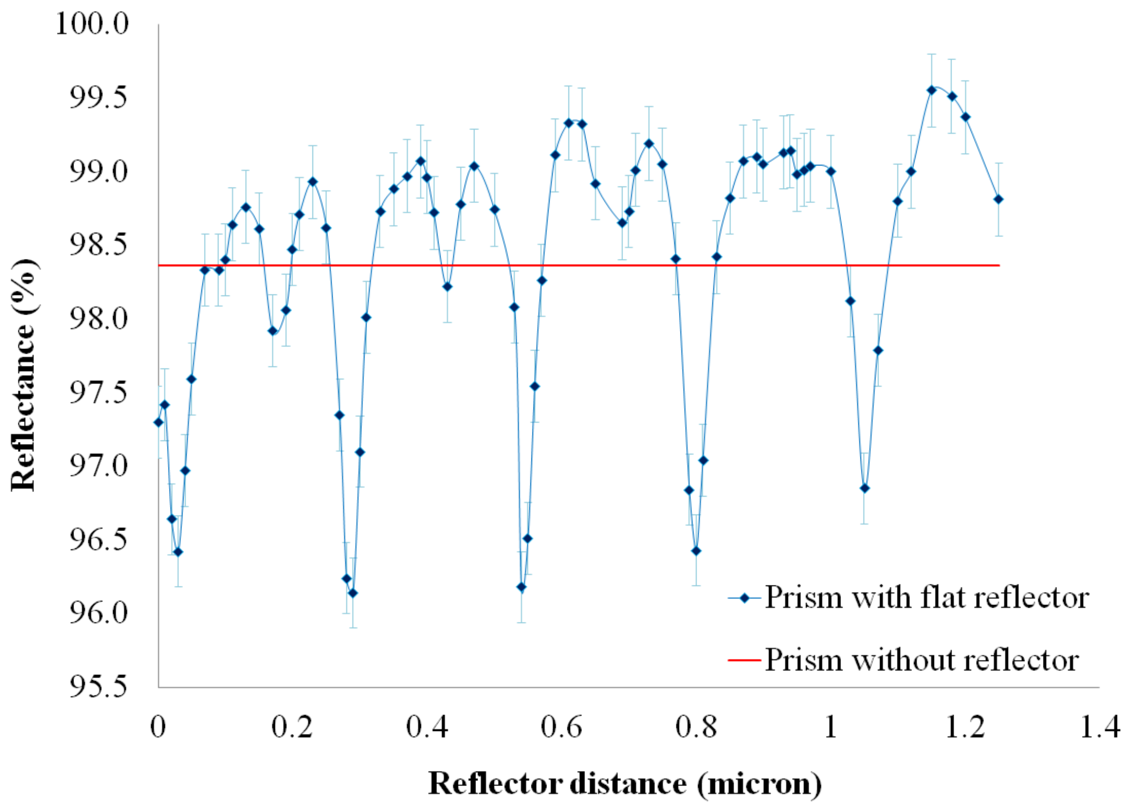

Figure 78. The reflectance of the prism and the flat sheet versus distance

Since the evanescent wave escapes from the prism tip and then propagates in space like a point source, it was suggested that a cylindrical reflector may be able to capture a larger amount of evanescent wave than a flat reflector. To test this, a flat sheet with cylindrical bump was modeled and the overall reflectance of the assembly was measured. Figure 79 illustrates the electrical field in the time domain as light is propagating in the computational domain. As it is illustrated in the figure, the semi-cylindrical structure reflects the evanescent wave back toward the prism. It was found that the overall reflectance of the system depends on the radius of the cylinder. Figure 80 represents the overall reflectance versus cylinder radius. As shown in the figure, the overall reflectance shows a periodic behavior with the period of $\frac{\lambda}{2} = 0.25\ \mu\text{m}$, similar to the flat sheet reflector.

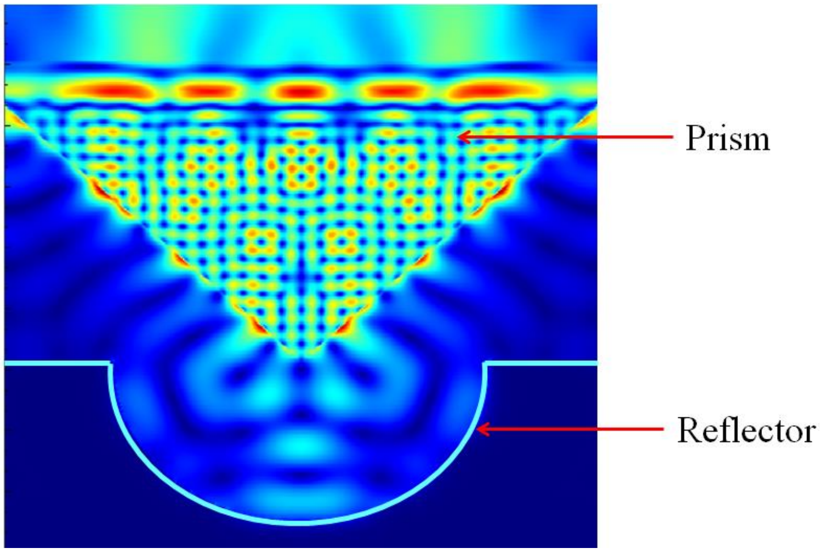

Figure 79. The flat sheet with cylindrical bump captures the evanescent wave and reflects it back to prism

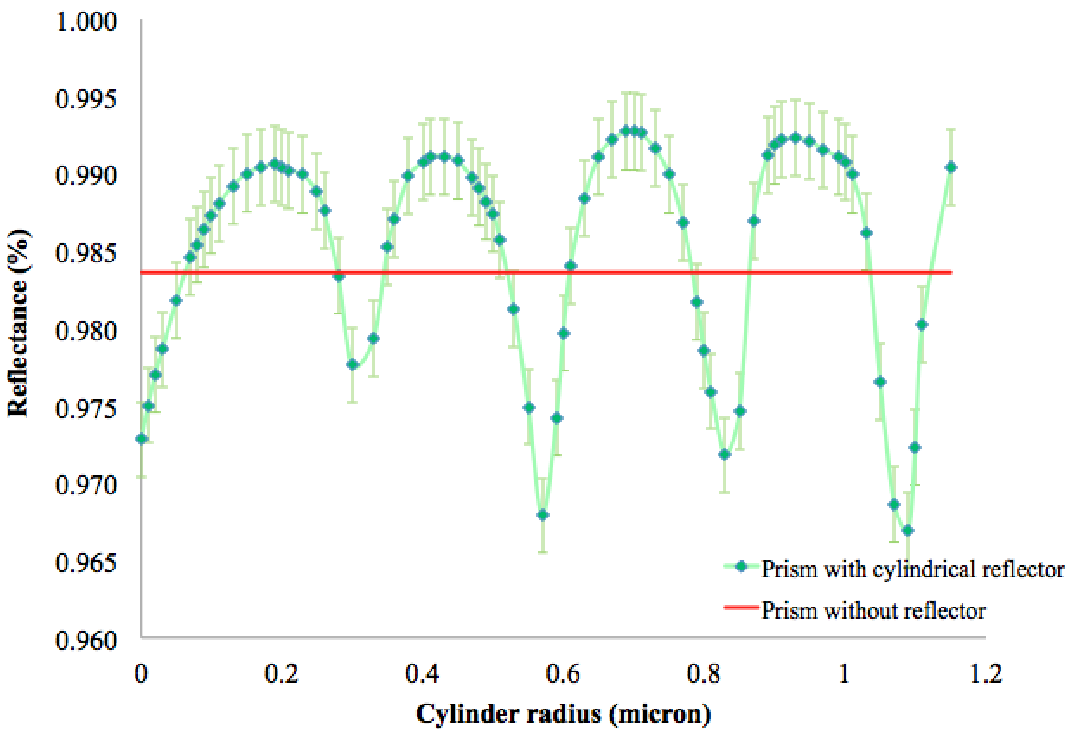

Figure 80. The reflectance of the prism and the semi-cylindrical reflector versus cylinder radius

The variation of the reflectance versus radius was also measured for two additional wavelengths, in order to assess the wavelength dependence. As shown in the Figure 81, all three wavelengths show a periodic behavior, each with the period of $\frac{\lambda}{2}$.

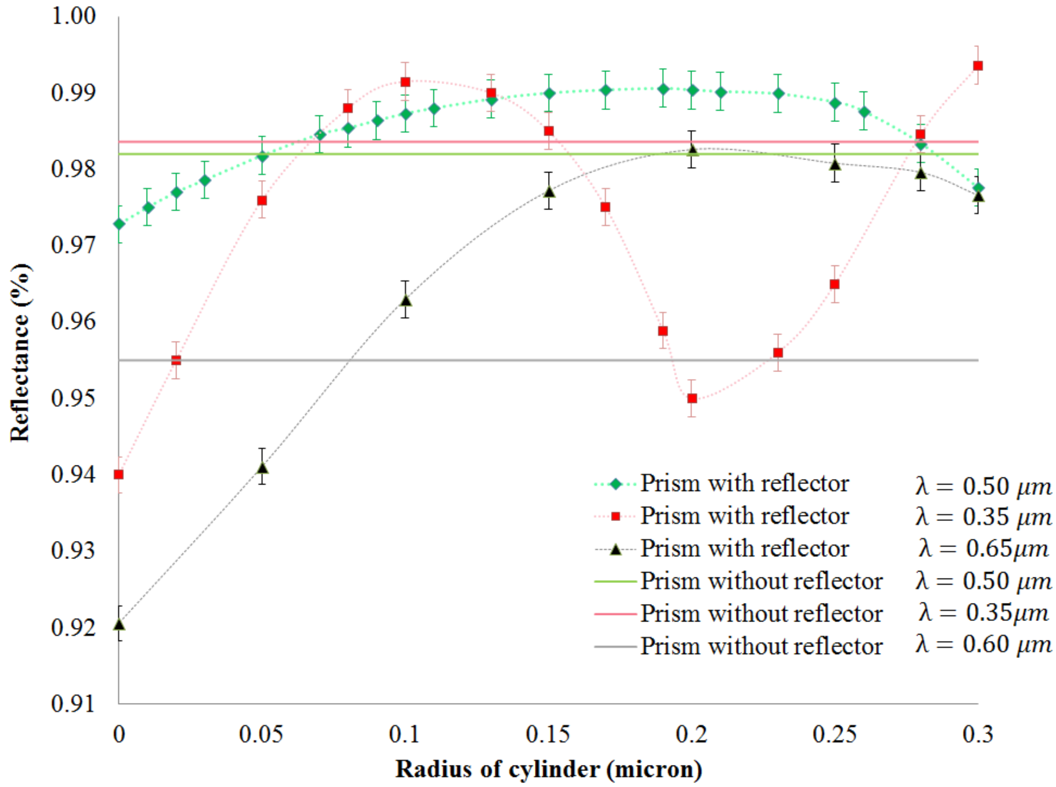

Figure 81. The variation of reflectance of the prism and the reflective structure for different wavelengths

On average, the overall reflectance of the prism with the semi-cylindrical reflector is 0.3% larger than the flat sheet reflector. This may be practical for some applications where a highly reflective thin film is required. However they both stop any light from exiting the prism while transmission of the light through the film is important for light guide application. For the current application of the film, more practical modification is required. As an example, a semi cylindrical shell with variable radius was also modeled, as shown in Figure 82, and the overall reflectance was measured, as shown in Figure 83.

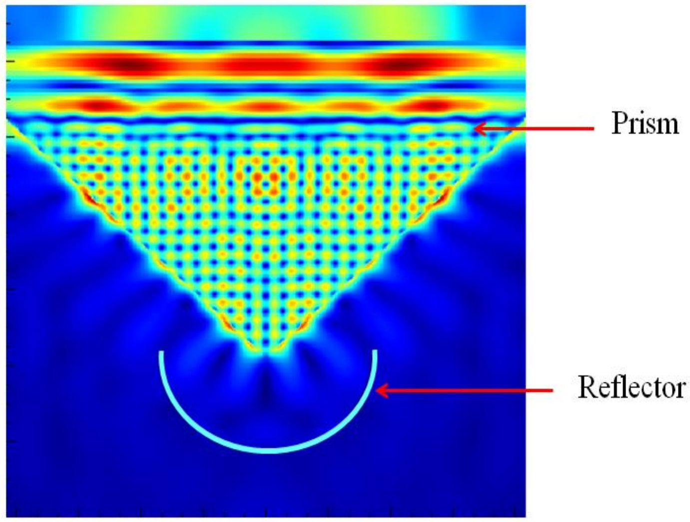

Figure 82. The prism structure and a semi-cylindrical shell

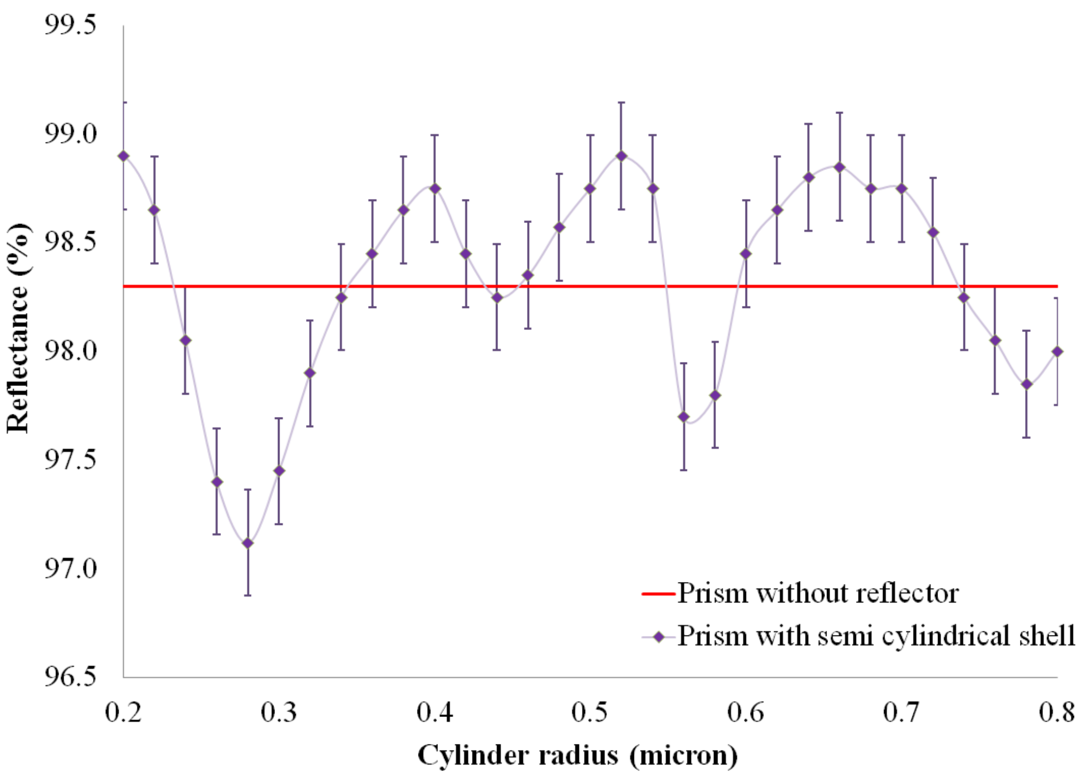

Figure 83. The reflectance of the prism and the semi-cylindrical shell versus cylinder radius

As illustrated in Figure 83, the cylindrical shell shows a potential to enhance the reflectance of the prismatic film as well. Even though on average, the overall reflectance of the cylindrical shell is slightly less than the other two designs, it may be more practical for some applications where the transmission of light through the prism film is important. The overall reflectance of the prism and the cylindrical shell shows a periodic behavior as well, however, it is not as repetitive as the other two reflectors.

In a simple case where there are two reflective layers, R_1 and R_2, as depicted in Figure 84, the overall reflectance of the optical system can be estimated as follow:

$$R_n = \frac{R_1 + R_2 - 2R_1R_2}{(1 - R_1R_2)} \tag{8-38}$$

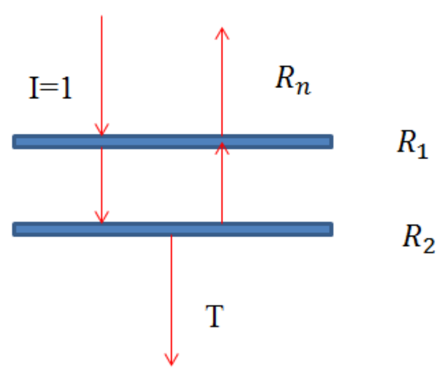

Figure 84. Interaction of light with two reflective layers

As it was measured before, the reflectance of the plain prism is 98.36% and the reflectance of the metal is 50%, the net reflectance of the system is expected to be around 98.38%. This means that adding a relatively poor reflector cannot simply enhance the overall reflectance of the prism by about 1.2%, which was caused by the constructive interference.

Even though this approach showed a potential to reduce the diffraction loss, it may be not be a very practical solution, as the condition for constructive interference is different for different wavelengths, Figure 81. However, for some applications where monochrome light source or with narrow bandwidth, this approach may be an appropriate solution.

8.7 Enhancing the optical imperfection

The main source of loss in the prismatic film is due to optical imperfection caused in manufacturing process. As we investigated the possibility of recovering part of the evanescent wave using a reflective structure, it was also interesting to study if the same technique could be used to recover the lost energy due to optical imperfections. To carry out this study, an imperfect prism with chamfered tip was modeled, where the dimension of the chamfered tip ranged from 5% to 10% of the prism width, shown in Figure 85. As depicted in Figure 85 (b), a significant fraction of the incident electromagnetic wave exits the prism tip. The reflectance of an imperfect prism with 0.15 μm chamfered tip is measured to be 89%.

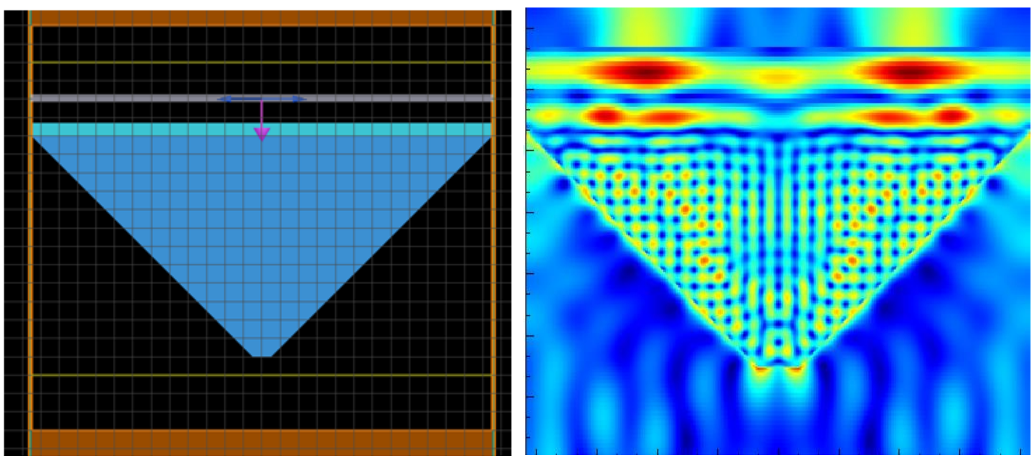

(a) (b)

Figure 85. The propagation of an EM wave through an imperfect prism with chamfered tip ((a) is the simulation set up, (b) the E-field in the time domain)

The overall reflectance of the system was measured for an assembly of two reflective structures, a flat sheet with a cylindrical bump and a semi-cylindrical shell. The time domain information of the electric field and the overall reflectance of the prism and reflective structure are shown for two structures respectively in Figure 86 and Figure 87.

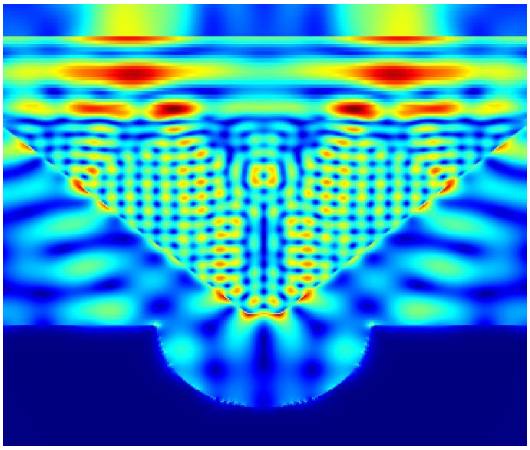

(a)

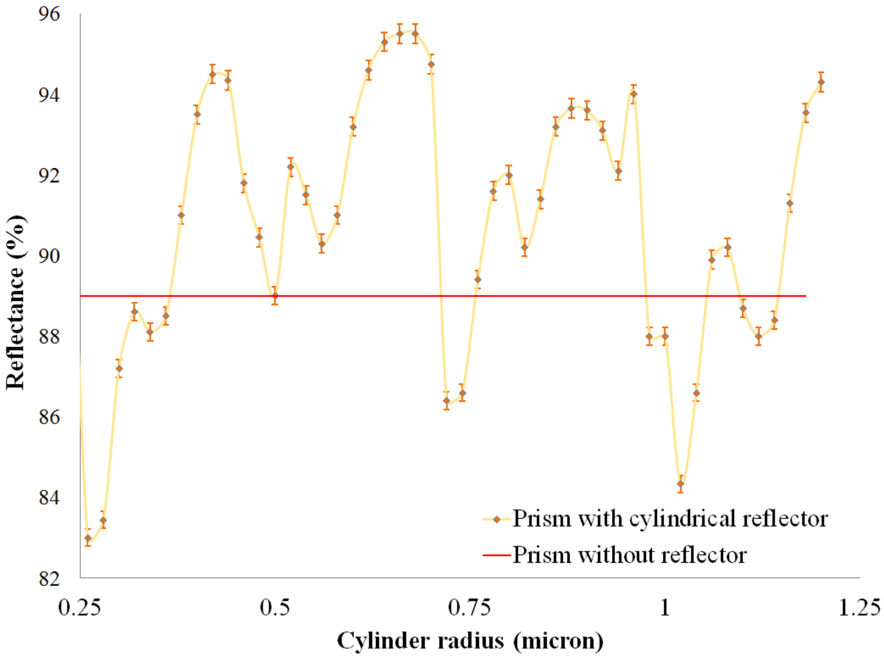

(b)

Figure 86. The imperfect prism and flat sheet with cylindrical bump
(a) The E-field in the time domain (b) the overall reflectance versus cylinder radius

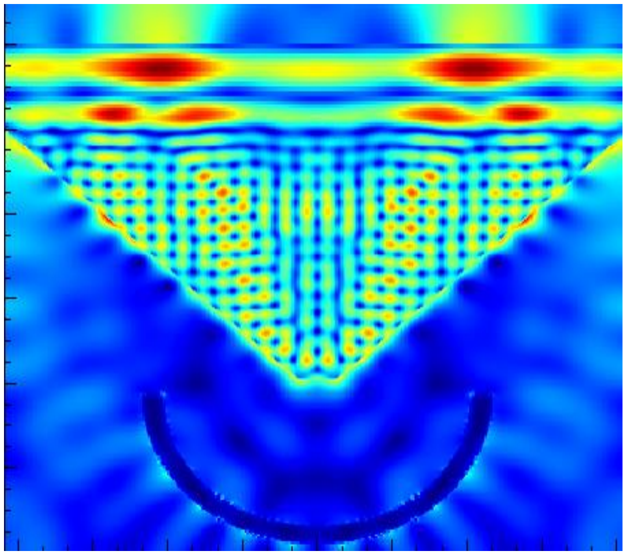

(a)

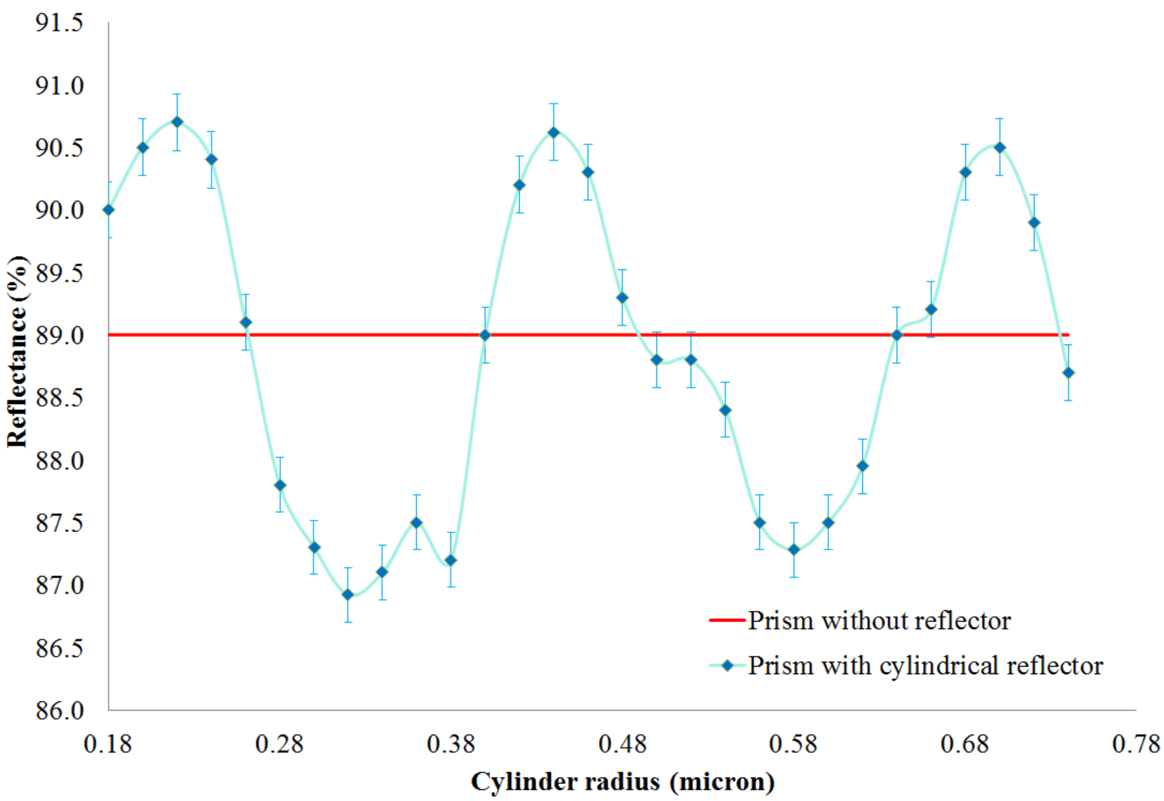

(b)

Figure 87. The imperfect prism and semi-cylindrical shell
(a) The E-field in the time domain (b) the overall reflectance versus cylinder radius

The simulation results showed that the proposed reflective structure has the potential to enhance the performance of the prismatic film. Comparing the simulation results of the two designs, it is apparent that the flat sheet with cylindrical bump can enhance the reflectance of the prism by about 0.5% more than the semi-cylindrical shell. However the cylindrical shell may provide a better solution, since it is more practical for applications where the transmission of light is important.

8.8 Potential method of implementing the modification on the prism film

The purpose of this research was to investigate the possibility of enhancing the reflectance of prismatic film by recovering part of the lost wave energy. As the simulation results have shown, the proposed method has the potential to improve the reflectance of the film.

Currently available prismatic films, which typically have a 300 μm prism width, are highly reflective with less than 2% loss. However, in future applications a much thinner film with nanostructures may be required. If the prism width is reduced by factor of a 100, the diffractive energy loss increases substantially, since it is proportional to the inverse of the prism width. The proposed method can be implemented with a nanostructured prismatic film to enhance its reflectance. Further study should be carried out for modifying the prism film.

As a practical implementation of the concept modeled, Figure 88 depicts a technique in which the overall concept can be implemented. The prismatic structure that is made out of a material with index of refraction close to 1.5 is moulded to a substrate made out of a theoretical material with very low index, close to air with a cylindrical structure. The cylindrical structure is then coated with highly reflective metal that would enhance the reflectance of film as shown in the previous simulation. This approach does not impact the transmission of light through the prism film which is essential in some applications including the light guide.

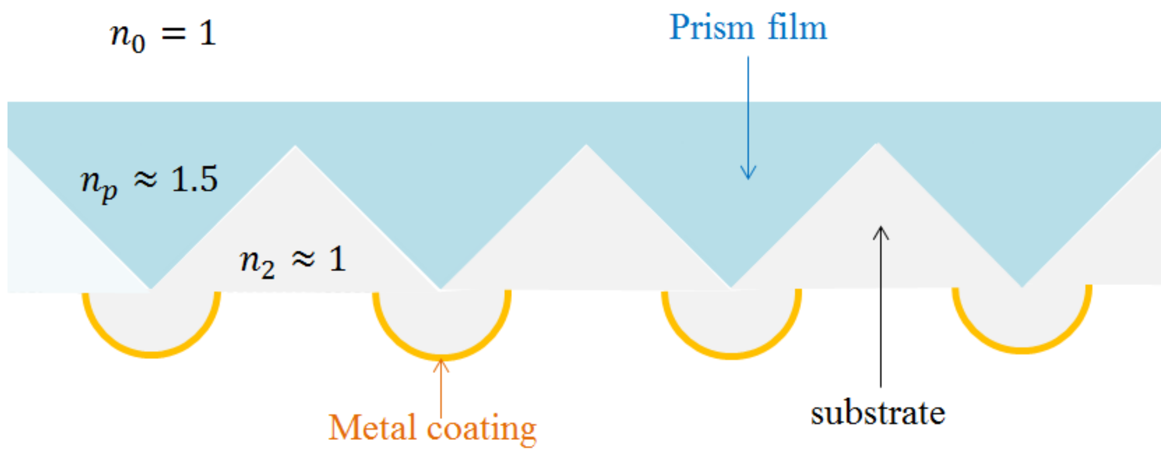

Figure 88. The semi-cylindrical reflector implemented to the prismatic film

Identifying a polymer that has very low index of refraction as well as very low absorption and scattering coefficients may be difficult. Hence the indices may be adjusted such that the ratio of the indexes remains the same and the prismatic structure has its dual functionality.

For more accurate analysis, further studies should be carried out for different indices of refraction and different prism dimensions. All simulations were done in 2D and the effect of motion of rays in third dimension was taken into account with the effective index of refraction. This analogy is valid for light a source that has a uni-axis wave vector, but for light sources with intrinsic divergence, a 3D simulation should be done to ensure more accurate result.

Chapter 9: Conclusion

The goal of this research was to design a new daylighting system capable of illuminating the core of a multistory building with sunlight, and to provide a detailed scientific evaluation of the performance of the system. Capturing sunlight at rooftop level and using the empty space adjacent to the building façades to deliver light to each floor is the unique and novel approach of the Two-Stage Core Sunlighting System for illuminating the building core with daylighting.

All elements of the Two-Stage Core Sunlighting System were analyzed in detail in order to optimize the overall performance of the system. The unique design of the rotary redirector component allows capturing sun efficiently throughout the day for all solar altitude and azimuthal angles. The rotary redirector can capture sunlight equally from all sides of the buildings, thus it can be mounted at the rooftop level of each façade. Hence, the Two-Stage Core Sunlighting System can be adapted to all buildings with almost any geometry and orientation. It was estimated that the Two-Stage Core Sunlighting System can provide daylight for the top six floors of the building, which would require a 3 m wide redirector hanging from the building edge.

The folded optical path concept, used in the concentrator element, allows concentrating light over a short distance, while maintaining a collimation angle of less than 2°. The high collimation of the output beam allows the use of a 7 cm thick light guide to transfer sunlight 15 m deep to the building core, with less than 23 % loss in the light guide. Since light can be captured from both sides of the building, the Two-Stage Core Sunlighting System can provide sunlight for any building with a 30 m wide floor plate. The concentrator is designed so as to have minimum aesthetic impact on the building. The lens assembly in the concentrator element can serve as a building façade shade element and the concentrator enclosure is designed to be only 15 cm thick, and thus able to vanish visually within the façade.

Raytracing simulation showed that for locations at latitude smaller than 35°, during summer and spring days the Two-Stage Core Sunlighting System can capture enough light to illuminate a typical multistory building purely with sunlight at 500 lux. However, during the autumn and winter days, sunlight needs to be partially supplemented with electrical lighting in a few hours a day, depending on the latitude. For example, for a place like Los Angeles with latitude of 35° this is supplemented period is 4 hours during the winter solstice, and at Honolulu with latitude of 21° this period is 2 hours. The Two-Stage Core Sunlighting System can be implemented at any location with any geographical and climate conditions, however, the energy calculation results showed that the system is more cost and energy effective at locations with latitudes smaller than 35° with annual sunshine probability larger than 60%.

Since the performance of the system is eventually limited by the properties of the applied materials, it is important that the loss in the applied material is minimal. To investigate the future potential improvement in the Two-Stage Core Sunlighting System, further studies were done on the prismatic microstructured film, which is one of the elements that are largely used in the Two-Stage Core Sunlighting System. A modelling study was carried out to investigate the sources of loss and potential methods to reduce the loss caused by the film. A few structures were considered as additions to the prismatic structure. The modified films were studied using Finite Difference Time Domain modeling which showed the potential for enhancing the performance of the prismatic film. The proposed modifications do not substantially reduce the loss in the currently available prismatic. However, the modification has more potential to improve the performance of a nanostructured film, which may have future applications.

In conclusion, the Two-Stage Core Sunlighting System can be adapted to most buildings with most geometries and it can be implemented into existing buildings. Unlike the other approaches, this Two-Stage Core Sunlighting System does not increase the energy load of the building and the impact of the system on the appearance of the building is minimal. A rough evaluation of cost and embodied energy of the system showed that the Two-Stage Core Sunlighting System has the potential to be broadly applied in commercial buildings and provides a practical and sustainable solution to the daylighting problem in the building industry.

References

[1] L. Whitehead, "Dual-stage sunlight redirection system". World Intellectual Property Organization Patent WO 2013155604 A1, 24 Oct 2013.

[2] L. A. Whitehead, "Sunlight redirecting mirror arrays". WO 2013059908 A1 Patent World Intellectual Property Organization, 2 May 2013.

[3] "TracePro- user manual (release 6.0)," Lambda research Corp, 2009. [Online]. Available: http://www.lambdares.com/. [Accessed 2014 9 2].

[4] J. Christoffersen, E. Peterson, and et al., "Windows and daylighting - a post occupancy evaluation of offices (SBI report)," International Daylighting Newsletter, vol. 2, no. 11, 1999.

[5] J. H. Heerwagen, G. H. Orians, "Adaptation to windowlessness: A study of the use of visual decor in windowed and windowless offices," Environment and Behavior, vol. 18, no. 5, pp. 623-639, 1986.

[6] H. H. Young, G. L. Berry, "The impact of environment on the productivity attitudes of intellectually challenged office workers," Human Factors, vol. 21, no. 4, pp. 399-407, 1979.

[7] K. Thapan, J. Andersen, "An action spectrum for melatonin suppression: evidence for a novel non-rod, non cone photorecptor system in humans," The Journal of Physiology, pp. 261-267, 2001.

[8] G.C. Brainard, J.P. Hanifin, et al, "Action spectrum for melatonin regulation in human: evidence for novel circadian photorecptor," The Journal of Neuroscience 21 (16), pp. 6405-

6412, 2001.

[9] D. Dilaura, K. Houser, R. Mistrick, G, Steffy, "Colour rendering," in The Lighting handbook, New York, Illuminating Engineering Society, 2011, p. 6.19.

[10] "Lamps and Ballast product guide," BC Hydro Power smart, [Online]. Available: http://www.bchydro.com/content/dam/hydro/medialib/internet/documents/psbusiness/pdf/ps_business_lamp_and_ballast_product_guide.pdf. [Accessed 28 1 2014].

[11] "United States Environmenta Protection Agency," [Online]. Available: http://www.epa.gov/climatechange/ghgemissions/sources.html. [Accessed 28 1 2014].

[12] "2010 Commercial Energy Use, by fuel type," U.S. Department of Energy, [Online]. Available: http://buildingsdatabook.eren.doe.gov/TableView.aspx?table=3.1.4. [Accessed 28 1 2014].

[13] R. Rise, M. M. Bilec, et al., "the economic benefit of green buildings: a comprehensive case study," The Engineering Ecconomist, no. 51, pp. 259-295, 2007.

[14] "LEED Canada for new construction and major renovation,," Canada Green Building Councill, [Online]. Available: http://www.cagbc.org/Content/NavigationMenu/Programs/LEED/GoingGreenwithLEED/default.htm. [Accessed 28 1 2014].

[15] L. Whitehead, D. Yen, R. Salikan, "Core Sunlighting technology offering a new approach to green building," Journal of Construction, vol. 53, no. 5, pp. 48-56, 2011.

[16] F. Linhart, S.K. Wittkopf, J. L. Scartezzini, "Performance of Anidolic Daylighting System in tropical cliamte- Parametric studies for identification of main influencing factors," Solar

Energy, vol. 84, pp. 1085-1094, 2010.

[17] L. A. Whitehead, M. Mossman, "Jack O'Lanterns and integrating spheres: Halloween physics," American Journal of Physics, vol. 74, no. 6, pp. 637-541, 2006.

[18] "Indoor lighting," in Lighting Handbook Reference and Application, New York, Illuminating Engineering Society of North America, 2000, pp. 8-12.

[19] G. Courret, J. L. Scartezzinin, et al, "Design and assessment of an anidolic light-duct," Energy and Building, vol. 28, no. 1, pp. 79-99, 1998.

[20] P. J. Littlefair, "Innovative daylighting: Review of system and evaluation methods," Lighting Research and Technology , vol. 22, no. 1, pp. 1-17, 1990.

[21] D. Molini, M. Montes and et al, "Horizontal daylighting system for office buildings," Energy and Buildings, vol. 67, pp. 525-530, 2013.

[22] J. T. Kim, G. Kim, "Overview and new developments in optical daylighting systems for building a healthy indoor environment," Building and Environment, vol. 45, pp. 256-269, 2010.

[23] D. J. Carter, "The measured and predicted performance of passive solar light pipe system," Lighting Research and Technology, vol. 34, no. 1, pp. 39-52, 2002.

[24] R. Wilson, J. C. Miano, P. Bentez, Nonimaging Optics., Burlington, San Diego, London: Elsevier Academic press, 2005.

[25] A. Rosemann, H. Kaase, "Lighting application for daylighting systems," Solar energy, vol. 78, pp. 772-780, 2005.

[26] M. S. Mayhoub, D. J. Carter DJ, "Toward hybrid lighting system: A review," Lighting

Research and Technology, vol. 42, pp. 51-71, 2010.

[27] Lapsa MV, Maxey LC and et al, "Hybrid solar lighting provides energy saving and reduces waste heat," Energy Engineering, vol. 104, no. 4, pp. 7-20, 2007.

[28] Mayhoub M, Carter D, "How hybrid lighting system can be integrated into building design?," PLEA conference, Lima, Peru, 2012.

[29] M. Wilson, A. Jacobs, et al., "Creating sunlight rooms in non-daylight spaces," in International Conference on Energy Efficient Lighting, Nice, France, 2002.

[30] A. Tsangrassoulis, L. Doulos, et al., "On the energy efficiency of a prototype hybrid daylighting system," Solar Energy, vol. 79, pp. 56-64, 2005.

[31] V. G. Hansen, "Innovative daylighting systems for deep-plan commercial buildings," Queensland University of Technology, 2006.

[32] "Himawari," Himawari, [Online]. Available: http://www.himawari-net.co.jp/e_page-index01.html. [Accessed 28 1 2014].

[33] Ono E, Cuello JL, "Design parameters of solar concentrating systems for CO2-mitigating algal photobioreactors," Energy, vol. 29, pp. 1651-1657, 2004.

[34] "Parans, Brochure," [Online]. Available: http://www.parans.com/eng/. [Accessed 20 1 2014].

[35] Whitehead L, Upward A, and et al, "Using core sunlighting to improve illumination quality and increasing energy efficiency of commercial buildings," in ASME international conference on Energy Sustainability, Arizona, USA, 2010.

[36] Rosemann A, Mossman M, Whitehead L, "Developement of cost-effective solar

illumination system to bring natural light into the building core," Solar Energy, vol. 82, pp. 302-310, 2008.

[37] "Building energy data book," U.S. Department of Energy, , [Online]. Available: http://buildingsdatabook.eren.doe.gov/ChapterIntro3.aspx. [Accessed 30 7 2014].

[38] "TracePro- user manual (release 6.0)," Lambda Research Corp, 2009. [Online]. Available: http://www.lambdares.com/. [Accessed 2014 9 2].

[39] E. Hecht, "Propagation of light," in Optics, San Fransisco, Addison Wesley, 2002, pp. 128-129.

[40] K. R. Symon, "The rotation of rigid body," in Mechanics, Massachusetts, Addison Wesley publishing comapny, 1960, pp. 450-458.

[41] W. R. Winston, The Optics of Nonimaging Concentrators: Light and Solar Energy, New York: Academic Press, 1978.

[42] G. N. Tiwari, "Solar Concnetrators," in Solar energy, fundamental, design, modeling and application, New Delhi, Narosa Publishing house, 2004, pp. 251-260.

[43] "Plastic optical fiber, Vol 25, P65," Information gatekeepers INC, [Online]. Available: http://www.igigroup.com/pub/reportseries/fopub.html. [Accessed 11 08 2014].

[44] E. Hecht, "Geometrical optics, field curvature," in Optics, San Francisco, Addison Wesley, 2002, p. 264.

[45] R. Uhl, T. Reddmann, "Divergence of sun-rays by atmospheric refraction at large solar zenith angles," Atmospheric Chemistry and Physics, vol. 4, pp. 1399-1405, 2004.

[46] L. Whitehead, "New simplified design procedures for prism light guide luminaires," Journal

of the Illuminating Engineering Society, pp. 21-27, 1998.

[47] L. Whitehead, R. A. Nodwell, F. L. Curzon, "New efficient light guide for interior illumination," Applied Optics, vol. 21, no. 15, pp. 2755-2758, 1982.

[48] M. Aden, A. Roesner, A. Olowinsky, "Optical characterization of polycarbonate: influence of additives on optical properties," Wiley InterScience, 2009.

[49] "3M optical lighting film," 3M, [Online]. Available: http://www.folienportal24.de/$WS/folienportal24/websale7_shop-folienportal24/produkte/medien/pdf/2301.pdf. [Accessed 14 8 2014].

[50] "ESR, Vikuiti," 3M, 2010. [Online]. Available: http://multimedia.3m.com/mws/mediawebserver?mwsId=66666UF6EVsSyXTtMxMyOXM6EVtQEVs6EVs6EVs6E666666--&fn=ESR%20ss2.pdf. [Accessed 25 3 2014].

[51] J. C. Artega-Velazques, and et all, "A measurement of the diffuse reflectivity of 1056 Tyvek in air and water," Nuclear Instruments and Methods in Physics Research, vol. 53, pp. 312-316, 2005.

[52] "K12 female conical prism," Liteline corporation, [Online]. Available: http://www.liteline.com/product_spec_sheet/K12-24%20CA-F-S.pdf. [Accessed 4 4 2014].

[53] J. C. Zwinkels, W. F. Davidson, C. X. Dodd, "Optical properties of UV transmitting acrylics for use in a heavy water Cerenkov detector," Applied Optics, vol. 29, no. 22, pp. 2340-2348, 1990.

[54] P. Yeh, C. Gu, "PD-LCDs," in Optics of liquide crystal display, New Jersey, Wiley, 2010, p. 402.

[55] L. G. Henyey, J. L. Greenstein, "Diffuse radiation in galaxy," American Astrtonomical Society, vol. 93, pp. 70-83, 1941.

[56] N. Zolek, S. Wojtkiewics, "Correction of anisotropic coefficient in original Henyey-Greenstein phase function for Monte Carlo simulation of light transport in tissue," Biocybernetics and Biomedical Engineering, vol. 28, no. 4, pp. 59-73, 2008.

[57] "The Lighting Handbook," Zumtobel Lighting , Oct 2013. [Online]. Available: http://www.zumtobel.com/PDB/teaser/EN/lichthandbuch.pdf. [Accessed 2014 10 06].

[58] "National Oceanic and Atmospheric Administration-Earth System Research Laboratory," [Online]. Available: http://www.esrl.noaa.gov/gmd/grad/solcalc/. [Accessed 1 3 2014].

[59] "Indoor lighting," in Lighting Handbook Reference and Application, New York, Illuminating Engineering Society of North America, , 2000, pp. 10-18.

[60] "Number of floors and type of ownership as of 2003, commercial sector," US department of Energy, 2003. [Online]. Available: http://buildingsdatabook.eren.doe.gov/TableView.aspx?table=3.2.3. [Accessed 2014 4 4].

[61] "National Climate data center, snshine probability," National Oceanic and Atmospheric Administration, [Online]. Available: http://www.ncdc.noaa.gov/oa/climate/online/ccd/avgsun.html. [Accessed 20 12 2012].

[62] "BC Hydro," Electricity Residential rate, [Online]. Available: https://www.bchydro.com/accounts-billing/customer-service-residential/residential-rates.html. [Accessed 8 4 2014].

[63] "U.S. Energy Information Administration," Electric Power Monthly, [Online]. Available:

http://www.eia.gov/electricity/monthly/epm_table_grapher.cfm?t=epmt_5_6_a. [Accessed 8 4 2014].

[64] "E-Grid GHG Annual OUtput Emsission Rates 2010," US. Environmental Protection Agency, [Online]. Available: http://www.epa.gov/cleanenergy/energy-resources/refs.html. [Accessed 8 4 2014].

[65] "Energy Efficiency of LED," US Department of Energy , [Online]. Available: http://apps1.eere.energy.gov/buildings/publications/pdfs/ssl/led_energy_efficiency.pdf. [Accessed 9 4 2014].

[66] Alibaba, "Alibaba," [Online]. Available: http://www.alibaba.com/showroom/pmma-commodity.html. [Accessed 15 4 2014].

[67] "Aluminum price," Mining market and investment, [Online]. Available: http://www.infomine.com/investment/metal-prices/aluminum/. [Accessed 15 4 2014].

[68] C. Designe, "Material life," [Online]. Available: http://media.cannondesign.com/uploads/files/MaterialLife-9-6.pdf. [Accessed 15 4 2014].

[69] C. Architect, "Measure of Sustainability," [Online]. Available: http://www.canadianarchitect.com/asf/perspectives_sustainibility/measures_of_sustainablity/measures_of_sustainablity_embodied.htm. [Accessed 15 4 2014].

[70] "PV FAQS," U.S. Department of Energy, Dec 2004. [Online]. Available: http://www.nrel.gov/docs/fy05osti/37322.pdf. [Accessed 28 1 2014].

[71] S. r. d. manual, "National Renewable Energy Laboratory (NREL)," [Online]. Available: http://rredc.nrel.gov/solar/pubs/redbook/. [Accessed 28 1 2014].

[72] "Solar pannel quote," Alibaba, [Online]. Available: http://www.alibaba.com/trade/search?fsb=y&IndexArea=product_en&CatId=&SearchText=solar+pannel. [Accessed 16 9 2014].

[73] I. Nawaz, G. N. Tiwari, "Embodied energy analysis of photovoltaic (PV) system based on macro and micro level," Energy Policy, vol. 34, pp. 3144-3152, 2006.

[74] L. Whitehead, W. Su, "Evaluation of prism light guide by finite-difference time-domain field modeling," Applied Optics, vol. 37, pp. 8536-8542, 1998.

[75] P. Lorrian, D. R. Corson, F. Lorrian, "Plane electromagnetic wave III," in Electromagnetic field and wave, New York, W. H. Freeman and Company, 1987, pp. 554-565.

[76] P. Lorrain, D. R. Corson, F. Lorrain, "Plane Electromagntic wave IV," in Electromagnetic waves , New York, W. H. Freeman and Company, 1987, pp. 579-584.

[77] Max Born, Emil Wolf, "Foundation of geometrical optics," in Principle of Optics, Cambridge, Cambridge University Press, 2001, p. 117.

[78] E. Hecht, "Geometrical Optics," in Optics, New York, Addison Wesley, 2002, p. 148.

[79] E. Hecht, "Electromagnetic theory, photons and Light," in Optics, New York, Addison Wesley, 2002, pp. 43-45.

[80] W. Yu, X, Yang and et al, in Electromagnetic simulation tecniques based on the FDTD method, New Jersey, John Wiley and Sons, 2009, pp. 1-16.

[81] Lumerical, "FDTD solutions getting started," [Online]. Available: http://nf.nci.org.au/facilities/software/Lumerical/7.5.6/FDTD_getting_started.pdf. [Accessed 9 5 2014].

[82] R. D. Knight, "Physics for scientists and engineers, a strategic approach," Addison Wesley, 2007, pp. 652-654.

[83] M. L. Rodrick, "Methods for calculating solar position and daylength including computer programs and subroutines," Government of western australia, 1992.

[84] I. Reda, A. Andreas, "Solar position algorithm for solar radiation application," National Renewable Labroratory, USA, 2008.

[85] N. D. Gupta, N. Kristensen, "Work environment satisfaction and employee health: panel," Eur J Health Econ, pp. 51-61, 2008.

Appendices

Appendix A : Sun position calculation

The azimuthal angle of sun, φ, can be calculated using following equation:

$$\tan\varphi = \frac{-\sin t}{\tan(decl)\cos(lat) - \sin(lat)\cos(t)}$$

where *decl* is the declination angle of sun, *lat* is the latitude of the location and *t* is the hour angle which is given by

$$t(arc\ degree) = T(hour) \times 15$$

$$T(hour) = local\ time - time\ zone + longitude + EOT - 180$$

where the equation of time, EOT, is the difference between actual day length and a mean day length. The actual length of day track the actual motion of sun and varies from 24 hours (length of a mean day) by $\pm 16min$. To calculate EOT, the length of day should be calculated via astronomical calculations.

Declination angle is the angle describing the difference between the orbital planes where earth rotates around itself and around the Sun, which is caused by the inclination of earth's orbital axis. It varies from $+23.45°$ at summer solstice and $-23.45°$ at winter solstice and is given by:

$$decl = 23.45\ \sin(\frac{360}{365}(d - 81))$$

where d is the day of the year with Jan 1st as d=1. The solar altitude angle α, can be calculated as followed:

$$\cos z = \sin(lat)\sin(decl) + \cos(lat)\cos(decl)\cos(t)$$

$$\alpha = 90 - z$$

The solar altitude needs to be corrected due to atmospheric parallax effect, which is given by the following equation in the first order:

$$\sin P = \frac{R}{D} \sin z$$

$$Z_{corrected} = Z_{calculated} + P$$

where R is the radius of earth and D is the distance earth to sun [83] [84]. I used an excel document form the National Ocean and Atmospheric Administration research Centre to calculate the solar position for some typical places throughout the year [58].

Appendix B : Macro code for TracePro (rotary redirector, single reflective mode)

```
(define AStart 6)
(define AFinish 90)
(define AIncrement 3)
(define FStart 0)
(define FFinish 360)
(define FIncrement 3)
(define a 1)
(define fi 1)
(define b 7)
(define PI 3.14159)
(define NX 1)
(define NY 1)
(define NZ 1)
(define SX 1)
(define SY 1)
(define SZ 1)
(define IX 1)
(define IY 1)
(define IZ 1)
(define RX 1)
(define RY 0)
(define RZ 1)
(define I 1)
(define R 1)
(define gama 1)
(define teta 1)
(define TargetFlux 1)
(define D 1000)
```

```
(define W 1)
(define d 77)
(define L 1)
(define Y 1)
(define Z 1)
(define LS 1)
(define L1 1)
(define L2 1)
(define h 1)

(do ( (FValue FStart (+ FValue FIncrement)))
 ((> FValue FFinish) FValue )
 (display FValue)
 (display " , ")

 (do ( (AValue AStart (+ AValue AIncrement)))
  ((> AValue AFinish) AValue )

  (set! a (* AValue (/ PI 180)))
  (set! fi (* FValue (/ PI 180)))
  (set! IX (- (* (cos a) (cos fi))))
  (set! IY (- (* (cos a) (sin fi))))
  (set! IZ  (sin a))
  (set! SX (* -1000 IX))
  (set! SY (* -1000 IY))
  (set! SZ (* -1000 IZ))
  (set! RX (sin (* b (/ PI 180))))
  (set! RZ (cos (* b (/ PI 180))))
  (set! I (sqrt( + (+ (* IX IX) (* IY IY)) (* IZ IZ))))
  (set! R (sqrt( + (+ (* RX RX) (* RY RY)) (* RZ RZ))))
```

```
    (set! NX (- (/ RX R) (/ IX I)))
    (set! NY (- (/ RY R) (/ IY I)))
    (set! NZ (- (/ RZ R) (/ IZ I)))
    (set! gama (atan (/ NY NX)))
    (set! teta (atan (/ NX (* NZ (cos gama)))))
    (set! W (/ d 1.5))
    (set! h (* (* -1 W) (sin teta)))
    (if (> h 0)
      (set! h (* -1 h)))
    (set! gama (/ (* gama 180) PI))
    (set! teta (/ (* teta 180) PI))

    (set! Y (/ d 2))
    (set! Z (+  Y W))
    (set! L1 (sqrt(- (* D D) (* 4 (* Y Y)))))
    (set! L2 (sqrt(- (* D D) (* 4 (* Z Z)))))
    (set! LS (/ (+ L1 L2) 2))

(modify:block (entity:get-by-name "Block 0") W LS 0.5)
    (edit:move (entity:get-by-name "Block 0") (/ W 2) 0.00 0.25)
    (entity:rotate (entity:get-by-name "Block 0") 0 0 0 0 1 0 teta)
    (edit:move (entity:get-by-name "Block 0") Y 0.00 0.00 #f #t)
    (entity:rotate (entity:get-by-name "Block 0") 0 0 0 0 0 1 gama)

    (modify:block (entity:get-by-name "Block 00") W L1 0.5)
    (edit:move (entity:get-by-name "Block 00") (/ W -2) 0.00 0.25 #f #t)
    (entity:rotate (entity:get-by-name "Block 00") 0 0 0 0 1 0 teta)
    (edit:move (entity:get-by-name "Block 00") Y 0.00 0.00 #f #t)
    (entity:rotate (entity:get-by-name "Block 00") 0 0 0 0 0 1 gama)
```

```
    (modify:block (entity:get-by-name "Block 1") W L1 0.5)
    (edit:move (entity:get-by-name "Block 1") (/ W 2) 0.00 0.25)
    (entity:rotate (entity:get-by-name "Block 1") 0 0 0 0 1 0 teta)
    (edit:move (entity:get-by-name "Block 1") (* -1 Y) 0.00 0.00 #f #t)
    (entity:rotate (entity:get-by-name "Block 1") 0 0 0 0 0 1 gama)

    (modify:block (entity:get-by-name "Block 2") W LS 0.5)
    (edit:move (entity:get-by-name "Block 2") (/ W -2) 0.00 0.25)
    (entity:rotate (entity:get-by-name "Block 2") 0 0 0 0 1 0 teta)
    (edit:move (entity:get-by-name "Block 2") (* -1 Y) 0.00 0.00 #f #t)
    (entity:rotate (entity:get-by-name "Block 2") 0 0 0 0 0 1 gama)

  (set! Y (+ d  Y))
    (set! Z (+  Y W))
    (set! L1 (sqrt(- (* D D) (* 4 (* Y Y)))))
    (set! L2 (sqrt(- (* D D) (* 4 (* Z Z)))))
    (set! LS (/ (+ L1 L2) 2))

    (modify:block (entity:get-by-name "Block 3") W LS 0.5)
    (edit:move (entity:get-by-name "Block 3") (/ W 2) 0.00 0.25)
    (entity:rotate (entity:get-by-name "Block 3") 0 0 0 0 1 0 teta)
    (edit:move (entity:get-by-name "Block 3") Y 0.00 0.00 #f #t)
    (entity:rotate (entity:get-by-name "Block 3") 0 0 0 0 0 1 gama)

    (modify:block (entity:get-by-name "Block 4") W L1 0.5)
    (edit:move (entity:get-by-name "Block 4") (/ W -2) 0.00 0.25 #f #t)
    (entity:rotate (entity:get-by-name "Block 4") 0 0 0 0 1 0 teta)
    (edit:move (entity:get-by-name "Block 4") Y 0.00 0.00 #f #t)
    (entity:rotate (entity:get-by-name "Block 4") 0 0 0 0 0 1 gama)
```

```
(modify:block (entity:get-by-name "Block 5") W L1 0.5)
(edit:move (entity:get-by-name "Block 5") (/ W 2) 0.00 0.25)
(entity:rotate (entity:get-by-name "Block 5") 0 0 0 0 1 0 teta)
(edit:move (entity:get-by-name "Block 5") (* -1 Y) 0.00 0.00 #f #t)
(entity:rotate (entity:get-by-name "Block 5") 0 0 0 0 0 1 gama)

(modify:block (entity:get-by-name "Block 6") W LS 0.5)
(edit:move (entity:get-by-name "Block 6") (/ W -2) 0.00 0.25 #f #t)
(entity:rotate (entity:get-by-name "Block 6") 0 0 0 0 1 0 teta)
(edit:move (entity:get-by-name "Block 6") (* -1 Y) 0.00 0.00 #f #t)
(entity:rotate (entity:get-by-name "Block 6") 0 0 0 0 0 1 gama)

(set! Z (+  Y W))
(set! L1 (sqrt(- (* D D) (* 4 (* Y Y)))))
(set! L2 (sqrt(- (* D D) (* 4 (* Z Z)))))
(set! LS (/ (+ L1 L2) 2))
```

repeat the same for all slats

```
(raytrace:set-grid-origin (position SX SY SZ) "Grid Source 1")
(raytrace:set-grid-orientation-direction-vectors (gvector IX IY IZ) (gvector 0.000000 1.000000 0.000000) "Grid Source 1")
(raytrace:all-sources)
(set! TargetFlux (raytrace:get-incident-flux (entity:get-by-name "target0")))
(display TargetFlux)
(newline)
(set! TargetFlux (raytrace:get-incident-flux (entity:get-by-name "target")))
(display TargetFlux)
(newline)
(set! TargetFlux (raytrace:get-incident-flux (entity:get-by-name "target1")))
```

```
  (display TargetFlux)
  (newline)
  (set! TargetFlux (raytrace:get-incident-flux (entity:get-by-name "target2")))
  (display TargetFlux)
  (newline)
  (set! TargetFlux (raytrace:get-incident-flux (entity:get-by-name "target3")))
  (display TargetFlux)
  (newline)
  (set! TargetFlux (raytrace:get-incident-flux (entity:get-by-name "target4")))
  (display TargetFlux)
  (newline)
  (edit:move (entity:get-by-name "Cylinder 1") 0.00 0.00 (* -1 h) #f #t)
  (edit:move (entity:get-by-name "Cylinder 2") 0.00 0.00 (* -1 h) #f #t)
  (edit:move (entity:get-by-name "Cylinder 3") 0.00 0.00 (* -1 h) #f #t)
  ;(display ",")
  (newline)
  )
(newline)
)
```

Appendix C : Matlab code used to calculate the orientation of reflective slats in double reflection mode

```
function E = myerr(s)

global phi;
global alpha;
global beta;
gama= s(1);
delta= s(2);
IX= -cos(degtorad(alpha))*cos(degtorad(phi));
IY= -cos(degtorad(alpha))*sin(degtorad(phi));
IZ= sin(degtorad(alpha));

NX= -sin(degtorad(beta))*cos(degtorad(gama));
NY= -sin(degtorad(beta))*sin(degtorad(gama));
NZ= -cos(degtorad(beta));

IN=IX*NX+IY*NY+IZ*NZ;

RX=IX-2*IN*NX;
RY=IY-2*IN*NY;
RZ=IZ-2*IN*NZ;

R=sqrt(RX^2+RY^2+RZ^2);

IIX=RX/R;
IIY=RY/R;
IIZ=RZ/R;

NNX= sin(degtorad(delta))*cos(degtorad(gama));
NNY= sin(degtorad(delta))*sin(degtorad(gama));
NNZ= cos(degtorad(delta));

IINN=IIX*NNX+IIY*NNY+IIZ*NNZ;
```

```
RRX=IIX-2*IINN*NNX;
RRY=IIY-2*IINN*NNY;
RRZ=IIZ-2*IINN*NNZ;

a=radtodeg(atan(RRX/RRZ));
b=radtodeg(atan(RRY/RRZ));
E=(a-7)^2+b^2;
```

Appendix D : Matlab code used to calculate the optimum rotational angle for double reflective mode

```
function [x,fval,exitflag,output,lambda,grad,hessian] = opt(x0,lb,ub)
% This is an auto generated MATLAB file from Optimization Tool.
global phi
global alpha
global beta
alpha=24;
beta=-6;
lb = [-180,-90];
ub = [180,0];
results = zeros(2,2);



 for phi = 1:3:360
     x0 = [phi-180,-30];

% Start with the default options
options = optimset;
% Modify options setting
options = optimset(options,'Display', 'off');
options = optimset(options,'Algorithm', 'interior-point');
[x,fval,exitflag,output,lambda,grad,hessian] = ...
fmincon(@myerr,x0,[],[],[],[],lb,ub,[],options);

results(idivide( int32(phi),3,'ceil'),1)=x(1);
results(idivide(int32(phi),3,'ceil'),2)=x(2);

end

 results

 dlmwrite('results.txt',results)
```

Appendix E : Macro code for TracePro (rotary redirector, double reflective mode)

```
(define FStart 0)
(define FFinish 360)
(define FIncrement 3)
(define alpha 30)
(define Beta 1)
(define delta 1)
(define gama 1)
(define a 1)
(define f 1)
(define PI 3.14159)
(define SX 1)
(define SY 1)
(define SZ 1)
(define IX 1)
(define IY 1)
(define IZ 1)
(define TargetFlux 1)
(define D 1000)
(define W 1)
(define d 77)
(define Y 1)
(define Z 1)
(define LS 1)
(define L1 1)
(define L2 1)
(define L 1)
(define table_beta "beta.txt")
(define beta_list (open-input-file table_beta))
(define table_gama "gama.txt")
```

```
(define gama_list (open-input-file table_gama))
(define table_delta "delta.txt")
(define delta_list (open-input-file table_delta))

(do ( (FValue  FStart  (+ FValue  FIncrement ) ) )
  ( (> FValue  FFinish ) FValue )

  (define Beta (read beta_list))
  (newline)
  (define gama (read gama_list))
  (newline)
  (define delta (read delta_list))

  (set! W (/ d 1.5))
  (set! a (* alpha (/ PI 180)))
  (set! f (* FValue (/ PI 180)))
  (set! IX (- (* (cos a) (cos f))))
  (set! IY (- (* (cos a) (sin f))))
  (set! IZ  (sin a))
  (set! SX (* -1000 IX))
  (set! SY (* -1000 IY))
  (set! SZ (* -1000 IZ))

  (set! Y (/ d 2))
  (set! Z (+  Y W))
  (set! L1 (sqrt(- (* D D) (* 4 (* Y Y)))))
  (set! L2 (sqrt(- (* D D) (* 4 (* Z Z)))))
  (set! LS (/ (+ L1 L2) 2))

  (modify:block (entity:get-by-name "Block 0") W LS 0.5)
```

```
(edit:move (entity:get-by-name "Block 0") (/ W 2) 0.00 0.25)
(entity:rotate (entity:get-by-name "Block 0") 0 0 0 0 1 0 (* -1 Beta))
(edit:move (entity:get-by-name "Block 0") Y 0.00 0.00 #f #t)
(entity:rotate (entity:get-by-name "Block 0") 0 0 0 0 0 1 gama)


(modify:block (entity:get-by-name "Block 00") W L1 0.5)
(edit:move (entity:get-by-name "Block 00") (/ W -2) 0.00 0.25 #f #t)
(entity:rotate (entity:get-by-name "Block 00") 0 0 0 0 1 0 delta)
(edit:move (entity:get-by-name "Block 00") Y 0.00 0.00 #f #t)
(entity:rotate (entity:get-by-name "Block 00") 0 0 0 0 0 1 gama)

(modify:block (entity:get-by-name "Block 1") W L1 0.5)
(edit:move (entity:get-by-name "Block 1") (/ W 2) 0.00 0.25)
(entity:rotate (entity:get-by-name "Block 1") 0 0 0 0 1 0 (* -1 Beta))
(edit:move (entity:get-by-name "Block 1") (* -1 Y) 0.00 0.00 #f #t)
(entity:rotate (entity:get-by-name "Block 1") 0 0 0 0 0 1 gama)


(modify:block (entity:get-by-name "Block 2") W LS 0.5)
(edit:move (entity:get-by-name "Block 2") (/ W -2) 0.00 0.25)
(entity:rotate (entity:get-by-name "Block 2") 0 0 0 0 1 0 delta)
(edit:move (entity:get-by-name "Block 2") (* -1 Y) 0.00 0.00 #f #t)
(entity:rotate (entity:get-by-name "Block 2") 0 0 0 0 0 1 gama)

(set! Y (+ d  Y))
(set! Z (+  Y W))
(set! L1 (sqrt(- (* D D) (* 4 (* Y Y)))))
(set! L2 (sqrt(- (* D D) (* 4 (* Z Z)))))
(set! LS (/ (+ L1 L2) 2))
```

```
(modify:block (entity:get-by-name "Block 3") W LS 0.5)
(edit:move (entity:get-by-name "Block 3") (/ W 2) 0.00 0.25)
(entity:rotate (entity:get-by-name "Block 3") 0 0 0 0 1 0 (* -1 Beta))
(edit:move (entity:get-by-name "Block 3") Y 0.00 0.00 #f #t)
(entity:rotate (entity:get-by-name "Block 3") 0 0 0 0 0 1 gama)

(modify:block (entity:get-by-name "Block 4") W L1 0.5)
(edit:move (entity:get-by-name "Block 4") (/ W -2) 0.00 0.25 #f #t)
(entity:rotate (entity:get-by-name "Block 4") 0 0 0 0 1 0 delta)
(edit:move (entity:get-by-name "Block 4") Y 0.00 0.00 #f #t)
(entity:rotate (entity:get-by-name "Block 4") 0 0 0 0 0 1 gama)

(modify:block (entity:get-by-name "Block 5") W L1 0.5)
(edit:move (entity:get-by-name "Block 5") (/ W 2) 0.00 0.25)
(entity:rotate (entity:get-by-name "Block 5") 0 0 0 0 1 0 (* -1 Beta))
(edit:move (entity:get-by-name "Block 5") (* -1 Y) 0.00 0.00 #f #t)
(entity:rotate (entity:get-by-name "Block 5") 0 0 0 0 0 1 gama)

(modify:block (entity:get-by-name "Block 6") W LS 0.5)
(edit:move (entity:get-by-name "Block 6") (/ W -2) 0.00 0.25 #f #t)
(entity:rotate (entity:get-by-name "Block 6") 0 0 0 0 1 0 delta)
(edit:move (entity:get-by-name "Block 6") (* -1 Y) 0.00 0.00 #f #t)
(entity:rotate (entity:get-by-name "Block 6") 0 0 0 0 0 1 gama)


(set! Y (+ d  Y))
(set! Z (+  Y W))
(set! L1 (sqrt(- (* D D) (* 4 (* Y Y)))))
(set! L2 (sqrt(- (* D D) (* 4 (* Z Z)))))
```

```
(set! LS (/ (+ L1 L2) 2))

**repeat the same for all slats**

(raytrace:set-grid-origin (position SX SY SZ) "Grid Source 1")
    (raytrace:set-grid-orientation-direction-vectors (gvector IX IY IZ) (gvector 0.000000
   1.000000 0.000000) "Grid Source 1")
(raytrace:all-sources)
(set! TargetFlux (raytrace:get-incident-flux (entity:get-by-name "target0")))
(display TargetFlux)
(newline)
(set! TargetFlux (raytrace:get-incident-flux (entity:get-by-name "target")))
(display TargetFlux)
(newline)
(set! TargetFlux (raytrace:get-incident-flux (entity:get-by-name "target1")))
(display TargetFlux)
(newline)
(set! TargetFlux (raytrace:get-incident-flux (entity:get-by-name "target2")))
(display TargetFlux)
(newline)
(set! TargetFlux (raytrace:get-incident-flux (entity:get-by-name "target3")))
(display TargetFlux)
(newline)
(set! TargetFlux (raytrace:get-incident-flux (entity:get-by-name "target4")))
(display TargetFlux)
(newline)
(newline)
)
```